Studies in NMR relaxation and diffusion: High-field applications to Petrophysics

by

Moacyr do Nascimento

Coordenação de Matéria Condensada,
Física Aplicada e Nanociência
December 10, 2020

Supervisor:
Prof. Ivan S. Oliveira

Abstract

This thesis contains the most relevant part of the work done by the author on NMR-based porous media characterization techniques at the NMR and Quantum Information lab of CBPF.

It starts with a short review of NMR applications to Petrophysics, reportedly, the science of physical processes that occur within the pore domain of a porous material. Most of NMR-based methods are concerned with geometric characterization of the pore structure and it is discussed both the type and the extent of such descriptions. A more in-depth but also considerably biased overview of NMR diffusive transport follows, laying much of the foundation for the subsequent chapters of original content and delineating the limitations and natural difficulties of the underlying theory and methods. It is believed, nevertheless, that this chapter is still able to offer an unified and a rather fresh perspective on a topic so amply and thoroughly discussed over the past half century. In particular, the algorithmic character of the theoretical treatment of NMR diffusion is emphasized and analyzed over several formalisms in order to establish a clear connection with essential numerical methods.

The beginning of second part contains a first-principles theory on one of the most common and effective scenarios that lead to NMR relaxation enhancement of fluid in porous media, namely, the presence of adsorbed or lodged paramagnetic impurities on the pore structure boundary. The concept of active surface elements is introduced and it is argued that NMR relaxation in the immediate vicinity of these centers is dependent upon surface normal orientation. The central hypotheses of the model and its predictions are then subjected to experimental tests for verification.

In the last chapter, the singularities of high-field NMR are exploited in devising a protocol that allows experimental observation of internal field autocorrelation functions. It is discussed what sort of information regarding domain geometry can be provided by such statistical characteristics and the method is put to test over model porous samples of known grain form and size. To the best of knowledge, it is the first time such an intrinsic property of the porous system is actively observed and, though research is still incipient, results look rather promising.

Keywords: Petrophysics, High-field NMR, surface relaxation, diffusion, internal field characteristics

Para os meus amigos, a quem amo e admiro.

Contents

CHAPTER 1

Introduction

Nuclear magnetic resonance (NMR) and porous media share a long history. Felix Bloch himself seems to have been the first to introduce the two subjects, in the early 1950s, when considering the effect of collisions on the NMR relaxation of gases saturating powders[8]. Ingeniously, he also correctly guessed the basic model that is used, to this day, for describing the many technological ramifications of that versatile phenomenon when it applies to one of Nature's most recurrent type of structure.

Pore systems are relevant in almost every branch of the natural sciences for either their ability to store or filter whatever they are able to confine to their intricate framework. The term typically refers to macroscopic aggregates of grains or fibers, yet it also applies to entirely consolidated solid bodies that, likewise, exhibit a vast system of pores which may or may not be communicated, forming a complex network of channels. Therefore, it encompasses a diverse range of naturally occurring materials: Rock, soil, wood, bone and virtually every other biological tissue are classical examples of porous media (see Fig.1.1). And, from a physical perspective, it is even possible to extend the definition to any structure having similar geometrical features, irrespective of its pore scale, as long the transport phenomena of interest agree to a classical description. As such, zeolites, amphiphilic aggregates and polymer solutions are all porous media but at the molecular level.

In turn, NMR-based methods happen to be extremely convenient for extracting geometrical information about a pore structure by probing the fluids that saturate

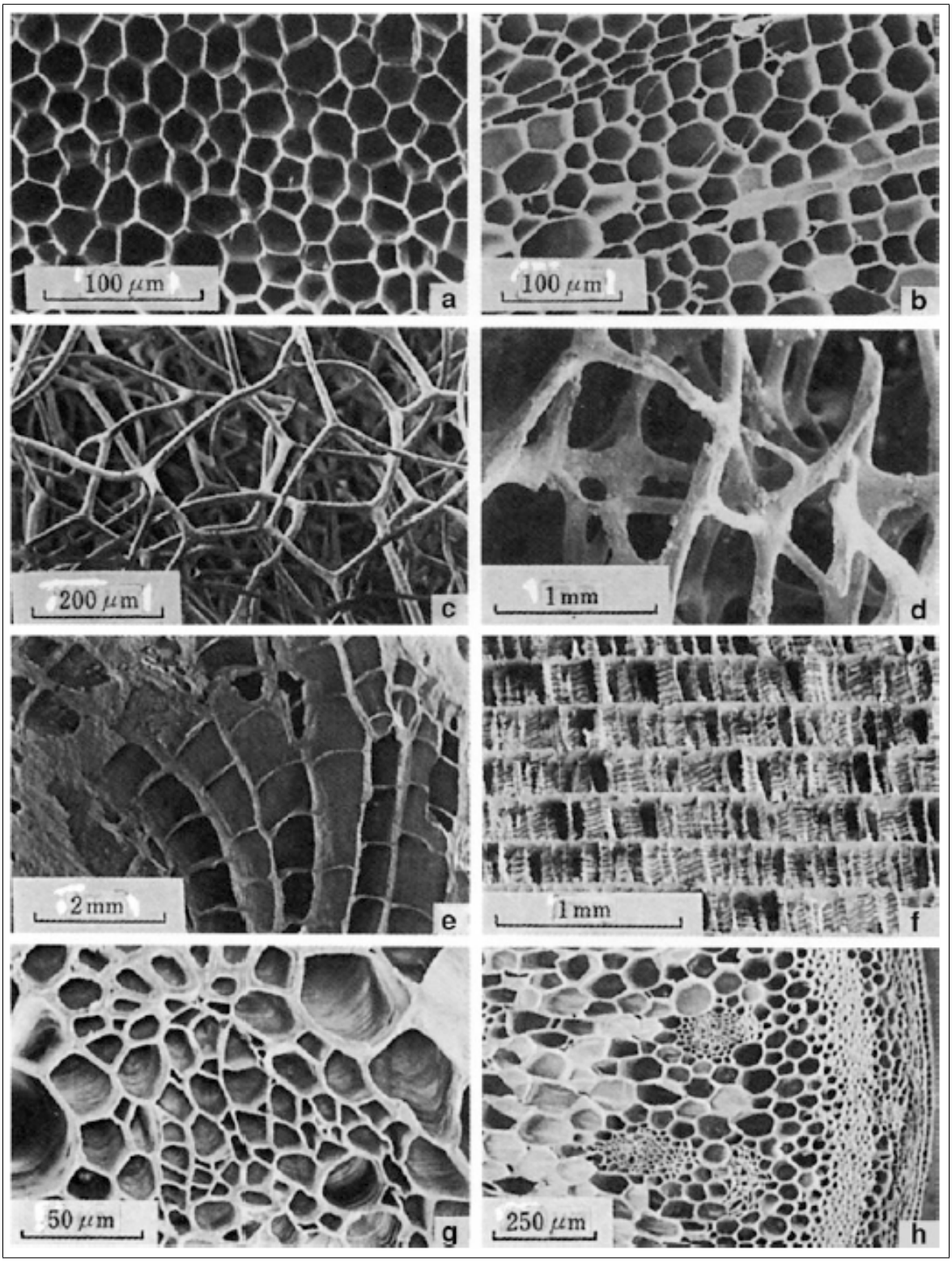

Figure 1.1: Natural pore structures: (a) cork, (b) balsa wood, (c) sponge, (d) cancellous bone, (e) coral, (f) cuttlefish bone, (g) iris leaf, and (h) plant stalk (Extracted from Nakajima[82])

it. To give a basic example, the porosity of a porous sample, defined as the ratio of pore to body volume, can be accurately measured through NMR via a simple tool calibration[63]. That is so because NMR signals are directly proportional to the amount of resonant nuclei in a sample, which is directly proportional to the volume of fluid contained in it. Therefore, porosity can be determined by normalizing a given signal to the signal produced by the same apparatus on a reference volume of the same fluid. Not only that but, as F.Bloch noted, signal decay is typically enhanced by molecular encounters with the confining structure; a fact that suggests NMR is sensitive to the surface-to-volume ratio of a pore domain as well.

These findings led to an impressive early development of NMR-based tools for water and hydrocarbon prospection[14,33,103], roughly a decade after magnetic resonance was announced to the scientific community as detectable in macroscopic bodies. During the same period, as researchers started to realize NMR is a powerful resource for chemical analysis[49,51,97] and characterization[76,95], oil companies and affiliated institutes were carrying laboratory experiments on fluid saturated porous samples aiming at equivalent applications[12,15,119].

1.1 Surface-induced Relaxation

NMR relaxation is a process affected by the molecular surroundings of nuclei. This is why, while resonant frequencies may be seen as nuclear properties, relaxations rates undoubtedly refer to substances. In typical containers, molecular interactions with boundaries are usually of negligible effect, however, as the surface-to-volume ratio of containers gets sufficiently large, fluid molecules become more and more frequently exposed to a distinct environment to the point that confinement alone seems to compel the formation of an altogether distinct substance[38]. Thus, in principle, NMR relaxation can not only separate the volumes occupied by multiple fluids in a porous sample but also determine what fraction of each wets its surface[15,119]. Both of these properties, saturation degree and wettability, are vital for assessing fluid quantity, configuration and mobility in a porous domain. Clearly, important factors in areas that have far-reaching implications in both industry and society such as hydrocarbon exploration and aquifer management.

Hence, in the context of porous media, considerable attention was given to the mechanisms by which solid boundaries and framework influence relaxation and to how structural information can be obtained from analyzing signal decays.

One important breakthrough came with the works of Torrey, Korringa, Seevers and co-workers[67,112]. In a beautifully designed experiment, they showed how a large nuclear magnetization develops in a saturated porous medium by exposing it to microwave radiation at the electronic resonant frequency of paramagnetic centers lodged at the fluid-solid interface. In contrast, Torrey *et al.*[112] point out that the concentration of these centers is typically very small and that, due to the low range of magnetic dipolar interactions, only nuclear spins at their immediate vicinity can experience this sort of electron-nucleus Overhauser effect. Surprisingly, the experiment shows how molecular diffusion can be a very effective process of nuclear magnetization transfer even in liquids. Moreover, their work reinforced the adequacy of non-equilibrium thermodynamic concepts, introduced in the NMR subject by Torrey himself[111], in the treatment of surface-induced effects; established for first time[1] how the enhancement in signal decay relates to the surface-to-volume ratio of a sample[112] and put on more solid foundation the discrete balance equations that were already being used to interpret the non-exponential character of signal decays[119], to the point of even incorporating field-dependence or **dispersion** of relaxation rates in the framework[67].

Magnetic coupling with sparse paramagnetic sites and effective molecular diffusion are indeed recognized to be the most basic features of NMR relaxation of fluids in porous media. Over time, several other modeling strategies, ranging from stochastic[77,93] to phenomenological[5,16,17], going back even to a detailed revision of non-equilibrium thermodynamic considerations[25], helped to consolidate the view.

The concept of a surface-affected *phase*, coating the inner walls of a saturated porous medium and exhibiting its own relaxation characteristics, was experimentally tested[38] in clays and, by the way, much more recently revisited with molecular dynamic simulations on model cementitious materials[36], confirming that nuclear spin behavior is already bulk-like beyond two or three molecular layers above the confining walls (at least for water).

Other mechanisms for relaxation enhancement were considered, yet, either proved to be too specific[2], like the influence of ferromagnetic grains or inclusions present in the solid structure[13], or found to be of negligible effect, as in the case of geometrical

[1] To the best of my knowledge.

[2] Although rocks with high iron content (about 15% in composition) are not unusual, iron compounds, typically, amount to 1-5% in the chemical constitution of geologically formed pore structures. The fraction is lower for porous media of biological origin such as wood or bone in which iron content falls in the order of 0.01% and, presumably, the occurrence for other possibly ferromagnetic impurities is even lower, regardless of material origin. Furthermore, the presence of ferromagnetic material can only enhance transverse magnetization decay.

constraints imposed by solid boundaries alone on nuclear rotational correlations[31].

The field dependence of relaxation rates presented by the Korringa-Seevers-Torrey (KST) theory has been generalized and extended in order to account for transverse relaxation as well[64] and, in this respect, fluid chemical polarity was proved to be an important factor in the selection of microscopic mechanisms that govern nuclear spin relaxation in confined systems[65,66], a feature that can be useful in the study of mixed-wet pore structures.

The effects of paramagnetic center concentration were throughly investigated[18,37,60,88]: Surface relaxation rates are found to increase linearly with concentration at a given field but dispersion profiles can vary remarkably on a given structure, depending on the chemical nature of paramagnetic sites. As a result, because of their ability to additionally provide chemical information, like characteristic times of adsorption[41] or coordination constraints[83], NMR-dispersion techniques became the favored method for investigating microporous media[65], in which chemical reactivity is often an relevant issue, but often finding applicability on characterizing macroporous systems as well[41].

The basic result following from all these studies is that, when diffusion is sufficiently effective, a porous structure affects the NMR signal decay by adding a term to the bulk relaxation rate of a fluid that is proportional to the surface-to-volume ratio of the medium. This, of course, implies that surface relaxation effects are inefficient for distinguishing interfacial regions because, in the course of an experiment, spins are mixed over nearly every accessible region of pore space. Diffusion is then said to be **fast**[17] or, equivalently, relaxation is **surface-limited**[5]. The proportionality coefficient, usually denote by ρ, is called **surface relaxivity**, although, it should be emphasized again, it is an interface property that, as seen, not only depends on concentration, chemical nature and oxidation state of paramagnetic centers, but also on the wetting fluid chemical polarity and reactivity.

Accordingly, NMR relaxation data of fully saturated pore structures can be used to estimate surface-to-volume ratios and, ultimately, to construct pore size distributions based on such quantity.

1.1.1 Pore size distributions

The underlying principle is simple. Assume a sample comprises only isolated pores. Since each pore contributes to the overall signal with is total resonant nuclear

magnetic moment and these, in turn, decay at rates which are pore-specific, the NMR relaxation signal takes the form[3]

$$M(t) = e^{-\frac{t}{\mathrm{T}}} \sum_m M_m \exp\left[-\left(\frac{\rho S_0}{V_0}\right)_m t\right]. \tag{1.1}$$

The decay is modulated by the fluid bulk relaxation, which can be independently measured, but, in most cases, the surface-induced terms completely dominate decay, so that factor can be entirely neglected [63].

Pores with identical relaxation rates are evidently grouped together and by normalizing the signal to its initial amplitude, a distribution of rates can be associated to the structure. Namely,

$$E(t) = \sum_m p_m e^{-s_m t} \equiv \int_0^\infty \mathrm{d}s\, p(s) e^{-st}, \tag{1.2}$$

wherein $s = \rho S_0/V_0$.

If the internal surfaces of the medium have similar microscopic characteristics, a requirement that usually means pore surfaces have been subjected to identical physicochemical processes, then surface relaxivity can be assumed uniform throughout the sample and so, apart from a axis dilation, distributions of surface-to-volume ratios (the NMR measure of pore size) can be derived.

Pore coupling

Frequently, however, a pore structure is communicated and so, the interpretation of NMR relaxation data becomes a bit more tricky. For one, the concept of pore in such systems can lose entirely its objective meaning. Several natural pore structures present no clear distinction among regions that should be considered pores or throats, the common jargon used for pore channels; that makes any pore space partitioning a fairly arbitrary procedure.

On the other hand, diffusion, effective as it can be, has its limitations as a mode of material transfer. For example, water molecules typically diffuse distances in the order of hundreds of micrometers over the duration of NMR relaxation experiment

[3] The distinction between longitudinal and transverse magnetization at this point is immaterial. Each experiment introduces obviously a particular characterization of relaxation coefficients, T and ρ, but, for the most part, the same equations apply for both types of experiments. Therefore, seeking notation simplicity, I leave it unspecified.

if unrestricted. The presence of solid boundaries, however, reduces molecular displacement as impinging particles are now reflected back and so forced to make longer trajectories to reach any given point in the pore domain. This puts a bound on how big a pore region can be for diffusion to be considered effective. Large pores may either violate the condition underlying Eq.(1.2), that is, spins are unable to access all available space, or they may be, in effect, partitioned into communicated regions in which the condition is locally satisfied (in a porewise sense) in spite of the fact they are open to transfers of magnetic moment with one another. The former case is expected, for example, in porous media that exhibit large vesicles, i.e., near spherical cavities, whereas the latter should hold on structures in which throats subtend rather small areas compared to pore surfaces.

It is instructive to consider the last scenario in more detail. Assume a partition for a highly communicated pore structure, meeting the aforementioned characteristics, is given. The transport of nuclear magnetization through pore connections can then be thought of as an additional mechanism for relaxation in pores.

Because, by assumption, diffusion is fast on homogenizing local nuclear spins densities, **pore to pore exchange** must be dominated by differences in magnetization between immediately communicated pores. In NMR-relaxation experiments, however, all pores usually start from the same initial condition: Uniform magnetization. So, as surface-induced decay sets in, throats to smaller pores essentially act as relaxing areas, as long as a magnetization difference is maintained across them, because the balance of magnetic moment over such channels is negative.

Smaller pores decay faster than larger pores, provided relaxivity is about the same all over the medium. An equal number of molecules is, nonetheless, expected to cross either way a given pore connection, implying magnetization transport towards smaller pores is always in deficit. Finally, the same reasoning can be applied to the effect of communication to bigger pores to reach the exact opposite conclusion.

Overall, magnetization transfers among pores make spin moment survive for longer at more confined regions and vanish quicker on more open ones, even though the process invariably shifts, towards faster decays, the rate distribution the same pore structure would present in its absence[4]. These seeming contradictory statements point to the fact that, due to pore coupling, it is generally incorrect to associate occurring relaxation rates to specific pore sizes.

[4]For the sake of argument, it helps to think of an equivalent structure in which throats have all been sealed by placing planes across the connections.

Much like in the same way the normal frequencies of a coupled system of springs cannot be pinned down to specific elements of the system, the observed decay rates in connected pore structures refer to **modes of relaxation and exchange** that reflect the entire topology of pore communication. If exchange, on the other hand, is sufficiently weak, it is reasonable to assume mode decay rates as approximations to actual pore relaxations and once more Eq.(2.15) applies.

The extent to which diffusive coupling is important in the characterization of porous samples is often investigated by analyzing the signal decay produced by a given fluid at different temperatures[33,63]. Nuclear spin relaxation mechanisms are very weakly temperature dependent[1], whereas molecular diffusion steadily increases as fluids become warmer[95]. Then, rate distributions pertaining to the same structure can be compared and reasonable increases in dispersion or the emergence of new statistical modes as temperatures vary are interpreted as indicators that exchange is relevant. These tests, however, must take into consideration that, although surface-induced relaxation mechanisms are fairly temperature independent *per se*, the physiochemical condition of the agents that promote them may not necessarily be over the desired temperature range. Some temperature-related effects like desorption lead to decreases in surface relaxivity, but changes in oxidation state and coordination characteristics of paramagnetic sites may go either way and could be misinterpreted as pore coupling effects.

Exponential analysis

The determination of pore size distributions brings on the issue of exponential analysis.

Non-exponential decays are pervasive in NMR-relaxation studies. They appear in the lineshape characterization of solids[28] or in the estimation of reaction rates in chemical solutions[76]. But, in these and other similar theories, there is a definite underlying model which allows them to account for signal behavior in terms of just few parameters. Such an expedient is nearly always inexistent for NMR-relaxation in porous media.

Although multipool[119] and pore-coupled[25,75] models have been proposed, they generally work the other way around by rather justifying fit parameters on the models themselves. This becomes a serious problem in terms of characterization of particular systems, because exponential analysis is highly susceptible to noise and dependent on *a priori* information. In other words, several and quite distinct rate distributions

can reproduce a given decay profile under a specified tolerance[55] and, without prior knowledge, the selection for a particular form is patently arbitrary.

There are many pore structures, mostly synthetic, which are homogeneous enough, statistically speaking, to be well characterized in terms of exponential decays. Under the assumption of negligible pore exchange, this suggests diffusion effectively partitions the pore space into regions that have nearly the same size (surface-to-volume ratio) and relaxivity. Non-exponential behavior, on the other hand, is even more frequently observed in relaxation experiments on porous media. Then, two- or three-exponential decays have enough parametric flexibility to fit any data set reasonably well; even still, when evidence from other characterizations, like microscopy or X-ray computerized tomography, does not cut a clear picture of to what regions of pore space each of the fit decay components should correspond[24].

Another approach makes use of the large disparity between diffusion length scales and sample sizes to advance instead a probabilistic model for pore distributions[26,62], normally, continuous and determined by few parameters. Signals are then fit to the Laplace transform, i.e., the moment generating function of the chosen distribution.

These methods are appealing in the sense that they try to characterize pore structures according to some stochastic process and, indeed, would lead to interesting conceptual leaps on porous media characterization, provided the underlying processes could in fact be outlined and the distributions fit to the observed decays. Often, non-exponential behavior cannot be described by unimodal forms, which leads to experimenters assigning multiple distributions to a particular data set.

In view of these difficulties, it is not surprising that preferred method for exponential analysis of NMR relaxation signals has always been Laplace inversion, ideally, a modelless mathematical procedure.

Laplace inverted distributions have the benefit of being data-driven, but they are also generated by standard linear methods. This feature is really an advantage because it allows for straightforward formulations of the inversion problem that ensure uniqueness of solutions[6,7,19,52], whereas non-linear methods, besides demanding less convenient implementations in general, may introduce additional non-uniqueness issues to a problem already suffering from ambiguity[116].

On the other hand, Laplace inversions remain extremely susceptible to noise and, for that, algorithms inescapably need to enforce **regularization**. Regularizing refers to any rule or procedure capable of removing or minimizing instabilities that develop in inversions due to the presence of noise in data.

It is not impossible to reformulate a linear discrete inverse problem in minimal terms that ensure existence and uniqueness of solutions[6], however, without regularization, inversions so produced will be plainly numerical nonsense. The challenge with it is not so much in the fact it is essential but, rather, in choosing how much regularization a problem really needs. Too little of it introduces noise-related artifacts in the computed solution, but too much worsens data conformity and can considerably blur the inversion objective. Hence, finding the optimum balance is important for both producing reasonable solutions and better outlining the available information.

As a result, regularized Laplace inversions are universally broad; for the matter at hand, it becomes very hard to tell whether the computed dispersion is really associated with pore size heterogeneity or, simply, a product of regularization. Furthermore, finding the optimal regularizer is often considered a computationally expensive step and some methods may even fail to converge under inversion constraints[30]. Many workers then just skip it, what, in practice, turns regularization a biased and somewhat arbitrary procedure. Despite these concerns, inversions are amply used for pore size characterization and correlate well with other methods, most notably, mercury injection porosimetry[33,63].

1.1.2 Multidimensional experiments

A second class of relaxation experiments that have grown partially from the convenient aspects of Laplace inversion comprises multidimensional NMR correlation sequences.

Two-dimensional NMR spectroscopy is used to characterize chemical exchange in solutions since the 1970s[34]; the techniques work particularly well in cases in which reaction rates are slow compared to nuclear relaxation at each substance, but their resolution is attached to the magnitude of relative nuclear frequency shifts. Alternatively, it is possible to study exchange by employing quite similar protocols but whose resolution instead is based on heterogeneities of nuclear relaxation rates in the considered chemical system[72].

These analyses necessarily substitute the familiar 2D inverse Fourier transforms used in spectroscopy for the much more difficult 2D inverse Laplace transforms. Yet, as more robust implementations of the latter started to gain popularity[99], the methods found their way in into the classic pore-to-pore exchange paradigm and, from there, were used to demonstrate a more direct estimation of diffusive coupling effects

and coefficients[115]; to introduce new pore size characteristics (exchange distances)[78] and, ultimately, provided more thoroughness and flexibility to NMR characterizations of porous media with the options for several types of correlation studies ($T_1 - T_2$, $T_2 - T_2$, $D - T_2$)[103].

These experiments are particularly suitable for probing exchange effects. Beyond the standard correlation maps, they also allow for direct time-domain signatures of pore coupling[98,104], what can be an interesting by-pass to the inversion-related problems.

Notwithstanding their popularity, multidimensional experiments can be somewhat time-consuming and, in some cases, fail to provide any additional information over that already accessible by a complete set of 1D relaxation experiments[57,58]

1.2 Restricted Diffusion

Random processes have always occupied a position of interest in the basic understanding of NMR phenomena.

Because nuclear spins are typically so weakly coupled to other degrees of freedom and have a relatively slow dynamics, their behavior is to a good approximation only sensible to certain statistical characteristics of their environment. Accordingly, rotational and translational random walks are evoked to account for nuclear position variables in the very first theories of NMR relaxation in fluids[11] and solid solutions[110] and, apart from recent molecular dynamic computational approaches, remain to this day the only viable expedient to deal with NMR relaxation in real systems theoretically.

At a more macroscopic level, on the other hand, stochastic models of motion are also remarkably useful and just as essential for the description of NMR experiments. Measured signals are strongly affected by heterogeneities in the applied magnetic field; even more so in systems wherein nuclear spins are mobile and therefore can experience different fields in the course of an experiment. Though molecular motion is quite complex, its effects on NMR can be surprisingly well-explained by simple probabilistic models. For instance, spin-echoes[50], the difference between FID and

CPMG attenuation[23][5] and other similar phenomena are all accounted for in unconfined fluid samples by assuming particle displacement is statistically distributed as a Wiener process.

The Brownian motion picture is so successful in NMR that it has established on its own a paradigm for the experimental characterization of molecular **self-diffusion** in spite of the fact that a fluid molecule in actual motion does not satisfy the same basic conditions of a Brownian particle[4]. NMR measurements of self-diffusion coefficients are nevertheless very consistent and used to characterize molecular mobility since the 1950s.

Given the adequacy of this description, it is no surprise that approaches to the same problem via diffusion equations work just as well; what can be more physically appealing because, though both views are equivalent[94], diffusion conceptually adheres to general framework of non-equilibrium thermodynamics and, for that fact, the resulting macroscopic model can be seen as somewhat independent of microscopic considerations.

Diffusion of nuclear magnetization is associated with the name of Torrey[111]. He was the first to identify the general applicability of the model and, apparently, it was also him who first extended the balance of nuclear magnetic moment to the walls of a confining structure in order to produce a general boundary condition[112]. Similar equations had been previously advanced by other researchers, like Bloembergen and Bloch, however, their derivations are rather *ad hoc* compared to Torrey's.

In any case, before pulsed field gradient (PFG) sequences were proposed, studies of diffusion via NMR remained mainly concerned with the effects of transport on NMR signal decay or with the determination of diffusion coefficients of pure substances[43]. Spin-echo attenuation is sensible to field heterogeneities and, under the assumption of unrestricted (Gaussian) diffusion, the first echo amplitude is determined by

$$E(t) = \exp\left[-\frac{t}{\mathrm{T}_2} - D_0\gamma^2|\boldsymbol{g}|^2\frac{t^3}{12}\right], \tag{1.3}$$

wherein $|\boldsymbol{g}|$ is the magnitude of the applied gradient and D_0 and γ denote respectively

[5]The Free Induction Decay and Carr-Purcell-Meiboom-Gill signals are staples on NMR practice. The former is simply the signal produced after an excitation pulse and the latter comprises a digitized sequence of spin echoes following a particular train of dephasing and refocalization periods. FID attenuation is strongly affected by external field heterogeneities; so much that FID can be used to characterize it. The CPMG sequence on the other hand was devised to correct for this effect and so provides a better characterization of nuclear relaxation proper.

the bulk diffusion coefficient and the gyromagnetic ratio of the spin-bearing nuclei.

The effects of confinement in the characterization of diffusion itself appear for the first time in the work of Woessner[117], who interpreted echo attenuation of fluids undergoing restricted diffusion in several porous media by Eq.(1.3). The **apparent diffusion coefficients** measured are in fact functions of the parameters of acquisition: They explicitly depend on echo time. In other words, the attenuation exponent does not show the cubic time behavior implied by Gaussian diffusion when fluids are confined to a porous structure. Shortly after, Robertson[87] showed that Eq.(1.3) is only asymptotically correct over times much smaller than the characteristic time of diffusion, L^2/D_0, for spins confined to a region between two infinite parallel planes, orthogonal to the applied field and separated by a distance L. Yet, the attenuation factor becomes a simple exponential decay at long times ($D_0 t \gg L^2$) and is approximately given by

$$E(t) = \exp\left[-\gamma^2 |\boldsymbol{g}|^2 L^4 \frac{t}{120 D_0}\right]. \tag{1.4}$$

This strong separation dependence points to the fact diffusion techniques can also provide relevant information on the geometrical features of a pore structure, complementary to the characterization of relaxation methods.

1.2.1 Pulsed Field Gradient Sequences

The ubiquity of non-Gaussian behavior in systems undergoing restricted diffusion became evident after PFG sequences were introduced[107]. There are many variant implementations of these sequences[106] designed to improve signal quality or correct particular features, like the influence of magnetic field heterogeneities due to susceptibility contrasts[69], but they are all equivalent in the sense that, ideally, their signal is determined by

$$E_{\boldsymbol{q}}(t) = \frac{1}{V} \int_\Omega \mathrm{d}^3 \boldsymbol{X} \int_\Omega \mathrm{d}^3 \boldsymbol{X}_0 \, G_t(\boldsymbol{X}, \boldsymbol{X}_0) e^{i\boldsymbol{q}\cdot(\boldsymbol{X}-\boldsymbol{X}_0)}, \tag{1.5}$$

wherein $G_t(\boldsymbol{X}, \boldsymbol{X}_0)$ is the associated **diffusion propagator** (Green function) to the underlying diffusion problem and $\boldsymbol{q}$ is an experimentally controllable parameter proportional to the externally applied field gradient. Gaussian behavior in this case is identified by a simple exponential decay of rate $D|\boldsymbol{q}|^2$; this feature makes deviations from Gaussian behavior particularly easy to spot.

A great example of non-Gaussian behavior is manifested by the long time asymptotics of restricted diffusion.

Whenever surface-induced relaxation is negligible, the propagator on bounded regions tends to an uniform distribution at long times, and therefore Eq.(1.5) reduces to the squared amplitude of the form-factor of the porous medium,

$$E_{\boldsymbol{q}}(t \to \infty) = \left| \frac{1}{V} \int_{\Omega} \mathrm{d}^3 \boldsymbol{X}\, e^{i\boldsymbol{q}\cdot\boldsymbol{X}} \right|^2 . \tag{1.6}$$

In this case, signal amplitude becomes virtually time independent but is expected to oscillate with $\boldsymbol{q}$ and the location of extrema can be used to estimate the characteristic length scale of the structure. Although this diffraction-like behavior was already realized by Stejskal[108] while exploiting the theoretical implications of PFG in simple confining structures, experimental observation of the effect was originally made by Callaghan *et al.*[21] on a monodisperse packing of micrometric spheres saturated by water. In practice, the use of diffusion-diffraction patterns for the characterization of porous media is limited to structures that exhibit some degree of order. In disordered media, oscillations in various length scales interfere with one another, making identification particularly challenging[46].

Alternative (asymmetrical) PFG sequences have been rather recently proposed to measure both amplitude and phase of the form-factor[71]; such a procedure in principle eliminates the process of length scale identification altogether since, through exhaustive acquisition, the indicator function of the porous structure becomes accessible.

All PFG sequences have one basic structure: The prototypical temporal profile, shown below, comprises three time intervals,

$$\underbrace{\frac{\pi}{2}\text{——}t_e\text{——}}_{\text{I}}\underbrace{\frac{\pi}{2}\text{————}t\text{————}}_{\text{II}}\underbrace{\frac{\pi}{2}\text{——}t_d\text{——}}_{\text{III}}\text{Acq.}$$

The first period is called **encoding**, normally starts from spin equilibrium and consists of an excitation pulse ($\pi/2$-pulse) followed by some procedure. In the original PFG sequence[107], for instance, a single gradient pulse is applied at this stage to encode spin positions. However, general protocols can involve several blocks of rephasing field pulses (π-pulses) in between gradient pulses of alternating polarity in order to minimize the influence of intrinsic field heterogeneities. These corrections be-

come really necessary in porous media studies when susceptibility contrasts between fluid and solid framework are sufficiently large[54].

In the second stage, the transverse magnetization is **stored** over the longitudinal axis and spins are allowed to diffuse over a time t, free from the influence of magnetic fields. This stage has also the benefit of reducing the relaxation rate to which nuclear magnetization is subjected as it effectively switches between transverse and longitudinal modes of relaxation.

The third and last time interval is where **decoding** happens. In symmetric implementations, an excitation pulse is used to bring the magnetization back to the transverse plane and an identical procedure to the one employed at encoding follows. By an appropriate choice of pulse phases in the whole sequence, nuclear spins effectively perceive this new stage *in reverse*; a stimulated echo builds up and its amplitude can be measured. Asymmetrical sequences have distinct encoding and decoding procedures. Pulses can be made relatively weaker and longer in one of the stages, nevertheless, in such a way that rephasing still occurs.

Narrow pulse approximation

The tacit assumptions of PFG-based studies is that encoding and decoding periods, t_e and t_d respectively, are sufficiently short in order that diffusion can be entirely neglected over these stages and, moreover, dephasing is much more efficiently imposed by the externally applied gradients than internal field heterogeneities. Combined, the two conditions constitute the basis of the so-called **narrow pulse approximation** (NPA), which formally corresponds to the limit $t_e \longrightarrow 0$ and $\boldsymbol{g} \longrightarrow \infty$ in such a way that $\gamma \boldsymbol{g} t_e \longrightarrow \boldsymbol{q}$.

Because of the NPA, the PFG signal, namely, the amplitude of the stimulated echoes is simply written in terms of the Fourier transform of the diffusion propagator. Such an explicit and simple expression like Eq.(1.5) is unique to PFG sequences and it follows directly from the NPA.

Time-dependent diffusion coefficients

One the most remarkable features of PFG sequences is that they allow for experimental observation of the displacement correlations of nuclei undergoing diffusion. It

follows from direct derivation of Eq.(1.5) that

$$\langle (\boldsymbol{X}_t - \boldsymbol{X}_0)_i (\boldsymbol{X}_t - \boldsymbol{X}_0)_j \rangle = - \lim_{\boldsymbol{q} \to 0} \frac{\partial^2}{\partial q_i \partial q_j} \ln E_{\boldsymbol{q}}(t). \tag{1.7}$$

Monitoring correlations in the case of restricted diffusion can reveal several geometric characteristics of the confining medium.

The short-time asymptotics of the mean squared displacement (MSD) allows for a separate measurement of surface-to-volume ratios[80], which, in turn, can be used for direct estimation of surface relaxivities and, equivalently, conversion of rate distributions into pore size distributions[54]. Time-dependent diffusion coefficients are operationally defined through Einstein's diffusion relation, namely,

$$D(t) \equiv \frac{\langle |\boldsymbol{X}_t - \boldsymbol{X}_0|^2 \rangle}{6t}. \tag{1.8}$$

A quite famous formula relates the short-time asymptotic behavior of $D(t)$ with the surface-to-volume of a porous structure,

$$\frac{D(t)}{D_0} = 1 - \frac{4}{9\sqrt{\pi}} \frac{S}{V} \sqrt{D_0 t} + \mathcal{O}\left(D_0 t\right). \tag{1.9}$$

Furthermore, higher order terms provide global properties like mean curvature of grains[80] and in-plane connectivity for tube-like structures[59].

Conversely, the long-time behavior of correlations reveals information about transport anisotropy, topology and conductive characteristics of the pore structure[92]. The long-time behavior of MSD, for instance, varies dramatically depending on the general connectivity of a pore structure. In isolated pores, the diffusion propagator tends to an uniform distribution, so, any position correlation approaches a definite constant related to the characteristic pore size of the medium. In connected structures, on the other hand, mean squared displacements develop a sort of Gaussian character as time becomes sufficiently large in the sense that they again become nearly proportional to t. The ratio between unrestricted and long-time MSD or, equivalently, the ratio of corresponding diffusion coefficients defines the **diffusive tortuosity** of the medium,

$$\frac{1}{\tau_D} \equiv \lim_{t \to \infty} \frac{D(t)}{D_0}. \tag{1.10}$$

Tortuosity is a concept to which has been given considerable attention in porous

media studies concerned with transport phenomena. It originally appeared in the context of fluid flow to account for the effect of streamline sinuosity in flow permeability, but, since then, has been employed to identify fractal and percolation features and to explain effective DC electrical conductivities and diffusion[40]. Tremendous effort has been placed on unifying these distinct characterizations notwithstanding the fact tortuosity cannot be a definite medium property as it originates from path averaging procedures that may be specific to the type of flow, conduction or transport process considered. With that said, it is known that electrical conductive and diffusive tortuosities become identical provided a purely reflective boundary condition applies in both underlying diffusion problems[91].

From an experimental standpoint, the observation of the so-called tortuosity limit in PFG studies is hindered by both bulk and surface-induced NMR-relaxation processes. In typical liquid substances, diffusing molecules move relatively small distances before their nuclear magnetization decays completely, as a result, diffusion studies will generally fail to probe long multipore length scales unless they fall below the diffusion bound imposed by the experiment. Two alternatives have been proposed to remedy this situation: Noble gas NMR-diffusion studies can satisfactory complement liquid studies as gases exhibit comparatively large diffusion coefficients, have bulk relaxation rates an entire order of magnitude lower and interact poorly with paramagnetic surface sites[74]; also, singlet-assisted NMR diffusion techniques enable an enormous increase in observed MSD by probing instead singlet nuclear states, which exhibit remarkable minute-long relaxation times[113], developed on specific, though liquid solutions. The gas diffusion method is simpler in the sense that it employs the same PFG sequences used in liquid-based studies but, incidentally, it is not much successful for probing short-time behavior due to violation of the NPA, presents some natural difficulties associated with sample preparation and produces signals with a lower signal-to-noise ratio because of poor thermal spin polarization. Singlet-assisted experiments, in turn, can be used to observe the entire time range of diffusive behavior, however, require the use of special molecules and quite involved PFG variants in order to prepare and read singlet states.

1.2.2 Beyond the NPA

Vanishingly narrow and infinitely high pulses are obviously abstractions beyond any experimenter's capacity. In practice, pulse durations can be as long as in the

tens of milliseconds and gradient intensities peak below 1000 Gauss/cm in most apparatuses and it is usually difficult to assert whether the NPA limit provides a good approximation to a particular sequence set-up. NPA violation can be a serious problem in characterizing porous media via PFG methods, for finite-width pulses can effectively alter the observed pore geometry: Isolated pores appear smaller and, in connected pore spaces, the distinction between pore and solid framework is progressively blurred as pulse duration increases[79].

On the other hand, there are several other experimental strategies that explicitly involve a diffusion component but cannot benefit whatsoever from the NPA. Yet, relevant information can be extracted from them. Notable examples are Hanh's echo sequence, which, as discussed, was amply used to study diffusion effects before PFG sequences were invented, and the famous CPMG, although immediately associated with relaxation studies[3].

Issues like these have prompted more general formulations of the echo amplitude relation to spin diffusion to account for arbitrary field gradient profiles[3,20,43]. The approaches are, nevertheless, equivalent and all founded on the idea that, under an inhomogeneous field, a moving spin accumulates a phase that depends both on the spatial configuration of the field and on its path. Namely,

$$\varphi_t = \gamma \int_0^t \mathrm{d}\, t' B(\boldsymbol{X}_{t'}, t'), \tag{1.11}$$

wherein B denotes only the longitudinal component of the applied field.

Accordingly, in the course of an experiment, every nucleus picks up a phase factor determined by $e^{-i\varphi_t}$. The total transverse magnetic moment of the sample, or equivalently, the measured signal is defined by the sum of all such contributions over the entire ensemble of diffusing nuclei, which, in typical conditions, is so large that one can safely assume to be sampling over all possible realizations of the spin phase process itself. Thus,

$$E(t) = \left\langle e^{-i\varphi_t} \right\rangle, \tag{1.12}$$

assuming the signal is normalized to unity and discounting relaxation effects.

The Gaussian paradigm

Whenever the underlying diffusion process, X_t, is normally distributed, as in the case of unrestricted diffusion, the spin phase, defined by Eq.(1.11), is also a Gaussian

variable[84]. Therefore

$$E(t) = \exp\left[-\frac{\langle\varphi_t^2\rangle}{2}\right], \tag{1.13}$$

provided $\langle\varphi_t\rangle = 0$, a satisfied condition in the set-up of most experiments. Furthermore, if the **phase encoding** is mainly done by externally applied linear gradients, then

$$\langle\varphi_t^2\rangle = \gamma^2 \sum_{ij} g_i g_j \int_0^t \mathrm{d}\, t_1 \int_0^t \mathrm{d}\, t_2 f(t_1) f(t_2) \langle X_{t_1,i} X_{t_2,j}\rangle . \tag{1.14}$$

wherein $f(t)$ denotes the gradient modulation profile. Making use of Einstein-Smoluchowski equation, $\langle X_{t_1,i} X_{t_2,j}\rangle = 2D_0\delta_{ij}\min(t_1,t_2)$, it is possible to define the so-called **b-value of the sequence**

$$b(t) = 2\gamma^2|\boldsymbol{g}|^2 \int_0^t \mathrm{d}\, t_2 \int_0^{t_2} \mathrm{d}\, t_1 f(t_2) f(t_1) t_1, \tag{1.15}$$

and to rewrite $E(t) = e^{-D_0 b(t)}$.

The Gaussian phase approximation (GPA)

A direct result of the above is that Gaussian behavior can be identified in arbitrary systems simply as mono-exponential decays with b-values. However, notice that the normal character now refers to the spin phase behavior rather than the diffusion process of nuclei. Given its definition, Eq.(1.11), the phase process must appear normally distributed whenever the underlying process, $\boldsymbol{X}_t$, is in fact or approximately Gaussian, or when t is so long that it is possible to define φ_t as a large sum of statistically independent phase increments and evoke the central limit theorem. Such reasoning suggests that, in cases of restricted diffusion, a Gaussian phase approximation (GPA) for the spin phase seems to be valid at both short and long diffusion times[3], yet for quite different reasons. If $D_0 t \ll L^2$, then very few nuclei reach the boundaries of the pore structure to be affected by it. So for most of particles the diffusion seems unrestricted and, thus, the process seems almost normal. On the other hand, if $D_0 t \gg L^2$, it is reasonable to assume that particle trajectories over sufficiently long time subintervals are uncorrelated and identically distributed, provided the porous medium is somewhat statistically uniform. Because in the latter case MSD tend to be shorter relative to unrestricted MSD calculated over the same period, the diffusion coefficients observed at long times are smaller. Whatever the case, apparent diffusion

coefficients (ADC) can be operationally defined by

$$\mathcal{D}(t) = -\frac{\ln E(t)}{b(t)}, \tag{1.16}$$

in order to monitor Gaussian regimes.

These ideas are fairly general in the sense that they apply regardless of gradient strength. A different argument that is frequently used to justify the GPA is the assumption of **weak encoding**[46].

If field gradients are weak to the point that φ_t does not grow beyond a small bound over the entire duration of an experiment, then high order statistical moments in the expansion of Eq.(1.12) can be neglected to yield

$$\begin{aligned} E(t) = \left\langle e^{-i\varphi_t} \right\rangle &= 1 - \frac{\langle \varphi_t^2 \rangle}{2!} + \frac{\langle \varphi_t^4 \rangle}{4!} - ... \\ &\approx 1 - \frac{\langle \varphi_t^2 \rangle}{2!} \approx \exp\left[-\frac{\langle \varphi_t^2 \rangle}{2} \right], \end{aligned} \tag{1.17}$$

assuming the odd-order moments all vanish. Together with Eq.(1.16), this result enables the definition of ADC for arbitrary sequences in the limit of vanishing b-values ($\boldsymbol{g} \longrightarrow 0$).

The GPA effectively reduces the generally intractable problem of determining the characteristic function of the spin phase process to the determination of its second moment. It is important to point out that ADC explicitly depend on the temporal profile of the sequences used and on the direction of applied gradients but not on their magnitudes. Consequently, they are not the same as time-dependent diffusion coefficients, which are formal reinterpretations of actual MSD, but have the advantage of being directly related to measured output. Retrospectively, real PFG sequences can only produce apparent diffusion coefficients as well; the identification of ADC and time-dependent diffusion coefficients in this cases is enforced by the NPA.

1.2.3 Internal field encoding

Magnetic field inhomogeneities are ubiquitous in NMR practice. They can originate from intrinsic set-up characteristics, like magnet design, or occur as a result of magnetic susceptibility contrasts present in the considered sample. To some extent **internal fields**, that is, intrinsic deviations from field homogeneity can be mitigated through the use shimming coils. But, in any case, there is always a residual field

whose influence on experimental results cannot be ignored.

Because all measurements in NMR are primarily based on spin phase coherence, internal fields promote **dephasing** and, consequently, signal decay is accelerated relative to the *true* rate of decoherence imposed by microscopic mechanisms. In the NMR jargon, this fact is usually summarized as $T_2^* \leq T_2$, in which T_2^* is a characteristic time scale of free induction decays (FID). Dephasing can make experimental determination of the transverse relaxation characteristics particularly challenging in systems for which internal field configuration is complex, as in the case of fluid saturated porous samples wherein the field structure reflects in a non-trivial manner the intricate geometry of pore space, as well magnetic properties of the materials. Yet, it can be used to encode, in principle, nuclear spin positions as well, only now in a completely different way than how is done by externally applied uniform gradients.

It is instructive to consider the ideal scenario in which spin phase is encoded instantaneously, akin to that of PFG sequences in the NPA limit, so the phase is directly proportional to the value of the field at a given position. Then, internal field encoding should assign the same **label** to spins momentarily positioned along an isovalue surface of the internal field, which is expected to somehow accompany domain geometry. Thus, instead of referring to definite positions on the sample, encoded phases carry only a sort of rough information on relative location. For example, if for a given pore structure the internal field is found to vary in magnitude more predominantly *across pores* rather than *within pores*, then internal field encoding could be useful in the study of diffusive transport among pores provided the scale of field variation is compatible with that of pore communication. Conversely, if internal field variations occur primarily within pores and are dependent on geometric features like pore shape or size, internal field encoding could provide information about these attributes, as long diffusion across pores can be neglected.

As it turns out, computer simulations indicate that the latter situation is likely the rule[101] and one the first applications of internal field encoding was suggested precisely with the intent of pore size characterization, a reliable alternative to pore size distributions based on NMR relaxation techniques[73,102]. The Decay due to Diffusion in Internal Field (DDIF) method remains as one of the few internal field encoding protocols to have ever been proposed, but now there seems to be considerable room for research in this area given the increasing availability of geometric representations of actual pore structures, as those produced by micro-X-ray computerized tomography. Computer simulation of diffusive transport and internal field encoding on

such domains may ultimately provide a general understanding of the processes and substantiate more informing data interpretations at the macroscopic level.

1.3 Outline of the thesis

Following this brief introduction, the remainder of the text is organized in three chapters.

Chapter 2 deals with the basic theory of nuclear magnetic diffusion and the general approach to the solution of problems introduced by such a theory. Many of the concepts and results here visited are there properly derived and, though the exposition is chiefly theoretical, experimental and computational ramifications are constantly brought forward where their pertinence is justified. This chapter comprises a more **in-depth revision** of the relevant bibliography, particularly, of the multiple correlation function method (MCF), systematically consolidated by Sen and co-workers and, independently, by Grebenkov[43], and of the GPA and the NPA. Nevertheless, the author believes some derivations are original, when not in content, at least in approach or view. The somewhat Einsteinian standpoint on the derivation of full Bloch-Torrey equation and relevant boundary conditions, the exact solution via the MCF method for the case of unrestricted diffusion under an uniform field gradient modulated by arbitrary temporal profile and the more direct derivation of the short-time asymptotics of time-dependent diffusion coefficients are all examples of modest, yet, original perspectives.

A microscopic model explaining the surface-induced relaxation is developed on Chapter 3. There the concept of active surface elements is introduced and it is seen that, although these elements may be all equivalent on the considered boundary, surface relaxivity is not generally the same all over it because of a dependence on inclination of active elements in respect to the external field. A high field theory is presented first, being the easier case, but a more general one is proposed in sequence, wherein it is postulated that local crystalline order plays a part on the electron-nucleus spin interaction. NMR relaxation is then analyzed for model porous samples in the light of the presented model under the assumption of fast diffusion. The findings are ultimately put to experimental test, employing natural and artificial porous systems having sufficient features to confirm or refute them. Finally, the fundamental aspects of the theory are revisited and its weak and strong points are discussed.

At last, on Chapter 4, the DDIF method is presented and discussed under the as-

sumption of narrow field modulations and weak encoding. The information provided by the technique is analyzed within the framework of Laplace operator eigenstructures. The discussion is considered instructive as it highlights the principal difficulties on interpretation of results. A slight variation of the method is proposed and it is shown that it can be used to observe experimentally the autocorrelation function of the internal magnetic field, seen as a stochastic process induced by particle diffusion. It is argued that the proposed modulated internal field (MIF) protocol has considerable advantage over traditional DDIF methods as its products are better suited for the data processing procedures and constraints that are usually employed and because it allows direct verification of encoding regimes, which is vital for a sound interpretation of results. The protocol is tested on relatively simple pore structures and results are presented and thoroughly discussed. Finally, the chapter ends with a brief discussion of what needs and remains to be done in order to understand better the characterization provided by such techniques.

Familiarity with many basic topics in nuclear magnetic resonance is assumed and, consequently, not discussed beyond the minimum necessary for a coherent exposition. An important tacit assumption, made in all subsequent chapters, is worth mention: Bloch equations adequately describe the intrinsic NMR relaxation of the saturating fluid in the systems under consideration. Once most applications of NMR in the geometric characterization of porous media are based on probing hydrogen nuclei associated to liquid phases, this is justified.

Finally, a couple of appendices follow the main text. There some peripheral discussions or expositions take place for the benefit of the reader. It is presented how the theoretical concept of effective temporal profile relates to the common experimental procedure of RF pulse phase cycling. Some general aspects of the statistical characterization of stochastic processes are presented very briefly and the normal process is used as an important illustration. A general (and surprisingly yet unpublished) representation for Robin diffusion propagators is derived and a more in-depth discussion of the magnetic interactions that promote NMR relaxation near boundary wall is given.

CHAPTER 2

Restricted Nuclear Spin Diffusion

Bloch equations constitute the elementary paradigm for describing nuclear magnetic resonance[1,28,96]:

$$\begin{aligned} \dot{m}_x &= \gamma(\boldsymbol{m} \times \boldsymbol{B})_x - \frac{m_x}{\mathrm{T}_2}, \\ \dot{m}_y &= \gamma(\boldsymbol{m} \times \boldsymbol{B})_y - \frac{m_y}{\mathrm{T}_2}, \\ \dot{m}_z &= \gamma(\boldsymbol{m} \times \boldsymbol{B})_z + \frac{m_0 - m_z}{\mathrm{T}_1}. \end{aligned} \tag{2.1}$$

The z-component is distinguished by the fact that, in the prototypical NMR set-up, the sample is always under the influence of an external static magnetic field whose direction is used to define the longitudinal axis of the coordinate system. Left alone, the system ultimately develops an equilibrium magnetic moment, m_0, parallel to $\boldsymbol{B}_0$.

A major idea behind this model is that changes of nuclear magnetic moment are governed by the torques magnetic fields of both macroscopic and microscopic origin exert on nuclear spins. These influences are, nevertheless, differentiated at the coarse-grained description level of Eq.(2.1) due to the natural smoothing associated with macroscopic observations. Hence, it is instructive to look at local magnetic fields as a sort of random superposition of harmonic components. Microscopic contributions are imagined to vary rapidly and throughout the spin system but most of these high-frequency fluctuations have a negligible effect on spin dynamics because of its resonant

character. On the other hand, it so happens that fields may exhibit some weak spectral component precisely at the Larmor frequency of the considered nuclei. Such resonant fluctuations can efficiently nutate nuclear magnetic moments if they occur **perpendicular** to the static field, thus functioning as a mechanism for relaxation to equilibrium.

Bloch[9] even anticipated that, while the resonant nutations interfere simultaneously with transverse and longitudinal spin components (the interchange of transverse and longitudinal moments promoted by them being in fact essential for maintaining a nuclear magnetization at equilibrium), the **coherence** of the spin system is additionally affected by local field fluctuations at zero frequency that happen **parallel** to $\boldsymbol{B}_0$, once these, in effect, lead to a heterogeneity of Larmor precession frequencies at the microscopic level. This is why, generally, $\mathrm{T}_2 \leq \mathrm{T}_1$.

The perspective that ensues from such separation of scales is that the contribution of microscopic magnetic fields to the overall balance of nuclear magnetic moment in a homogeneous medium simply amounts to relaxation terms that somehow characterize the microscopic spin environment.

The phenomenological picture introduced by Bloch equations, however, is not complete, for it so happens that truly homogeneous magnetic fields are nothing more than theoretical abstractions; in practice, fields can be made less and less inhomogeneous as it is desired but some degree of heterogeneity is unavoidable. Then, Eq.(2.1) still apply on a local level, provided the spin-bearing particles do not move beyond the scale of field heterogeneity. But if not, transfers of **nuclear magnetization** between different portions of the sample must be incorporated to the balance of magnetic moment.

An easy way to correct for the effect, at least formally, is to add a flux contribution to the global balance of a region. Namely,

$$\frac{\mathrm{d}}{\mathrm{d}t}\int_\Omega \mathrm{d}^3\boldsymbol{X}\, m_i = \int_\Omega \mathrm{d}^3\boldsymbol{X}\, \left[\gamma(\boldsymbol{m}\times\boldsymbol{B})_i - \frac{m_i}{\mathrm{T}_i}\right] - \int_{\partial\Omega} \mathrm{d}S\, (\boldsymbol{J}_i\cdot\boldsymbol{n}) \tag{2.2}$$

wherein the explicit position dependence of magnetization and field variables is omitted for the sake of notation simplicity; m_i is used to denote either m_x, m_y or $m_z - m_0$ and $\boldsymbol{J}_i$, the corresponding magnetization fluxes. By convention, magnetic moment increases within a region when fluxes are inward.

Since the above balance holds for arbitrary regions of the sample, localization

follows,

$$\frac{\partial m_i}{\partial t} = \gamma(\boldsymbol{m} \times \boldsymbol{B})_i - \frac{m_i}{\mathrm{T}_i} - \nabla \cdot \boldsymbol{J}_i, \tag{2.3}$$

and all that is left to completely determine the continuity of nuclear magnetic moment is a **flux law**. If, for example, the substance under consideration is a fluid under flow, convection of nuclear magnetization can be accounted for by means of a simple relation like $\boldsymbol{J}_i = m_i \boldsymbol{u}$, in which $\boldsymbol{u}$ denotes the fluid's velocity field.

The ubiquitous process of nuclear magnetization transport that has tremendous impact on NMR applications is, however, **diffusion**.

Diffusive transfers occur in liquids and gases due to thermal molecular agitation, but also in solids by various mechanisms such as solute transport or spin-direction exchange. There are several approaches in modeling diffusion effects: Phenomenological[5,8,16,44,111], probabilistic[77,93,94] and even sort of first-principle formulations[109]. They are all equivalent in the sense they all incorporate at some stage the idea, first introduced by Einstein in the context of Brownian motion[86], that diffusive transport follows simply from property heterogeneity and some underlying stochastic motion. Accordingly, changes in spin magnetization due to diffusion accompany the statistical structure of displacements of spin-bearing particles on the considered medium. This introduces the concept of a **diffusion propagator**, $G_\tau(\boldsymbol{X}, \boldsymbol{X}_0)$, as the probability density function of a particle originally located at a point $\boldsymbol{X}_0$ to be moved to point $\boldsymbol{X}$ after a time τ. Then,

$$\nabla \cdot \boldsymbol{J}_i \equiv -\lim_{\tau \to 0} \int \mathrm{d}^3 \boldsymbol{X}_0 \, G_\tau(\boldsymbol{X}, \boldsymbol{X}_0) \left(\frac{m_i(\boldsymbol{X}_0, t) - m_i(\boldsymbol{X}, t)}{\tau} \right). \tag{2.4}$$

It is instructive to discuss some aspects of each term in the right-hand side of the definition. First, notice that the propagator does not show an explicit dependence on the t, the instant in which displacements occur; this reflects the assumption G_τ describes a statistical character of equilibrium. In other words, that the underlying particle motion presents the same mean characteristics irrespective of the time of observation. By separating the integrals, it is possible to check that the first one amounts to the spin magnetic moment that is transported by diffusion into the vicinity of $\boldsymbol{X}$ after τ, whereas the second one is merely a convenient way to describe the magnetic moment that was already there and it follows from the fact that, over any sufficiently long period, particle displacement to any small region must be a sure event, i.e., one of unity probability. Therefore, Eq.(2.4) simply establishes that the flux of nuclear

magnetic moment is locally defined by the rate of change of nuclear magnetization due to diffusive transport. Because of the flux sign convention, divergences must be negative when transport induces magnetic moment increase and so the minus sign is explained.

Now, provided the magnetization field is smooth all over the medium, it is possible to use Taylor expansion to rewrite the above flux law in a more fitting way for analysis

$$\nabla \cdot \boldsymbol{J}_i = \boldsymbol{u} \cdot \nabla m_i - \sum_{jk} D_{jk} \frac{\partial^2 m_i}{\partial X_j \partial X_k} + \dots , \tag{2.5}$$

wherein

$$\boldsymbol{u}(\boldsymbol{X}) = \lim_{\tau \to 0} \int \mathrm{d}^3 \boldsymbol{X}_0 \, \frac{G_\tau(\boldsymbol{X}, \boldsymbol{X}_0)}{\tau} \left(\boldsymbol{X} - \boldsymbol{X}_0 \right) , \tag{2.6a}$$

$$D_{jk}(\boldsymbol{X}) = \lim_{\tau \to 0} \int \mathrm{d}^3 \boldsymbol{X}_0 \, \frac{G_\tau(\boldsymbol{X}, \boldsymbol{X}_0)}{2!\tau} \left(\boldsymbol{X} - \boldsymbol{X}_0 \right)_j \left(\boldsymbol{X} - \boldsymbol{X}_0 \right)_k , \tag{2.6b}$$

with coefficients related to higher order terms being similarly defined. The $\boldsymbol{u}$ and D_{jk} respectively correspond to the **drift** and **diffusion** tensors. Symmetry conditions can be used to reduce the number of coefficients. In fluids, for example, $G_\tau(\boldsymbol{X}, \boldsymbol{X}_0)$ is usually assumed to be translationally invariant and isotropic, implying a zero drift field and an uniform and isotropic diffusion tensor. In this case, it follows that

$$\boldsymbol{J}_i = -D_0 \nabla m_i \tag{2.7}$$

is the simplest flux law compatible with Eq.(2.5), with

$$D_0 = \lim_{\tau \to 0} \int \mathrm{d}^3 \boldsymbol{X}_0 \, \frac{G_\tau(\boldsymbol{X}, \boldsymbol{X}_0)}{6\tau} \left| \boldsymbol{X} - \boldsymbol{X}_0 \right|^2 , \tag{2.8}$$

provided neglect of higher order terms is reasonable[1].

Finally, Eq.(2.4) can be incorporated to the local balance of nuclear magnetization described by Eq.(2.3) to yield

$$\frac{\partial m_i}{\partial t} = \gamma (\boldsymbol{m} \times \boldsymbol{B})_i - \frac{m_i}{\mathrm{T}_i} + D_0 \nabla^2 m_i . \tag{2.9}$$

[1] As it turns out, diffusion is either simple in the above sense or amazingly complex, meaning that the diffusion flux law must necessarily include infinitely many higher order contributions to ensure some basic diffusive features like absence of transport in the absence of property heterogeneity [85].

2.1 The Bloch-Torrey equation

In principle, the result of any experimental protocol can be calculated by solving Eq.(2.9) under suitable initial and boundary conditions. A specific spatial configuration and temporal profile of the externally applied field jointly set up what is in practice called a NMR sequence. Therefore $\boldsymbol{B}(\boldsymbol{X}, t)$ is everywhere and at all times defined. On the other hand, closed-form solutions for arbitrary sequences are incredibly difficult to obtain and so it is instructive to consider a more piecewise approach to general problems.

Every NMR sequence comprises some basic elements: Field and field-gradient pulses, idle times, acquisition windows, phase cycling. And recognizing the structure of these elements is essential to find when and how particular approximations apply.

For instance, field pulses are typically so short that both relaxation and diffusive transport can be entirely neglected over their duration. As a result, nuclear magnetization simply rotates about the direction of $\boldsymbol{B}$ with an angular frequency defined by $\gamma|\boldsymbol{B}|$. This effect is useful to excite the nuclear spin system, that is, to remove it from equilibrium and to interchange nuclear magnetization among components. Moreover, spin nutation can only be effectively performed by field pulses that introduce a (albeit weak) transverse field component that oscillates with the Larmor frequency of the considered nuclei: This is in fact the resonant phenomenon associated with pulsed NMR. The phase of oscillation is also important as it dictates to which direction the nuclear magnetization nutates relative to a frame of reference that rotates about the static field with frequency γB_0, the so-called **rotating frame** illustrated on Fig.2.1. Other than that, just the nutation angle is relevant from a theoretical standpoint. These considerations imply that field pulses can be considered vanishingly short and regarded in the analysis rather by their effects instead of their form.

A gradient pulse is the generic terminology for any process that introduces a momentary spatial heterogeneity in the resultant applied field, $\boldsymbol{B}$. Due to build constraints, poor calibration or even magnetic susceptibility contrasts within the sample, there is always a **static** magnetic field inhomogeneity added to the external field, $\boldsymbol{B}_0$, which can be considered the dominant or the spatially averaged field. These heterogeneities, though typically small, introduce clearly observable effects like quicker dephasing of the spin system. As it turns out, it can be considerably advantageous to further enhance and modulate such effect through the use of gradient pulses, particularly, in studies concerned with diffusion. On the other hand, gradient pulse durations

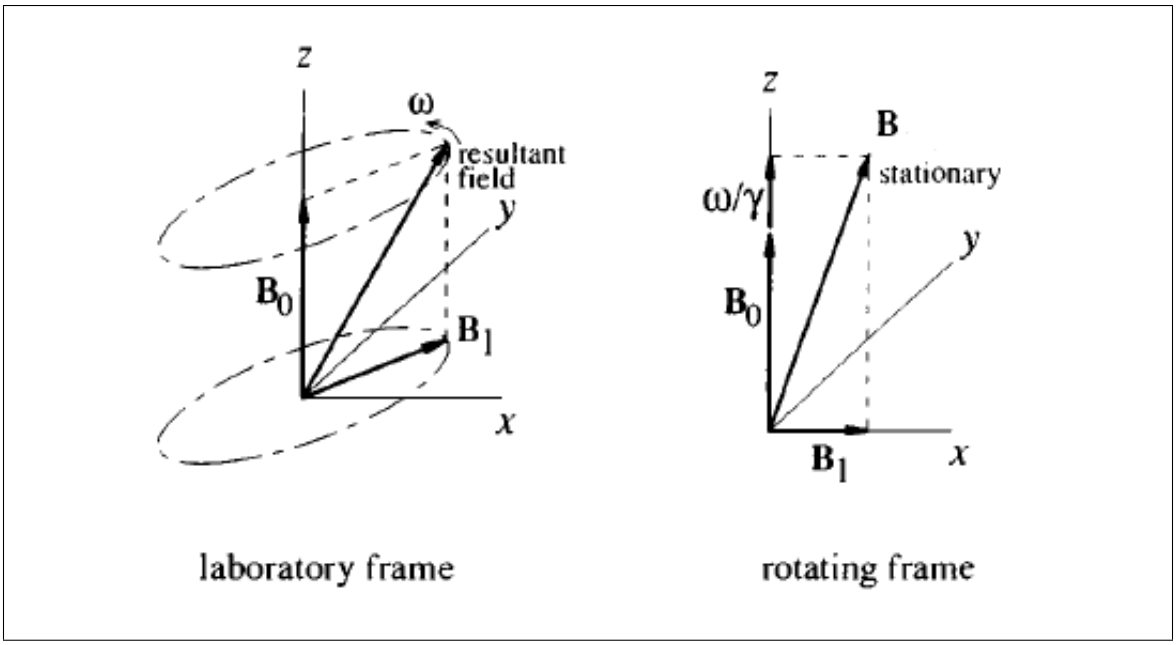

Figure 2.1: The difference from laboratory and rotating frames: The oscillating RF component is perceived as as a static field in the frame that rotates with the speed of oscillation (Extracted from Cowan[28])

may be sufficiently long for diffusive transport to become relevant over the intervening time; thus, it is not at first hand clear whether a similar approximation to the one used for field pulses applies. Incidentally, a narrow pulse approximation (NPA) is the cornerstone of the entire class of NMR protocols known as Pulsed Field-Gradient (PFG) sequences.

In any case, pulsed gradients and internal field heterogeneities[2] are usually small compared to $\boldsymbol{B}_0$ and this means that

$$\hat{\boldsymbol{B}} \cdot \hat{\boldsymbol{B}}_0 = 1 + \mathcal{O}\left(\frac{|\boldsymbol{b}|^2}{B_0^2}\right), \tag{2.10a}$$

$$|\boldsymbol{B}| = B_0 + b_z + \mathcal{O}\left(\frac{|\boldsymbol{b}|^2}{B_0^2}\right). \tag{2.10b}$$

So, up to the second order, the effects of field heterogeneity are determined by just the longitudinal component of the inhomogeneity, $\boldsymbol{b}$. In short, there is usually a spread in Larmor frequencies but no relevant tilt in the precession axis. The approximation conveniently decouples the longitudinal nuclear magnetization component in Eq.(2.9),

[2]Internal is here used in the sense of intrinsic and as opposed to externally controllable as inhomogeneities introduced by gradient pulses. The terminology is well-consolidated in the specialized literature.

which yields

$$\frac{\partial m}{\partial t} = -\left[\frac{1}{\mathrm{T}_2} + i\gamma\left(B_0 + b_z\right)\right] m + D_0\nabla^2 m \tag{2.11a}$$

$$\frac{\partial m_z}{\partial t} = \frac{m_0 - m_z}{\mathrm{T}_1} + D_0\nabla^2 m_z \tag{2.11b}$$

once the transverse (complex) magnetization $m \equiv m_x + im_y$ is introduced[3].

The above system, instead of Eq.(2.9), comprises the basic equations of modern NMR techniques. In this framework, the longitudinal magnetization is uninfluenced by magnetic fields apart from the instantaneous effects of magnetic field pulses. In accord, a $\pi/2$-pulse can immediately swap transverse and longitudinal magnetization components, the direction of swapping being determined by the pulse phase, and π-pulses can be used to invert longitudinal magnetization and complex-conjugate transverse magnetization[28] (See Appendix A).

Whenever relaxation rates are uniform through the sample, as assumed so far, a further simplification ensues. It is possible to define **surviving** nuclear magnetizations

$$m \equiv e^{-(\frac{1}{\mathrm{T}_2}+i\gamma B_0)t} M \tag{2.12a}$$

$$m_z \equiv m_0 + e^{-\frac{t}{\mathrm{T}_1}} M_z \tag{2.12b}$$

wherein, in the transverse case, the uniform Larmor precession imposed by the static field is conveniently account for by the complex exponential.

To put it in traditional NMR jargon, the surviving nuclear magnetizations are defined in the rotating frame of reference whereas the original magnetizations are described in the so-called laboratory frame. By inserting these definitions on Eq.(2.11),

$$\frac{\partial M_z}{\partial t} = D_0\nabla^2 M_z \tag{2.13}$$

[3]The definition of a complex magnetization may seem artificial at first but it should be noted that the transverse (complex) nuclear magnetization is precisely the measurable quantity in modern NMR spectrometers. From a mathematical perspective, there is nothing special about the definition. It, in fact, follows naturally from a **spherical tensor** description of the spin magnetization vector, which is useful for theoretical treatment in many instances. Notice that such description introduces two transverse complex magnetization components, namely, m and m^*, and that, in general, both components are necessary to account for nuclear magnetization dynamics. One great simplification introduced by Eq.(2.10) is that the approximation effectively decouples all spherical components, incidentally, making the information contained in m^* redundant.

and

$$\frac{\partial M}{\partial t} = -i\gamma b_z M + D_0 \nabla^2 M. \tag{2.14}$$

And, although Eq.(2.9) is in fact the original system proposed by Torrey[111], nowadays, it is Eq.(2.14) that is commonly referred to as the Bloch-Torrey equation[43] and there are several reasons for its notoriety.

First of all, M relates directly to the observed NMR signal. Modern NMR spectrometers employ heterodyne detection techniques, which means the resultant output is demodulated, i.e., observed in the rotating frame, and acquired in quadrature, real and imaginary components are recorded. Namely,

$$E(t) = e^{-\frac{t}{T_2}} \int_\Omega \mathrm{d}^3\boldsymbol{X}\, M(\boldsymbol{X}, t). \tag{2.15}$$

Furthermore, appropriate phase cycling can effectively switch back and forth the full complex transverse magnetization, M, for M_z. This is useful for interrupting dephasing of whatever origin over some time, even though magnetization is still lost by longitudinal relaxation, however, at a much weaker rate. Such procedures fit neatly into a framework based on Eq.(2.14) alone, as swapping can be considered simply as turning on and off field inhomogeneities. This notion brings about the concept of effective **temporal profile** of a NMR sequence[43], which in sum allows for the description of a generally complex experimental protocol in terms of a simple modulation function.

How to identify the temporal profile a given sequence is explored at Appendix A. At this point, the important result is that, for a large class of NMR sequences[46,106], the observed signal can be predicted at all times by solving the Bloch-Torrey equation under an effective dephasing field determined by

$$b_z(\boldsymbol{X}, t) = B(\boldsymbol{X}) f(t) + b(\boldsymbol{X}) g(t), \tag{2.16}$$

wherein B and b denote respectively the external and internal field inhomogeneity configuration and $f(t)$ and $g(t)$, their respective temporal profiles. Commonly employed temporal profiles are depicted at Fig.2.2.

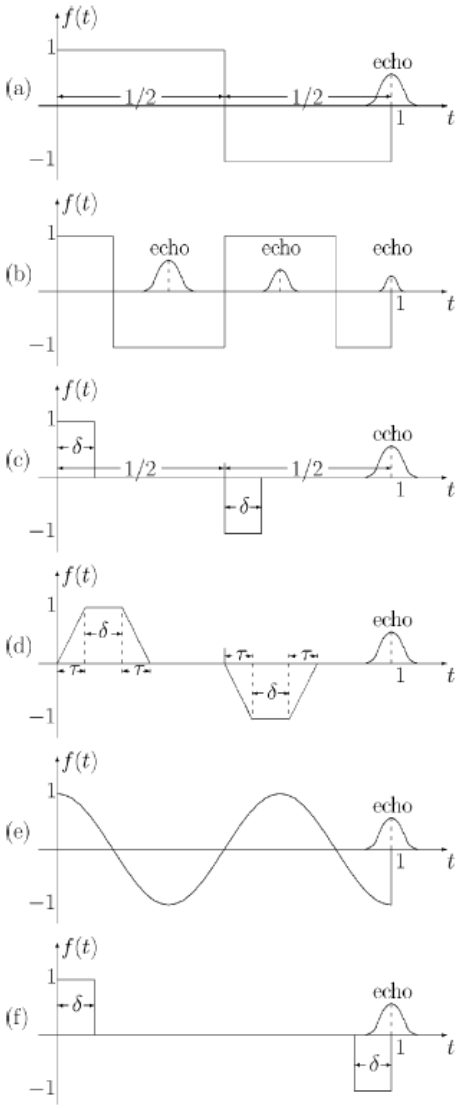

Figure 2.2: Common effective temporal profiles of NMR sequences: (a) Hahn echo, (b) CPMG, (c) rectangular PFG, (d) trapezoidal PFG, (e) Cosine modulated gradient and (f) PFG-SE (Extracted from Grebenkov[43])

2.1.1 Initial and Boundary conditions

Solving the Bloch-Torrey equation, a PDE, presupposes that initial and boundary conditions are given. Since every pulsed NMR experiment starts with the equilibrium spin density being flipped from the longitudinal axis, the initial condition is assumed to be uniform and proportional to m_0 over the probed sector of the sample and zero elsewhere. In the case of bounded domains, the probed volume can always be identified with the sample geometry entirely, so $M(\boldsymbol{X}, 0) = c_0 m_0$ everywhere, with c_0 being a complex number determined by the type and phase of the excitation pulse. There are many situations, however, in which is more convenient to treat sample geometry in terms of a domain that extends indefinitely (this is normally the case for typical test tubes, wherein boundary effects can usually be neglected, or connected pore structures that stretch beyond the active interval of a NMR probe) and hence it becomes necessary to introduce an **indicator function** for the probed region,

$$H(\boldsymbol{X}) = \begin{cases} 1 & \text{if } \boldsymbol{X} \in \Omega \\ 0 & \text{if } \boldsymbol{X} \notin \Omega \end{cases} \tag{2.17}$$

in which, unless stated otherwise, $\partial\Omega$ is assumed to define regular boundary. Accordingly,

$$M(\boldsymbol{X}, 0) = c_0 m_0 H(\boldsymbol{X}) \tag{2.18}$$

is the relevant initial condition to NMR studies[4].

Determining appropriate boundary conditions, on the other hand, is less straightforward. For unbounded domains without internal boundaries, because the initial excitation is localized, a reasonable boundary condition is imposed by

$$M(\boldsymbol{X}, t) \longrightarrow 0 \text{ as } |\boldsymbol{X}| \longrightarrow \infty \text{ for all } t. \tag{2.19}$$

Yet, in every other situation actual boundaries are present, it must be considered how the presence of an interface affects the balance of nuclear magnetic moment on its surroundings. Fluid-fluid interfaces, as those formed in emulsions, may be permeable in the sense that nuclear magnetization is exchanged across them, unavoidably affecting the spin density on both sides. Solid walls, in turn, are generally impermeable but, there, molecules can be adsorbed over sufficiently long times and encounter surface

[4]Notice that under the assumptions of Eq.(2.10) the equilibrium magnetization is actually heterogeneous. However, in virtue of the linearity of Bloch-Torrey equation, the first-order correction contributes negligibly to the observed signal and can be ignored.

structures that introduce new important mechanisms of spin relaxation.

The general structure of boundary conditions can nevertheless be guessed from an argument similar to the one that produced the diffusion flux law, Eq.(2.7), and it starts by considering the overall flux through a small Gaussian pillbox centered at a particular interface point, noting that on either side an expansion like Eq.(2.5) is valid. The hypotheses of translational invariance and isotropy of the diffusion propagator are no longer valid near interfaces, so both drift and diffusion tensors must exhibit a sharp spatial dependence upon crossing the boundary. Some rotational symmetry however should still remain about the normal axis, implying that there can only exist drifts orthogonal to the surface and that longitudinal and transverse diffusive transport are locally uncoupled. In the limit the height of the pillbox goes to zero, these considerations suggest a balance

$$\int_{A(\boldsymbol{X})} \mathrm{d}A \; [\boldsymbol{J}_i] \cdot \boldsymbol{n} = \int_{A(\boldsymbol{X})} \mathrm{d}A \; \left[k\, m_i + D \frac{\partial m_i}{\partial \boldsymbol{n}} \right] \tag{2.20}$$

in which [ ] denotes the jump of its argument across the boundary. In general, drift and normal diffusion coefficients are different at both sides of the interface. There are in fact microscopic expressions for these quantities akin to Eq.(2.6) but determined only by the normal characteristics of the local diffusion propagator. Notice also that drifts related to boundary presence do not generally correspond to a flow component; they result simply from the breaking of rotational invariance near interfaces. Imposing continuity on flux densities finally reduces the above condition to

$$k_- m_i^{(-)} + D_- \frac{\partial m_i^{(-)}}{\partial \boldsymbol{n}} = k_+ m_i^{(+)} + D_+ \frac{\partial m_i^{(+)}}{\partial \boldsymbol{n}}, \tag{2.21}$$

in which $\pm$ signs indicate the side of interface on which the expressions are evaluated.

The drift coefficients get many different names depending on the context they are applied: Interface permeability, inter-medium exchange coefficients, surface relaxivity. The important result for now is that they are generally distinct and can be non-uniform, i.e., take different values across surfaces and interfaces. An important relation that follows directly from Eq.(2.21) upon assumption of uniformity on both drift coefficients and magnetization components is the so-called **detailed balance condition**,

$$k_+ m_0^{(+)} = k_- m_0^{(-)}; \tag{2.22}$$

it points to the fact that spin exchange between different media does not cease upon equilibrium but rather happens in a very precise manner that maintains equilibrium characteristics.

The diffusion coefficients D_+ and D_-, in turn, are not strictly equal to the respective bulk diffusion coefficients of each medium but are generally regarded to be.

The **boundary compatibility condition** expressed by Eq.(2.21) can be particularized to several standard situations.

In the event that the medium under consideration is coupled to a very large reservoir of spin moment or in contact with a number of small systems in which diffusive processes are immaterial, only inhomogeneities in the medium itself are of any relevance to the magnetization balance, so

$$D_0 \frac{\partial m_i}{\partial \boldsymbol{n}} + (k_0 m_i - k' m_i') = 0. \tag{2.23}$$

Cohen and Mendelson[25] coupled a balance of nuclear magnetic moment over **small sites** lodged on a solid boundary, equivalent to Eq.(2.3), to the above condition to show that it reduces to

$$D_0 \frac{\partial m_i}{\partial \boldsymbol{n}} + \frac{h}{\mathrm{T}_i^{(s)}} m_i + h \frac{\partial m_i}{\partial t} = 0, \tag{2.24}$$

provided spin dynamics at surface sites can be described by Bloch equations and that exchange is much faster than surface relaxation, namely, $k_0 \mathrm{T}_i^{(s)} \gg 1$. The parameter h has dimension of length and is associated with the characteristic height of the small surface structures. They argued this parameter should be small, typically the width of a couple molecular layers. The relaxation times $\mathrm{T}_i^{(s)}$ correspond to local spin relaxation mechanisms and can become orders of magnitude higher than bulk relaxation times if surface sites harbor paramagnetic centers, in which case the simple (Bloch-like) decay is automatically justified[5].

Cohen and Mendelson's boundary condition can be further simplified whenever the characteristic size of domains, L, is much greater than h. In practice, this is always the case unless one is dealing with microporous materials. The last term of Eq.(2.24) can be neglected and hence the expression falls into the category of homogeneous Robin boundary conditions,

$$D_0 \frac{\partial m_i}{\partial \boldsymbol{n}} + \rho_i m_i = 0. \tag{2.25}$$

[5]See Chapter 3

The ratio $h/\mathrm{T}_i^{(s)}$ determines the surface relaxivity at a given boundary point and it is usually denoted by ρ_i. As discussed in Chapter 1, this boundary condition has played a crucial role in the understanding and description of NMR relaxation experiments on porous media.

Finally, the boundary compatibility condition also applies to the situation in which there is nothing to account for on one side of the boundary, as in the case of solid wall whose only function is to bounce back the particles that impinge on it. Then, Eq.(2.21) strictly reduces to

$$D_0 \frac{\partial m_i}{\partial \boldsymbol{n}} + k_0 m_i = 0, \tag{2.26}$$

but it is reasonable to assume that, in such cases, the diffusion propagator also has local reflection symmetry; this ultimately implies a zero drift and, accordingly,

$$\frac{\partial m_i}{\partial \boldsymbol{n}} = 0 \tag{2.27}$$

becomes the expected boundary condition. The regime of **reflected diffusion** follows from such homogeneous Neumann boundary condition when it applies to all boundary points.

The boundary conditions determined by Eqs.(2.25, 2.27) share one final convenient attribute: Both express relations that refer to a single domain and do not explicitly depend on time. Consequently, they automatically apply to the Bloch-Torrey equation, Eq.(2.14). Nevertheless, one must constantly heed to the fact that, when surface relaxivities are introduced, the diffusive characteristics of each magnetization component might differ and so switching between components may bring about an additional complexity to a sequence.

2.2 Diffusion propagators

Having presented all necessary elements to characterize restricted nuclear spin diffusion, it is time to consider a formal method of solution.

Notwithstanding its apparent simplicity, the Bloch-Torrey equation is too difficult to solve under any relevant boundary conditions even at simple domains[43]. Diffusion problems, on the other hand, albeit also hard to solve, admit a formal general solution through the use of Green functions. Accordingly, any initial and bound-

ary value problem involving Eq.(2.13) is solved in terms of the solution of particular (fundamental) problem. Namely,

$$M_z(\boldsymbol{X},t) = \int_\Omega \mathrm{d}^3\boldsymbol{X}_0\, G_{t-t_0}(\boldsymbol{X},\boldsymbol{X}_0) M_z(\boldsymbol{X}_0,t_0) \tag{2.28}$$

wherein

$$\begin{aligned} &\frac{\partial}{\partial t} G_t(\boldsymbol{X},\boldsymbol{X}_0) = D_0 \nabla^2_{\boldsymbol{x}} G_t(\boldsymbol{X},\boldsymbol{X}_0), \\ &G_0(\boldsymbol{X},\boldsymbol{X}_0) = \delta(\boldsymbol{X}-\boldsymbol{X}_0), \quad \forall\, \boldsymbol{X},\boldsymbol{X}_0 \in \Omega \quad \text{and} \\ &D_0 \frac{\partial G_t}{\partial \boldsymbol{n}} + \rho_1(\boldsymbol{X}) G_t = 0, \quad \forall\, \boldsymbol{X} \in \partial\Omega. \end{aligned} \tag{2.29}$$

Notice how Eq.(2.28) emulates the notion of diffusive transport discussed in the preceding sections. The longitudinal magnetic moment within a vicinity of a point $\boldsymbol{X}$ in Ω, at any given instant, equals the sum of spin magnetic moment of all the particles that have been diffused towards $\boldsymbol{X}$ over a considered period of time. It reflects not only the characteristics of previous spin densities but the process of particle diffusion as well. In reality, there is no distinction between the fundamental solution of a diffusion problem and the postulated diffusion propagator in Eq.(2.4), apart from the fact that the former is a particularization of the latter in the sense that all assumptions made in the derivation of the differential equations and boundary conditions are simply necessary requirements for specifying the diffusion process under consideration.

The diffusion propagator possesses some properties worth listing. The relation expressed in Eq.(2.28) can be used recursively to show that propagators always satisfy the Chapman-Kolmogorov identity,

$$G_{t-t_0}(\boldsymbol{X},\boldsymbol{X}_0) = \int_\Omega \mathrm{d}^3\boldsymbol{X}'\, G_{t-t'}(\boldsymbol{X},\boldsymbol{X}') G_{t'-t_0}(\boldsymbol{X}',\boldsymbol{X}_0) \tag{2.30}$$

for arbitrary $t' \in [t_0, t]$. This imbues diffusive transport with a kind of short-memory dynamics and imposes other relevant dynamical restrictions like sign-preservation. This last property can also be easily demonstrated.

Assume $G_t(\boldsymbol{X},\boldsymbol{X}_0) \geq 0$ for every pair of points $\boldsymbol{X},\boldsymbol{X}_0$ in Ω over a time interval $0 < t \leq \tau$. This means the diffusive response in the entire domain to every possible infinitely concentrated initial condition is non-negative during some finite time interval. Then, Chapman-Kolmogorov identity implies that $G_t(\boldsymbol{X},\boldsymbol{X}_0) \geq 0$ holds under the same requirements up to 2τ, for if it were to be violated at any intermediate

instant, $\tau < t' \leq 2\tau$,

$$\int_\Omega \mathrm{d}^3\boldsymbol{X}'\, G_{t'-\tau}(\boldsymbol{X},\boldsymbol{X}')G_\tau(\boldsymbol{X}',\boldsymbol{X}_0) < 0 \tag{2.31}$$

which cannot hold since the integrand by assumption is non-negative. The argument can now be repeated to show the propagation remains non-negative up to any time $2^N\tau$ and therefore indefinitely.

To prove that $G_t(\boldsymbol{X},\boldsymbol{X}_0)$ in fact does not change sign during some short, though finite initial period, for the entire class of problems encompassed by Eq.(2.29), seems to be way more difficult; here, the condition is conjectured affirmatively[6].

To summarize it in a simple corollary: Diffusive transport cannot flip spin magnetization. Changes in magnetic moment result exclusively from transfers between regions and boundary relaxation.

Now, regarding signal decay, notice that integration of Eq.(2.29) over the entire domain yields

$$\frac{\mathrm{d}}{\mathrm{d}t}\int_\Omega \mathrm{d}^3\boldsymbol{X}\, G_t(\boldsymbol{X},\boldsymbol{X}_0) = -\int_{\partial\Omega} \mathrm{d}S\, \rho_1(\boldsymbol{X})G_t(\boldsymbol{X},\boldsymbol{X}_0), \tag{2.32}$$

implying that the integral on the left-hand side is monotonically decreasing with time. In the particular case of reflected diffusion, the integral is constant and equal to 1, because of the initial condition. To illustrate these ideas, consider the signal produced by an inversion recovery sequence[7] ($c_0 = -2$)

$$\begin{aligned} E(t) &= m_0V_0 - 2m_0e^{-\frac{t}{\mathrm{T_1}}}\int_\Omega \mathrm{d}^3\boldsymbol{X}\int_\Omega \mathrm{d}^3\boldsymbol{X}_0\, G_t(\boldsymbol{X},\boldsymbol{X}_0)H(\boldsymbol{X}_0) \\ &= E_0\left(1 - 2e^{-\frac{t}{\mathrm{T_1}}}\int_\Omega \mathrm{d}^3\boldsymbol{X}\int_\Omega \mathrm{d}^3\boldsymbol{X}_0\, G_t(\boldsymbol{X},\boldsymbol{X}_0)P(\boldsymbol{X}_0)\right), \end{aligned} \tag{2.33}$$

wherein $E_0 = m_0V_0$ corresponds to the total magnetic moment in the excited region, accordingly, the signal amplitude, whereas $P(\boldsymbol{X}) = H(\boldsymbol{X})/V_0$ defines the probability

[6]The conjecture is hinted by the fact that away from boundary points the short-time behavior of the diffusion propagator is nearly Gaussian. Near boundary responses should also exhibit closely a reflected or partially reflected Gaussian character over sufficiently small times. Providing an actual proof for these statements over arbitrary geometries, however, seems to be too mathematically involved and so I pose it as a conjecture. Unfortunately, I was unable to find a reference that proves the point but remark that, at least for the Neumann boundary condition, the result must follow due to the probabilistic nature of diffusion propagators.

[7]Recall that NMR methods effectively measure the actual rotating nuclear magnetic moment of a sample and not the surviving magnetic moments. See Eq.(2.12).

density of spin excitation. If there is no surface relaxation, interchanging integral yields

$$E(t)/E_0 = 1 - 2e^{-\frac{t}{\mathrm{T}_1}} \int_\Omega \mathrm{d}^3\boldsymbol{X}_0\, P(\boldsymbol{X}_0) = 1 - 2e^{-\frac{t}{\mathrm{T}_1}}. \tag{2.34}$$

This is a quite general result. Without surface relaxation, recovery signals remain unaffected by the presence of a boundary. The underlying reason for this phenomenon is easily explained in terms of the eigenstructure of the Laplace operator (see Section 2.3). Conversely, if $\rho_1 \neq 0$, the monotonic decrease described in Eq.(2.32) implies a faster saturation that is strictly non-exponential. Signal behavior then reflects specific characteristics of the confining structure, but the analysis is not exactly amenable. One general simple piece of information, though, can be retrieved from the initial rate of saturation,

$$\frac{\mathrm{d}E(0)}{\mathrm{d}t} = 2\left(\frac{1}{\mathrm{T}_1} + \int_{\partial\Omega} \mathrm{d}S\, \rho_1(\boldsymbol{X})P(\boldsymbol{X})\right) = 2\left(\frac{1}{\mathrm{T}_1} + \frac{\bar{\rho}_1 S_0}{V_0}\right) E_0 \tag{2.35}$$

in which $\bar{\rho}_1 \equiv 1/S_0 \int_{\partial\Omega} \mathrm{d}S\, \rho_1(\boldsymbol{X})H(\boldsymbol{X})$ denotes the **mean surface relaxivity** over the probed surface S_0. As it turns out, in many pore structures the observed nuclear moment recovery can be reasonably well described in terms of a single exponential and so Eq.(2.35) can be assumed to hold approximately for all times. Incidentally, this is how surface-induced relaxation rates are measured in practice.

2.2.1 Multiple Correlation Functions

The diffusion propagator defined in Eq.(2.29) pertains to the diffusive transport of longitudinal magnetization. Transverse surface relaxivities tend to be higher than longitudinal ones and, consequently, the dynamics of nuclear magnetic moment components is distinguished in another aspect. This issue is obviously absent in the case of reflected diffusion, where diffusive transport is determined purely by the geometry of the confining structure. In any case, a second diffusion propagator is completely defined by formulating the fundamental problem in terms of ρ_2.

The existence of an underlying diffusion propagator can be evoked to establish an important identity involving the solutions of Bloch-Torrey equation. It follows by multiplying Eq.(2.14) by the diffusion propagator[8] $G_{t-t'}(\boldsymbol{X}, \boldsymbol{X}')$ and integrating the

[8]For economy of notation, I do not distinguish between longitudinal and transverse propagators unless it is necessary to avoid confusion.

second spatial variable over the entire domain, namely,

$$\begin{aligned}\int_\Omega \mathrm{d}^3\boldsymbol{X}'\, G_{t-t'}(\boldsymbol{X},\boldsymbol{X}')\frac{\partial}{\partial t'}M(\boldsymbol{X}',t') = \\ -i\int_\Omega \mathrm{d}^3\boldsymbol{X}'\, G_{t-t'}(\boldsymbol{X},\boldsymbol{X}')\gamma b_z(\boldsymbol{X}',t')M(\boldsymbol{X}',t') \\ + D_0\int_\Omega \mathrm{d}^3\boldsymbol{X}'\, G_{t-t'}(\boldsymbol{X},\boldsymbol{X}')\nabla'^2 M(\boldsymbol{X}',t').\end{aligned} \tag{2.36}$$

Then, Green's theorem, the permutation symmetry of G_t on its spatial variables[9] and the fact G_t and M satisfy the same boundary conditions must all be used to show that

$$\begin{aligned}\int_\Omega \mathrm{d}^3\boldsymbol{X}'\,\frac{\partial}{\partial t'}\left(G_{t-t'}(\boldsymbol{X},\boldsymbol{X}')M(\boldsymbol{X}',t')\right) = \\ -i\int_\Omega \mathrm{d}^3\boldsymbol{X}'\, G_{t-t'}(\boldsymbol{X},\boldsymbol{X}')\gamma b_z(\boldsymbol{X}',t')M(\boldsymbol{X}',t'),\end{aligned} \tag{2.37}$$

which, integrated on t' over $[0,t]$, yields

$$\begin{aligned}M(\boldsymbol{X},t) = \int_\Omega \mathrm{d}^3\boldsymbol{X}'\, G_t(\boldsymbol{X},\boldsymbol{X}')M(\boldsymbol{X}',0) \\ -i\int_0^t \mathrm{d}\,t'\int_\Omega \mathrm{d}^3\boldsymbol{X}'\, G_{t-t'}(\boldsymbol{X},\boldsymbol{X}')\gamma b_z(\boldsymbol{X}',t')M(\boldsymbol{X}',t').\end{aligned} \tag{2.38}$$

The identity reveals how dephasing is a process intertwined to diffusive transport. It can be used iteratively to show that

$$M(\boldsymbol{X},t) = \sum_{k=0}^{\infty}(-i)^k\, M^{(k)}(\boldsymbol{X},t), \tag{2.39}$$

wherein

$$M^{(0)}(\boldsymbol{X},t) = \int_\Omega \mathrm{d}^3\boldsymbol{X}'\, G_t(\boldsymbol{X},\boldsymbol{X}')M(\boldsymbol{X}',0), \tag{2.40a}$$

$$M^{(k)}(\boldsymbol{X},t) = \gamma\int_0^t \mathrm{d}\,t'\int_\Omega \mathrm{d}^3\boldsymbol{X}'\, G_{t-t'}(\boldsymbol{X},\boldsymbol{X}')b_z(\boldsymbol{X}',t')M^{(k-1)}(\boldsymbol{X}',t'), \tag{2.40b}$$

provided, of course, the series converges. Incidentally, the procedure establishes a method for finding solutions of the Bloch-Torrey equation under arbitrary encoding

[9] This follows from the fact that the generator of diffusive motion, namely, the underlying Laplace operator in Eq.(2.29) is self-adjoint.

by systematically developing high order contributions. Notice that again the diffusion propagator is brought back to the center of description.

The decomposition of the transverse magnetic moment into infinite contributions implies the measured NMR signal is determined accordingly. In fact, (without loss to generality, $c_0 = 1$)

$$E(t) = E_0 e^{-\frac{t}{\mathrm{T}_2}} \left(\sum_{k=0}^{\infty} (-i)^k \, \Phi^{(k)}(t) \right), \tag{2.41}$$

in which the various functions $\Phi^{(k)}(t)$ are defined by

$$\Phi^{(k)}(t) = \gamma^k \int_0^t \mathrm{d}\, t_k ... \int_0^{t_2} \mathrm{d}\, t_1 \, \langle b_z(\boldsymbol{X}_k, t_k) ... \, b_z(\boldsymbol{X}_1, t_1) \rangle \,, \tag{2.42}$$

the time variables being labeled in ascending order. The **multiple correlation functions** (MCF) of the dephasing field are determined as

$$\begin{aligned} \langle b_z(\boldsymbol{X}_k, t_k) ... \, b_z(\boldsymbol{X}_1, t_1) \rangle = \int_{\Omega^{k+2}} \mathrm{d}^3\boldsymbol{X} \mathrm{d}^3\boldsymbol{X}_k ... \, \mathrm{d}^3\boldsymbol{X}_0 \Big[G_{t-t_k}(\boldsymbol{X}, \boldsymbol{X}_k) ... \\ b_z(\boldsymbol{X}_2, t_2) G_{t_2-t_1}(\boldsymbol{X}_2, \boldsymbol{X}_1) b_z(\boldsymbol{X}_1, t_1) G_{t_1}(\boldsymbol{X}_1, \boldsymbol{X}_0) P(X_0) \Big]. \end{aligned} \tag{2.43}$$

At least formally, the MCF method solves the question of how the observed NMR signal is determined in terms of the underlying restricted diffusion problem and encoding sequence parameters. On the other hand, explicit evaluation of the MCF is already unfeasible for the simplest domains but semi-analytical calculations are possible and have been performed by several authors [3,43,70]. On more general structures, however, the method needs to be implemented fully as a computational scheme. Then, the expressions resulting from Eq.(2.43) can still be worked a little more in order to simplify the basic algorithm; this is done below when introducing the eigenstructure of Laplace operators (Section 2.3). At this point, it is instructive to present another view on how multiple correlation functions also come about.

2.2.2 The spin phase process

One fundamental concept in NMR is that field heterogeneity leads to loss of coherence simply because spins located at different positions in a sample may precess with distinct Larmor frequencies. A relative phase difference then builds up over time and this makes transverse nuclear magnetization decay faster. Accordingly, such process

is neatly explained by the Bloch-Torrey equation.

Assume for the moment that $D_0 = 0$ in Eq.(2.14), so it can be explicit integrated to yield a signal

$$E(t) = E_0 e^{-\frac{t}{\mathrm{T}_2}} \int_\Omega \mathrm{d}^3\boldsymbol{X}\, \exp\left(-i\gamma \int_0^t \mathrm{d}t'\, b_z(\boldsymbol{X}, t')\right) P(\boldsymbol{X}). \tag{2.44}$$

Notice how the domain integral corresponds to the expectation of a variable, namely, the accumulated spin phase over the observation period at the position $\boldsymbol{X}$; thus, the signal can be alternatively written as

$$E(t) = E_0 e^{-\frac{t}{\mathrm{T}_2}} \left\langle e^{-i\phi_t} \right\rangle. \tag{2.45}$$

More generally, the above relation is expected to hold even in situations diffusion cannot be neglected. The idea is essentially the same, but now the spin phase variable must reflect the entire trajectory of nuclei from excitation to the point of observation. As a result,

$$\phi_t = \gamma \int_0^t \mathrm{d}t'\, b_z(\boldsymbol{X}_{t'}, t'). \tag{2.46}$$

The position of nuclei, being only known probabilistically, bestows a more involved stochastic character to the accumulated spin phase, yet the transverse magnetic moment of each nucleus in the sample simply picks up a factor determined by $e^{-i\phi_t}$ and the measured signal is again defined by the sum of all such contributions. In macroscopic samples, the number of nuclei is so large that it is safe to assume a typical measurement samples over all possible realizations of the spin phase process conditioned to a initial position, hence, by averaging over the entire excited region, Eq.(2.45) follows.

Now, one clear advantage of Eq.(2.45) is conceptual, for it encompasses a basic relation of nuclear spin behavior and the observed output of NMR experiments. But, additionally, it marks the spin phase as the accessible quantity for characterization of the underlying processes involved and, from a statistical point of view, it also establishes NMR as an experimental method for investigation of the class of stochastic processes that are defined through Eq.(2.46) (the **characteristic function** of a random process φ_t is defined by $\left\langle e^{-ih\varphi_t} \right\rangle$ and contains all statistical information regarding the process[84]). On the other hand, closed-form expressions for $\left\langle e^{-i\phi_t} \right\rangle$ are available only for a rather small and restricted class of processes, so, as a rule, the relation has but limited applicability.

A similar expansion to Eq.(2.41), however, results directly from expansion of phase factor,

$$E(t) = E_0 e^{-\frac{t}{\mathrm{T}_2}} \left(\sum_{k=0}^{\infty} (-i)^k \frac{\langle \phi_t^k \rangle}{k!} \right), \tag{2.47}$$

and the **spin phase moments** are generally defined by

$$\langle \phi_t^k \rangle = \gamma^k \int_0^t \mathrm{d}\, t_k ... \int_0^t \mathrm{d}\, t_1 \, \langle b_z(\boldsymbol{X}_k, t_k) ... \, b_z(\boldsymbol{X}_1, t_1) \rangle \,, \tag{2.48}$$

wherein no time order is presumed in the field correlation functions, which are then symmetric under permutation of arguments.

An equivalent definition can be derived from the above expression by enforcing order on the time variables. Notice that the integration interval can be partitioned on $k!$ subdomains which are all identical in sense that each can defined by means of a permutation of variables on the basic set, $0 \leq t_1 \leq ... \leq t_k \leq t$. Because field correlation functions in the above definition are symmetric under the same permutation, the integral can decomposed into a sum of $k!$ integrals of identical value, therefore

$$\langle \phi_t^k \rangle = \gamma^k k! \int_0^t \mathrm{d}\, t_k ... \int_0^{t_2} \mathrm{d}\, t_1 \, \langle b_z(\boldsymbol{X}_k, t_k) ... \, b_z(\boldsymbol{X}_1, t_1) \rangle \,, \tag{2.49}$$

in which field correlation functions are now understood to be time-ordered and thus formally characterized by the probability density of the position process. Namely[10]

$$\begin{aligned} \langle b_z(\boldsymbol{X}_k, t_k) ... \, b_z(\boldsymbol{X}_1, t_1) \rangle = \int_{\Omega^{k+1}} & \mathrm{d}^3 \boldsymbol{X}_k ... \, \mathrm{d}^3 \boldsymbol{X}_0 \, b_z(\boldsymbol{X}_k, t_k) ... \, b_z(\boldsymbol{X}_1, t_1) \\ & \times P(\boldsymbol{X}_k, t_k; ... \, ; \boldsymbol{X}_1, t_1 | \boldsymbol{X}_0) P(\boldsymbol{X}_0). \end{aligned} \tag{2.50}$$

Finally, in the absence of surface relaxation, diffusion propagators strictly define the conditional probability density of a position random process pertaining to the considered nuclei. The process is Markovian, which means that it is fully determined by G_t and the initial probability density, P. Thus, the k-point probability function

[10] Recall the spin phase defined in Eq.(2.46) is in fact a stochastic process conditioned to the initial position of a nucleus, whereas the expectation in Eq.(2.45) assumes this process is being averaged over all excited initial positions. Accordingly, all phase moments must be averaged over the same initial distribution; this explains why the determination of k-point phase moments requires in fact $k+1$ integrals. All correlations in fact are mean functions of the conditioned correlations.

becomes simply

$$P(\boldsymbol{X}_k, t_k; \ldots; \boldsymbol{X}_1, t_1|\boldsymbol{X}_0) = G_{t_k - t_{k-1}}(\boldsymbol{X}_k, \boldsymbol{X}_{k-1}) \ldots G_{t_1}(\boldsymbol{X}_1, \boldsymbol{X}_0). \tag{2.51}$$

It is instructive to compare the field correlations determined by the above and Eq.(3.6) with the multiple correlation functions defined in Eq.(2.43). They are in fact identical when the conditions imposed on diffusive transport are the same, specifically, if there is no surface relaxation, for then integration of the $\boldsymbol{X}$ variable can be made regardless.

The comparison proves two things: The phase-signal relation, Eq.(2.45), follows directly from Bloch-Torrey equation, in fact, it represents the formal solution to problems posed in terms of the latter; secondly, multiple correlation functions generalize the more intuitive field correlations that result from probability theory to situations in which the diffusion propagator cannot strictly define a probability density function.

In turn, it is possible to give a clear interpretation to the high order signal contributions:

$$\Phi^{(k)}(t) = \frac{\left\langle \phi_t^k \right\rangle}{k!} \tag{2.52}$$

provided averaging is defined in the generalized sense.

A simplification that is of practical importance stems from the decomposition of the dephasing field into spatial and temporal profiles, Eq.(2.16), provided a single contribution is present or dominant.

For definiteness, let $b_z(\boldsymbol{X}, t) = B(\boldsymbol{X})f(t)$, so

$$\left\langle \phi_t^k \right\rangle = \gamma^k k! \int_0^t \mathrm{d}\, t_k \ldots \int_0^{t_2} \mathrm{d}\, t_1 f(t_k) \ldots f(t_1) \left\langle B(\boldsymbol{X}_k) \ldots B(\boldsymbol{X}_1) \right\rangle . \tag{2.53}$$

Notice that correlation functions do not generally lose their time-dependence; it is inherent to the explicit dependence on the diffusion propagators used to define them. But now it is possible to discriminate what pertains to external manipulation from what is consequent to diffusion. Moreover, correlation functions are seen by definition to involve only time differences, that is,

$$\left\langle B(\boldsymbol{X}_k) \ldots B(\boldsymbol{X}_1) \right\rangle \equiv F^{(k)}(t - t_k, t_k - t_{k-1}, \ldots, t_2 - t_1, t_1 - 0). \tag{2.54}$$

Particularly in absence of surface relaxation, the explicit dependence on t can dropped.

Gaussian processes

There is one case in which Eq.(2.45) can be determined explicitly and consequently the Bloch-Torrey equation can be solved for general temporal profiles.

If the underlying diffusion process is normally distributed, then the (conditioned) spin phase process is also Gaussian[68,84], implying it is completely defined in terms of its first two moments. The characteristic function of a Gaussian process is known to be determined by

$$\left\langle e^{-i\phi_t}\right\rangle_0 = \exp\left[-i\left\langle\phi_t\right\rangle_0 - \frac{\left\langle\phi_t^2\right\rangle_0 - \left\langle\phi_t\right\rangle_0^2}{2}\right]. \tag{2.55}$$

wherein the zero subscript indicates the expectations are conditioned to a starting point $\boldsymbol{X}_0$. Refraining from averaging over the initial spin density in Eq.(2.53), the following definitions are obvious

$$\left\langle\phi_t\right\rangle_0 = \gamma\int_0^t \mathrm{d}\,t_1 f(t_1)F_0^{(1)}(t_1) \tag{2.56}$$

and

$$\left\langle\phi_t^2\right\rangle_0 = 2\gamma^2\int_0^t \mathrm{d}\,t_2\int_0^{t_2}\mathrm{d}\,t_1 f(t_2)f(t_1)F_0^{(2)}(t_2-t_1,t_1). \tag{2.57}$$

Now, in NMR diffusion studies, a typical form of field inhomogeneity is that induced by a linear gradient. Specifically, $B(\boldsymbol{X}) = \boldsymbol{g}\cdot\boldsymbol{X}$. This form also follows in the case of homogeneous samples (non-porous) subject to nearly uniform external fields as a first order approximation. In any case, the field correlations reduce to

$$F_0^{(1)}(t_1) = \boldsymbol{g}\cdot\left\langle\boldsymbol{X}_1\right\rangle_0 = \boldsymbol{g}\cdot\boldsymbol{X}_0 \tag{2.58}$$

and

$$F_0^{(2)}(t_2-t_1,t_1) = \sum_{jk} g_j g_k\left\langle X_{1,j}X_{2,k}\right\rangle_0 = \left(\boldsymbol{g}\cdot\boldsymbol{X}_0\right)^2 + 2D_0|\boldsymbol{g}|^2 t_1, \tag{2.59}$$

the right-hand side expression result from Eq.(B.8).

The first phase moment is thus easily calculated,

$$\left\langle\phi_t\right\rangle_0 = \gamma\boldsymbol{g}\cdot\left\langle\boldsymbol{X}_1\right\rangle_0 = \gamma F(t)\boldsymbol{g}\cdot\boldsymbol{X}_0 \tag{2.60}$$

wherein $F(t)$ denotes the primitive of the effective temporal profile of the sequence, whereas

$$\begin{aligned}\frac{\langle\phi_t^2\rangle_0 - \langle\phi_t\rangle_0^2}{2} &= 2\gamma^2 D_0|\boldsymbol{g}|^2 \int_0^t \mathrm{d}\, t_2 \int_0^{t_2} \mathrm{d}\, t_1 f(t_2) f(t_1) t_1 \\ &= 2\gamma^2 D_0|\boldsymbol{g}|^2 \int_0^t \mathrm{d}\, t_1 \int_{t_1}^t \mathrm{d}\, t_2 f(t_2) f(t_1) t_1,\end{aligned} \tag{2.61}$$

the last step resulting from direct analysis of the integration domain. Then,

$$\begin{aligned}\frac{\langle\phi_t^2\rangle_0 - \langle\phi_t\rangle_0^2}{2} &= 2\gamma^2 D_0|\boldsymbol{g}|^2 \int_0^t \mathrm{d}\, t_1\, t_1 F'(t_1)\left[F(t) - F(t_1)\right] \\ &= \gamma^2 D_0|\boldsymbol{g}|^2 \int_0^t \mathrm{d}\, t_1 \left[F(t) - F(t_1)\right]^2\end{aligned} \tag{2.62}$$

after successive integral by parts.

The signal can finally be determined by averaging Eq.(2.55) over the initial spin density, therefore

$$\begin{aligned}E(t) = E_0 e^{-\frac{t}{\mathrm{T_2}}} &\left(\int \mathrm{d}^3\boldsymbol{X}_0\, e^{-i\gamma F(t)\boldsymbol{g}\cdot\boldsymbol{X}_0} P(\boldsymbol{X}_0)\right) \\ &\times \exp\left[-\gamma^2 D_0|\boldsymbol{g}|^2 \int_0^t \mathrm{d}\, t_1 \left[F(t) - F(t_1)\right]^2\right]\end{aligned} \tag{2.63}$$

since the conditioned phase variance turned out to be independent of $\boldsymbol{X}_0$.

The above result was first derived by Kenkre *et al.*[61] by solving the Bloch-Torrey equation directly. They also apply it to several temporal profiles and initial spin densities. Their result remains as the only known general explicit solution to the Bloch-Torrey equations under a linear magnetic gradient[46]. The presented derivation however is somewhat simpler and can be considered more physically appealing as it is based on considerations made on the spin phase process itself. In any case, it is a good exercise to understand the subtleties and natural difficulties of the MFC method in more general problems.

Finally, it is instructive to point out some general and practical aspects of Eq.(2.63). As written, it describes the NMR signal of a sequence as if it were monitored continuously. This is seldom the case in modern NMR techniques. Rather, acquisition is digitized *a priori* when only spin echo amplitudes are measured (spin echoes are specially convenient from an experimental standpoint because they can provide sufficient separation between stimulation and detection events in a sequence). **Spin**

echo-based sequences have characteristic oscillating temporal profiles, which means $F(t)$ generally has many zeros. Incidentally, the times at which $F(t) = 0$ are known as refocalization times and usually correspond to the times of acquisition. If all measured points, $\{t_n\}$, of a sequence, therefore, satisfy the **rephasing condition**,

$$F(t_n) = \int_0^{t_n} \mathrm{d}\, t f(t) = 0, \tag{2.64}$$

signal decay (specifically for a nuclear spin sample undergoing **unrestricted diffusion**) becomes independent of the initial spin density, though choice for a particular excitation region can still influence signal amplitude. The pre-factor in Eq.(2.63) can be dropped and the decay modulation curve simply given as

$$E(t_n) = E_0 e^{-\frac{t_n}{T_2}} \exp\left[-\gamma^2 D_0 |\boldsymbol{g}|^2 \int_0^{t_n} \mathrm{d}\, t_1 F(t_1)^2\right] \tag{2.65}$$

Residence-time processes and the Bloch-Torrey Equation

A curious aspect of spin phase process is its close relation to residence-time stochastic processes[47].

Given a position stochastic process, $\boldsymbol{X}_t$, defined over a domain Ω, and an indicator function $H(\boldsymbol{X})$ for a sub-domain $\Omega_0 \subseteq \Omega$, the residence time of a particle on Ω_0 over a total time t, i.e., the amount of time it spends within Ω_0, starting from an initial observation up to a final time t, is a random variable conditioned to the initial position, $\boldsymbol{X}_0$, defined by

$$T_t\left[\Omega_0\right] = \int_0^t \mathrm{d}t'\, H(\boldsymbol{X}'_t). \tag{2.66}$$

The definition is intuitively sound. Since $H(\boldsymbol{X}) = 0$ if $\boldsymbol{X} \notin \Omega_0$, the integral only counts time intervals for which the particle is within the considered sub-domain along a particular trajectory.

Compare the above definition to Eq.(2.46) and, for the sake of argument, assume there is no explicit time dependence on b_z. Apart from physical dimensions, if b_z could be tailored into the shape of an indicator function, the NMR decay would allow experimental observation of the statistical characteristics of residence-time stochastic processes. Alternately, the spin phase process could be thought as directly proportional to a generalized residence-time process that is weighed by the spatial configuration of the dephasing field, normalized by its maximum amplitude, with the caveat that the association conceptually breaks down whenever b_z changes sign within the

domain.

Finally, because the definitions for both types of process are formally the same, the residence-time stochastic processes of Brownian particles can be studied through PDE identical to the Bloch-Torrey equation, Eq.(2.14), a fact known to mathematicians for quite some time. With the advent of micro-X-ray computerized tomography, μ-CT, the structure of actual porous media is becoming increasingly available and these processes can be studied from a computational point of view by the methods presented in this text[47].

2.3 The eigenstructure of Laplace operators

The calculation of spin phase moments when particle diffusion is restricted by boundaries is an extremely involved procedure, mostly, due to the fact that diffusion propagators are no longer defined by expressions amenable to theoretical analysis. Yet, as already pointed out, the MCF method does allow the problem to be handled numerically in a quite elegant and simple manner. Since it all rests on the solution of the fundamental problem for a particular type of boundary condition and domain, looking into how general solutions of restricted diffusion problem can be fundamentally expressed is beneficial.

An arbitrary initial value problem with homogeneous boundary conditions as

$$\begin{aligned} \frac{\partial M}{\partial t} &= D_0 \nabla^2 M, \\ M(\boldsymbol{X}, 0) &= m_0(\boldsymbol{X}), \quad \forall\, \boldsymbol{X} \in \Omega \quad \text{and} \\ D_0 \frac{\partial M}{\partial \boldsymbol{n}} &+ \rho(\boldsymbol{X}) M = 0, \quad \forall\, \boldsymbol{X} \in \partial\Omega. \end{aligned} \tag{2.67}$$

is solved by separating time and spatial variables and introducing the eigenstructure of the underlying Laplace operator, namely, the infinite set of eigenvalues and eigenfunctions that, accordingly, satisfy[11]

$$\begin{aligned} \nabla^2 u_n(\boldsymbol{X}) &= -\lambda_n^2 u_n(\boldsymbol{X}), \quad \forall\, \boldsymbol{X} \in \Omega \quad \text{and} \\ \frac{\partial u_n}{\partial \boldsymbol{n}} &+ k(\boldsymbol{X}) u_n = 0, \quad \forall\, \boldsymbol{X} \in \partial\Omega, \end{aligned} \tag{2.68}$$

[11] From this point on, unless stated otherwise, the fundamental domain Ω is assumed to be bounded and having a regular boundary. This ensures the eigenstructure is discrete and eigenfunctions are normalizable[48].

wherein $k(\boldsymbol{X}) = \rho(\boldsymbol{X})/D_0$. The solution is expressed in terms of the infinite series

$$M(\boldsymbol{X}, t) = \sum_{n=0}^{\infty} M_n e^{-D_0 \lambda_n^2 t} u_n(\boldsymbol{X}) \tag{2.69}$$

where the coefficients, M_n, are determined by the **projections** of the initial condition $m_0(\boldsymbol{X})$ onto the eigenfunctions themselves, assumed to be normalized,

$$M_n = \int_\Omega \mathrm{d}^3\boldsymbol{X}\; u_n^*(\boldsymbol{X}) m_0(\boldsymbol{X}). \tag{2.70}$$

This form is verified directly by substitution on Eq.(2.67) and using the orthogonality of Laplace eigenfunctions.

The class of Laplace operators defined in Eq.(2.68) are all self-adjoint [27,48], implying the eigenvalues are real and the eigenfunctions comprise a complete orthogonal set on Ω. Furthermore, because the surface field $k(\boldsymbol{X})$ is real and non-negative, the eigenvalues are all non-positive, hence it is permissible to denote them as the opposite of squared numbers. The latter property is actually easy to be demonstrated by multiplying Eq.(2.68) by $u_n^*(\boldsymbol{X})$, integrating the result over the entire domain and using Green's first identity plus the boundary condition:

$$\lambda_n^2 = \int_\Omega \mathrm{d}^3\boldsymbol{X}\; |\nabla u_n(\boldsymbol{X})|^2 + \int_{\partial\Omega} \mathrm{d}S\, k(\boldsymbol{X})\, |u_n(\boldsymbol{X})|^2\,, \tag{2.71}$$

the right-hand side being obviously non-negative.

Eigenfunctions can be assumed real, but it is generally convenient to consider complex eigenfunctions, particularly in domains that exhibit some rotational symmetry. Notice that if an eigenvalue is non-degenerate, its corresponding eigenfunction must be real, otherwise two linearly independent functions would solve the same eigenvalue problem and consequently the eigenvalue would be degenerate. The reasoning also implies that the complex conjugate of an eigenfunction is also an eigenfunction corresponding to the same eigenvalue. Finally, eigenvalues, hence eigenfunctions, can be ordered in terms of increasing magnitude, i.e.,

$$0 \leq \lambda_0^2 \leq \lambda_1^2 \leq \ldots \leq \lambda_k^2 \leq \ldots\,. \tag{2.72}$$

Now, Eq.(2.70) can be inserted in Eq.(2.69) directly to yield, after some rearrange-

ment of terms,

$$M(\boldsymbol{X},t)=\int_{\Omega}\mathrm{d}^{3}\boldsymbol{X}_{0}\left(\sum_{n}e^{-D_{0}\lambda_{n}^{2}t}u_{n}(\boldsymbol{X})u_{n}^{*}(\boldsymbol{X}_{0})\right)m_{0}(\boldsymbol{X}_{0}). \tag{2.73}$$

Direct comparison of the above expression with Eq.(2.28) and the fact that both procedures are valid for arbitrary initial conditions imply (in the distributional sense) the identity:

$$G_{t}(\boldsymbol{X},\boldsymbol{X}_{0})=\sum_{n=0}^{\infty}e^{-D_{0}\lambda_{n}^{2}t}u_{n}(\boldsymbol{X})u_{n}^{*}(\boldsymbol{X}_{0}). \tag{2.74}$$

Besides the introduction of a formal representation for the diffusion propagator, the eigenstructure of Laplace operators offer some genuine insights on the geometrical aspects of restricted diffusion, particularly so in the case of Neumann-Laplace operators whose eigenstructure is defined in terms of purely geometrical relations. It is even possible to show that as long as one is **not** interested on local (pointwise) details of eigenfuctions, or equivalently of the transport problem, Robin-Laplace operators can be expressed in terms of the eigenstructure of the Neumann-Laplace operator defined over the same domain. Therefore, eigenvalues and eigenfunctions of the former can all be determined in respect to the basis introduced by the latter (see Appendix C), much like in the same manner an operator can be expressed in the basis of a particular observable in Quantum Mechanics. Accordingly, in this text, Neumann eigenfunctions are considered to be fundamental geometric characteristics of a domain and, from Eq.(2.71), so are the eigenvalues.

Back to the matter of geometric insights, the first one to be pointed out is the fact that an uniform function satisfies the Neumann-Laplace eigenvalue problem with $\lambda^{2}=0$. This means that the fundamental **mode of transport** for reflected diffusion is uniform, given by

$$u_{0}(\boldsymbol{X})=\frac{1}{\sqrt{V_{0}}}, \tag{2.75}$$

due to normalization. Furthermore, this mode is non-degenerate as it follows directly from Eq.(2.71) that any mode with a zero eigenvalue must be uniform. Actually, the lowest eigenvalue of any Robin-Laplace operator is also simple, so the fundamental mode is always non-degenerate, regardless the type of diffusive transport considered[48]; also, Robin fundamental modes do not change sign over the entire domain and can always be made positive, a property akin to Eq.(2.75).

The orthogonality of eigenfunctions thus implies

$$\int_{\Omega} \mathrm{d}^3\boldsymbol{X}\, u_n(\boldsymbol{X}) = 0 \quad \forall\, n > 0, \tag{2.76}$$

hence all superior modes of transport change sign within the domain or, in other words, all superior eigenfunctions have nodal points. The notion suggest an interesting picture for the spatial configuration of superior modes and, incidentally, a qualitative interpretation on the physical meaning of Neumann eigenvalues in the context of diffusion.

Assume that, for any given mode, nodal points form a surface or a collection of surfaces that effectively partitions Ω into regions in which the eigenfunction has a definite sign. For the sake of argument, picture this nodal mesh defining regular subdomains. Now, say a sample is prepared in an initial density that exactly matches the spatial configuration of a superior mode. In response to material inhomogeneity, transport must occur between regions of high (positive) concentration to regions of low (negative) concentration and, as a result, through diffusion, concentration changes. However, because the initial state is a mode of diffusive transport, theses changes must take place in such a specific manner that the spatial configuration of inhomogeneities remains unaltered. In this particular setting, diffusion can only lead to a global attenuation of concentration, which in fact is known to governed by a factor $e^{-(D_0 t)\lambda_n^2}$, due to Eq.(2.69). On the other hand, recall that the typical displacement of particles undergoing **unrestricted** diffusion is proportional to $\sqrt{D_0 t}$, so this figure must fix an upper bound for the extent of restricted diffusive transport and serve as an estimate of displacements under confinement as well. Hence, particles must move a distance in the order of λ_n^{-1} before a substantial material exchange can occur between regions of high and low concentration to promote a visible attenuation. Incidentally, λ_n^{-1} determines the length scale on which changes in sign occur in a given mode or, said differently, the characteristic size of compartments determined by its nodal mesh.

This interpretation is particularly relevant from the perspective of intricate structures, such as those defined by porous media, for it suggests that the Neumann-Laplace eigenstructure of the domain may be used to characterize it geometrically in a more objective manner.

Mathematicians have long known that the eigenstructure of Laplace operators offer some degree of geometrical characterization for the domains in which they are defined. The question of how much, however, is more recent and the problem is

perhaps best illustrated in the provocative title of Kac's famous paper: "Can one hear the shape of drum?" [59]. Over 25 years had passed when a definite negative answer was finally published [42], but the fact remains that a great deal of geometrical information like volume, bounding area, mean boundary curvature and topological attributes can still be discovered from a Laplace eigenstructure or, more concisely, from a corresponding propagator.

2.3.1 Matrix formalism

The representation of the diffusion propagator provided by Eq.(2.74) can be used to express multiple correlation functions more compactly. By inserting the expansion in Eq.(2.43) and carrying out the integrals, it follows that

$$\begin{aligned}\langle b_z(\boldsymbol{X}_k,t_k)\dots b_z(\boldsymbol{X}_1,t_1)\rangle = \sum_{n,n_k,\dots,n_1} & \langle U|u_n\rangle\, e^{-\mathcal{D}_0\lambda_n^2(t-t_k)}\,\langle u_n|b_z(t_k)|u_{n_k}\rangle \\ & \times \dots e^{-\mathcal{D}_0\lambda_{n_2}^2(t_2-t_1)}\,\langle u_{n_2}|b_z(t_1)|u_{n_1}\rangle\, e^{-\mathcal{D}_0\lambda_{n_1}^2 t_1}\,\langle n_1|P\rangle\end{aligned} \tag{2.77}$$

in which the bracket notation is used to express the domain integrals involved[12].

Notice how the expression above can be understood in the familiar language of quantum mechanical states. Each $|u_n\rangle$ represents a basis vector introduced by diagonalization of the appropriate Laplace operator, $-\Lambda^2$. In this picture, the diffusion propagator is seen also as an operator that takes an initial density into another and, accordingly, it is represented as $e^{-D_0\Lambda^2 t}$. Incidentally, the dephasing field acts in this analogy as a sort of applied potential whose matrix elements are defined by

$$\langle u_n|b_z(t)|u_{n'}\rangle = \int_\Omega \mathrm{d}^3\boldsymbol{X}\; u_n^*(\boldsymbol{X})b_z(\boldsymbol{X},t)u_{n'}(\boldsymbol{X}) \tag{2.78}$$

As a result,

$$\begin{aligned}\langle b_z(\boldsymbol{X}_k,t_k)\dots b_z(\boldsymbol{X}_1,t_1)\rangle &= \Big\langle U\Big|e^{-D_0\Lambda^2(t-t_k)}b_z(t_k) \\ &\qquad \times \dots e^{-D_0\Lambda^2(t_2-t_1)}b_z(t_1)e^{-D_0\Lambda^2 t_1}\Big|P\Big\rangle \\ &= \left\langle U\left|e^{-D_0\Lambda^2 t}\left(\prod_{l=1}^{k} e^{D_0\Lambda^2 t_l}b_z(t_l)e^{-D_0\Lambda^2 t_l}\right)\right|P\right\rangle,\end{aligned} \tag{2.79}$$

[12] Dirac notation is convenient whenever one is dealing with general Hilbert spaces. The usage is not necessarily common in the NMR diffusion literature but the meaning of relations expressed in terms of it is particularly clear and easy to grasp by anyone familiar with basic Quantum Mechanics. Here, the notation is employed for its economy and didactic value.

notice the product is implemented through left-to-right matrix multiplications. The kets $|P\rangle$ and $|U\rangle$ denote respectively those associated with the initial spin density and the uniform (pick-up) function.

Introduction of the Laplace eigenstructure, therefore, reduces the computation of MCF to a problem of matrix multiplication. The matrices involved, nevertheless, are of infinite dimension; strictly, there is no mathematical advantage of one formulation over the other and Laplace eigenstructures can be just as hard or unfeasible to calculate as diffusion propagators. But, considered as the basis of a numerical scheme for computation of MCF, the matrix formulation encompassed in Eq.(2.79) can indeed be advantageous due to the rapid convergence of matrix products[3,43]. It is important to realize that the contribution of high diffusion modes falls very rapidly, so field correlations can be computed reasonably well in terms of a finite set of low order eigenfunctions, the number of which can vary from just a few to a couple dozen depending on how short are simulation times.

The numerical treatment of MFC also recognizes the fundamental role of the Neumann-Laplace eigenstructure in the analysis of restricted diffusion. The matrices in Eq.(2.79) can of course be represented in any complete basis over Ω, but notice that, because both pick-up and initial density functions are usually uniform in NMR diffusion experiments[13] both functions are proportional to the fundamental Neumann mode. In fact, the proportionality factors of each perfectly cancel one another, making MCF defined in terms of the single matrix element $\langle 0| \quad |0\rangle$, wherein the notation $|n\rangle$ is used specifically to denote Neumann eigenfunctions. Furthermore, the fact only non-local characteristics of diffusion transport are experimentally accessible allows one to conveniently choose the Neumann basis as the fundamental system for computation and exploit methods of representation to Robin problems as in Grebenkov's imaginary dephasing field approach[44] or as through the more direct method developed in Appendix C.

[13]The pick-up can be safely assumed to be uniform in all cases, but non-uniform excitations are commonplace in imaging techniques which, in contrast to diffusion methods, employ soft pulses to excite small position-encoded regions of the sample[22]

The equivalence of formalisms

Once a basis of functions for Ω is provided, the matrix formalism can be applied directly to the Bloch-Torrey equation. Accordingly,

$$\frac{\mathrm{d}}{\mathrm{d}t}\left|M\right\rangle = -i\gamma b_z(t)\left|M\right\rangle - D_0\Lambda^2\left|M\right\rangle \tag{2.80}$$

wherein $|M\rangle$ is understood to be an infinite vector defined by the solution components in the considered basis. By integrating this equation iteratively, an alternative derivation of MCF and spin phase moments definitions can be given. In fact, a formal expression for the characteristic function of the spin phase process can be derived directly from the usual quantum mechanical approach to time-dependent Hamiltonian:

$$\begin{aligned}\left\langle e^{-i\phi_t}\right\rangle &= \left\langle 0\left|e^{-D_0\Lambda^2 t}\left(I+\sum_{k=1}^{\infty}(-i\gamma)^k\int_0^t \mathrm{d}\,t_k ... \int_0^{t_2}\mathrm{d}\,t_1\prod_{l=k}^{1}e^{D_0\Lambda^2 t_l}b_z(t_l)e^{-D_0\Lambda^2 t_l}\right)\right|0\right\rangle \\ &= \left\langle 0\left|e^{-D_0\Lambda^2 t}\mathcal{T}\exp\left[-i\gamma\int_0^t \mathrm{d}\,t' e^{D_0\Lambda^2 t'}b_z(t')e^{-D_0\Lambda^2 t'}\right]\right|0\right\rangle\end{aligned} \tag{2.81}$$

in which $\mathcal{T}$ denotes the time-ordering operator amply used in Quantum mechanics. Notice how the argument of the exponential mimics an applied potential considered in the interaction picture. The very same expression is obtained by inserting the MCF expressions in Eq.(2.79) into the phase moments definition and summing all contributions in Eq.(2.45). This proves all formalisms presented so far are completely equivalent.

Piecewise constant encoding

Dealing directly with the Eq.(2.80) leads to more straightforward derivations in the particular situation the considered NMR sequence is defined in terms of a piecewise constant temporal profile. Since a great number of actual NMR experiments satisfy this condition, it is instructive to consider it in detail.

If $f(t)$ is piecewise constant, it is determined completely in terms of a sequence of amplitudes, f_n, and a partition of the time-domain

$$0 < t_1 < t_2 < ... < t_n < ... . \tag{2.82}$$

Over a single sequence block, Eq.(2.80) can be formally integrated

$$|M(t)\rangle = e^{-\left(i\gamma f_n B + D_0\Lambda^2\right)(t-t_{n-1})}\,|M(t_{n-1})\rangle \tag{2.83}$$

in which B denotes the matrix representation of the applied field inhomogeneity. Notice that in general B and Λ^2 do not commute, which means the operator $i\gamma f_n B + D_0\Lambda^2$ is not normal and, therefore, not generally diagonalizable. In any case, the above result can be used recursively to establish

$$|M(t)\rangle = \left(\prod_{n=1}^{N(t)} e^{-\left(i\gamma f_n B + D_0\Lambda^2\right)(t_n - t_{n-1})}\right)|M(0)\rangle \tag{2.84}$$

wherein $N(t)$ determines the number of sequence blocks covered up to a time t; also, $t_{N(t)} \equiv t$ and $t_0 \equiv 0$. Finally, the observed signal is determined by projection onto the fundamental Neumann mode, $|0\rangle$. Equivalently,

$$\left\langle e^{-i\phi_t}\right\rangle = \left\langle 0\left|\prod_{n=1}^{N(t)} e^{-\left(i\gamma f_n B + D_0\Lambda^2\right)(t_n - t_{n-1})}\right|0\right\rangle. \tag{2.85}$$

The result is exact for piecewise constant sequences, but it can work as an approximation scheme for sequences with completely general temporal profiles through an appropriate discretization of $f(t)$. This is in essence Callaghan's matrix method[20]. As a numerical procedure, Eq.(2.85) is preferable to Eq.(2.81), for typically requiring the computation of fewer matrix exponentials. In practical sequences, $f(t)$ often shows some repeatability and regularity in time, which can reduce profoundly the number of distinct matrix exponentials needed to determine the signal. On the other hand, Eq.(2.81) can be quite useful from an analytical standpoint, viewed as perturbation series. Such reasoning provides justification for one of the most relevant approximations in the analysis of NMR signals.

2.3.2 The Gaussian phase approximation (GPA)

Clearly, the degree of encoding imposed on a given nuclear spin system, that is, the typical magnitude of the spin phase accumulated in the course of an experiment is controlled by both duration and amplitude of field heterogeneities. The time factor is always a controllable aspect of NMR sequences, in fact, it usually comprises the basic

parametric set at the disposition of an experimenter. Therefore, it is always possible to control the degree of encoding in a sequence by adjusting the duration of gradient pulsing or internal field modulation. For set-ups in which field heterogeneities are externally applied, encoding can be controlled by adjusting gradient strength as well.

A suitable regime for both theoretical and experimental analysis is provided by **weak encoding**: If the accumulated spin phase is typically small throughout the sample, then contributions to the observed signal associated with spin phase moments tend to decrease in relevance with their increasing order and hence the measured output can be reasonably well characterized by just a few leading moments.

The analysis is much simpler under the assumption that diffusion is purely reflected and encoding is governed by a single type of magnetic inhomogeneity. As such, consider Eq.(2.81) up to the second moment,

$$\begin{aligned}\left\langle e^{-i\phi_t}\right\rangle = &\left\langle 0\left|e^{-D_0\Lambda^2 t}\right|0\right\rangle - i\gamma\int_0^t \mathrm{d}\,t_1 f(t_1)\left\langle 0\left|e^{-D_0\Lambda^2(t-t_1)}Be^{-D_0\Lambda^2 t_1}\right|0\right\rangle \\ &- \gamma^2\int_0^t \mathrm{d}\,t_2\int_0^{t_2}\mathrm{d}\,t_1 f(t_2)f(t_1)\left\langle 0\left|e^{-D_0\Lambda^2(t-t_2)}Be^{-D_0\Lambda^2(t2-t_1)}Be^{-D_0\Lambda^2 t_1}\right|0\right\rangle \\ &+ \dots .\end{aligned} \tag{2.86}$$

Now, because $|0\rangle$ is an eigenvector of Λ^2 with zero eigenvalue, $e^{-D_0\Lambda^2 t}|0\rangle = |0\rangle$ for arbitrary t; the characteristic function can be simplified into

$$\begin{aligned}\left\langle e^{-i\phi_t}\right\rangle = &1 - i\gamma\int_0^t \mathrm{d}\,t_1 f(t_1)\langle 0|B|0\rangle \\ &- \gamma^2\int_0^t \mathrm{d}\,t_2\int_0^{t_2}\mathrm{d}\,t_1 f(t_2)f(t_1)\left\langle 0\left|Be^{-D_0\Lambda^2(t2-t_1)}B\right|0\right\rangle + \dots .\end{aligned} \tag{2.87}$$

The first order field correlation $\langle 0|B|0\rangle$ is constant and corresponds to the spatial average of the dephasing field, $\bar{B}$, which, without loss of generality can be taken equal zero[14]. In turn, the second order MCF reduces to the **autocorrelation function** of

[14]It is not hard to prove that any $\bar{B}\neq 0$ can be incorporated beforehand into the definition of the surviving nuclear magnetization, Eq.(2.12a), as a frequency shift factor $\exp\left[-i\gamma\bar{B}F(t)\right]$, wherein once again $F(t)$ denotes the primitive of the effective temporal profile of the sequence. This follows directly from the Bloch-Torrey equation. Just make $B(\boldsymbol{X}) = \bar{B} + B'(\boldsymbol{X})$ and factor $\exp\left[-i\gamma\bar{B}F(t)\right]$ out of M in Eq.(2.14) to produce the result.

the dephasing field, which can be expanded into

$$\begin{aligned}\langle B_t B_0\rangle &\equiv \left\langle 0\left|Be^{-D_0\Lambda^2 t}B\right|0\right\rangle \\ &= \sum_{n=0}^{\infty} B_{0n}e^{-D_0\lambda_n^2 t}B_{0n} = \sum_n |B_{0n}|^2 e^{-D_0\lambda_n^2 t},\end{aligned} \tag{2.88}$$

since the diffusion propagator is diagonal on the considered basis.

Several properties of the field autocorrelation are worth remarking. First of all, the limits

$$\left\langle 0\left|B^2\right|0\right\rangle = \lim_{t\to 0}\langle B_t B_0\rangle = \overline{B^2} \tag{2.89a}$$

$$\langle 0|B|0\rangle^2 = \lim_{t\to\infty}\langle B_t B_0\rangle = 0. \tag{2.89b}$$

Second, the $\langle B_t B_0\rangle$ is a non-negative and monotonically decreasing function of time. It is also easy to see that correlation is always lost at a rate that is faster than or equal the rate of the lowest diffusion mode excited by the field, i.e., $\langle B_t B_0\rangle \leq \overline{B^2}e^{-D_0\lambda_1^{*2}t}$. Furthermore[15],

$$\begin{aligned}\left.\frac{\mathrm{d}}{\mathrm{d}t}\langle B_t B_0\rangle\right|_{t=0} &= -D_0\sum_n |B_{0n}|^2\lambda_n^2 \\ &= \frac{D_0}{V_0}\int_\Omega \mathrm{d}^3\boldsymbol{X}\, B(\boldsymbol{X})\nabla^2 B(\boldsymbol{X}) = -D_0\overline{|\nabla B|^2}.\end{aligned} \tag{2.90}$$

It is also possible to identify a measure to the amount of dephasing imposed by a given field configuration over time through definition of the so-called **field scattering kernel**[118]

$$\left\langle \Delta B^2(t)\right\rangle \equiv \frac{1}{2}\left\langle \left(B(\boldsymbol{X}_t) - B(\boldsymbol{X}_0)\right)^2\right\rangle = \overline{B^2} - \langle B_t B_0\rangle, \tag{2.91}$$

notice the second identify follows directly from expansion of the squared variation. Accordingly, the typical rate of dephasing is starts from zero and monotonically reaches a plateau defined by $\overline{B^2}$

Back to the matter at hand, it is seen that signal decay is dominated by the second

[15] There are couple subtleties related to Eq.(2.90). Though the final identity holds for the actual dephasing field, the previous one is in fact defined in terms of the representation of $B(\boldsymbol{X})$ in the Neumann-Laplace basis. The two fields are equal almost everywhere[105], that is, their difference determines a function of zero measure on Ω. Particularly, the fields must differ drastically on the domain boundary, where the normal derivative of the representation must vanish identically while the actual field must satisfy the necessary continuity requirements imposed by Maxwell equations.

spin phase moment in the weak encoding regime. An useful *ansatz* therefore is to assume decay is in fact governed **only** by this term, that is,

$$\begin{aligned}\left\langle e^{-i\phi_t}\right\rangle &= 1-\gamma^2\int_0^t \mathrm{d}\,t_2\int_0^{t_2}\mathrm{d}\,t_1 f(t_2)f(t_1)\left\langle B_{t_2-t_1}B_0\right\rangle + \ldots \\ &\equiv \exp\left[-\gamma^2\int_0^t \mathrm{d}\,t_2\int_0^{t_2}\mathrm{d}\,t_1 f(t_2)f(t_1)\left\langle B_{t_2-t_1}B_0\right\rangle\right]\end{aligned} \tag{2.92}$$

so it behaves as if the spin phase process were normal. This association encapsulates the **Gaussian phase approximation**, which has been frequently used to account for signal behavior in general pulsed field gradient sequences[43,46].

Finally, if the dephasing field is the product of externally applied gradients, then $B(\boldsymbol{X}) = \boldsymbol{g}\cdot\boldsymbol{X}$ and the autocorrelation function becomes proportional to correlations of the position process. Namely,

$$\left\langle B_t B_0\right\rangle = \sum_{jk} g_j g_k \left\langle X_{t,j}X_{0,k}\right\rangle, \tag{2.93}$$

which shows that changing the direction of the applied gradient allows investigation of the influence of confinement in distinct directions. This flexibility is particularly important in studies concerned with the characterization of geometrical features of porous media or soft matter as it allows among other things the identification of statistical anisotropy.

A great deal of structural information is provided by position correlations (see Section 2.4); in practice, they encompass the basic objective of NMR diffusion studies. However, as it is now obvious from the look of Eq.(2.92), the relation between restricted diffusion characteristics and actually measured quantities can be quite involved. In spin echo-based sequences, for example, echo amplitude is generally profoundly dependent on sequence parameters. Incidentally, for such sequences, echo attenuation is determined exclusively by the field scattering kernel, provided the rephasing condition is always satisfied. This result follows from Eq.(2.92) directly, as

$$\left\langle e^{-i\phi_t}\right\rangle = \exp\left[\frac{\gamma^2}{2}\int_0^t \mathrm{d}\,t_2\int_0^{t_2}\mathrm{d}\,t_1 f(t_2)f(t_1)\left\langle \Delta B^2(t_2-t_1)\right\rangle\right], \tag{2.94}$$

since $e^{-\frac{\gamma^2}{2}\overline{B^2}F(t)^2} = 1$ under rephasing.

Apparent diffusion coefficients (ADC)

Through the GPA, it is possible to isolate, somewhat, the effects of confinement from other operational aspects. The basic idea is to take the exact Gaussian behavior of unrestricted diffusion as reference and compare to it the attenuation of a restricted case. An effective characterization of reflected diffusion can then be given through the definition of **apparent diffusion coefficients**,

$$\mathcal{D}_{jk}(t) \equiv \frac{\int_0^t \mathrm{d}\, t_2 \int_0^{t_2} \mathrm{d}\, t_1 f(t_2) f(t_1) \left\langle X_{t_2-t_1,j} X_{0,k} \right\rangle}{\int_0^t \mathrm{d}\, t' F(t')^2}. \tag{2.95}$$

Notice how the expression above generalizes the Einstein-Smoluchowski equation, $D_0 \delta_{jk} = \langle X_{t,j} X_{0,k} \rangle / 2t$, by recalling that the dominator follows from the integral relation in the numerator provided the position autocorrelation is assumed to be that of a Gaussian process (see Eq.(2.62) and assume rephasing).

In the simplest scenario, confinement cannot break the rotational symmetry of position autocorrelations, so a single ADC characterizes diffusion in the considered medium and

$$\left\langle e^{-i\phi_t} \right\rangle = e^{-\mathcal{D}(t) b(t)}, \tag{2.96}$$

wherein

$$b(t) = -\gamma^2 |\boldsymbol{g}|^2 \int_0^t \mathrm{d}\, t' F(t')^2 \tag{2.97}$$

denotes the so-called **b-value** of the sequence.

It is important to stress the fact that ADC do not only depend upon acquisition times, which may lead to confusion with **time-dependent diffusion coefficients** (see Section 2.4), but also are particular of the considered NMR sequence. They introduce a multitude of characterizations for diffusion, restricted to a given domain, that are not in general equivalent. An illuminating review of these aspects is provided by Grebenkov[45].

The effects of surface relaxation

Surface relaxation can complicate the above analysis greatly. For a Robin-Laplace operator, $e^{-D_0 \Lambda^2 t}$ is no longer diagonal on the Neumann basis. As a result, the zero order term introduces a non-exponential decay, the first order MCF becomes time-dependent, even though $\bar{B} = 0$, and higher MCF exhibit a much more involved time-dependence than otherwise.

Fortunately, in many actual pore structures, surface relaxation can be considered a weak decay mechanism when compared to nuclear spin dephasing due to diffusion under field inhomogeneities. As demonstrated on Appendix C, if surface relaxivity is sufficiently small, it is reasonable to retain its effect only in the eigenvalue structure of the Laplace operator while leaving the eigenfunction set unaltered, because higher order corrections to signal decay are small compared to unity. This amounts to a zero-order approximation of $e^{-D_0\Lambda^2 t}$ in which only secular behavior is considered. More importantly,

$$e^{-D_0\Lambda^2 t}\left|0\right\rangle = e^{-\bar{\rho}\frac{S_0}{V_0}t}\left|0\right\rangle, \tag{2.98}$$

in which $\bar{\rho}$ denotes the mean surface relaxivity, and

$$\left\langle e^{-i\phi_t}\right\rangle = e^{-\bar{\rho}\frac{S_0}{V_0}t}\left\langle e^{-i\phi_t}\right\rangle_{\rho=0}, \tag{2.99}$$

resulting from substitution of the above on moment expansion of $\left\langle e^{-i\phi_t}\right\rangle$[16].

2.4 Displacement correlation functions

Diffusion studies were originally proposed[107] and continue to be performed under a linear field inhomogeneity; the field gradient, $\boldsymbol{g}$, is assumed sufficiently strong to govern encoding completely (if the susceptibility contrasts within the sample are not too great, it is even possible to satisfy simultaneously this condition and the weak strength requirements of the GPA). This typical set-up makes position correlation functions particularly relevant for the understanding of NMR decay or, conversely, make NMR diffusion methods an useful resource for probing Brownian motion characteristics. In view of Eq.(2.94) and the fact that common diffusion techniques are spin echo-based, mean squared displacements (MSD) or, more generally, displacement correlation functions are, however, more adequate for signal interpretation and description. The statistical information contained in the two sets of functions is, of

[16]In fact, there is a subtlety regarding Eq.(2.99), for all eigenvalues of the Neumann-Laplace operator pick up a correction term associated with the surface relaxivity field. Therefore, $\left\langle e^{-i\phi_t}\right\rangle_{\rho=0}$ is not strictly identical to the characteristic function of purely reflected case. However, such corrections present no source of difficulty in the analysis and contribute negligibly to the decay of superior modes, given the approximation. Thus, for analytical purposes, the identification is reasonable and Eq.(2.99) is justified.

course, identical, as

$$\frac{1}{2}\left\langle \left(\boldsymbol{X}_t - \boldsymbol{X}_0\right)_j \left(\boldsymbol{X}_t - \boldsymbol{X}_0\right)_k \right\rangle = \langle X_{0,j} X_{0,k}\rangle - \langle X_{t,j} X_{0,k}\rangle \,. \tag{2.100}$$

For a domain Ω, not necessarily bounded, displacement correlations make up a second order tensor whose matrix components are determined by

$$\langle \Delta X_j(t) \Delta X_k(t)\rangle = \int_\Omega \mathrm{d}^3\boldsymbol{X} \int_\Omega \mathrm{d}^3\boldsymbol{X}_0 \, \Delta X_j \, \Delta X_k \, G_t(\boldsymbol{X}, \boldsymbol{X}_0) P(\boldsymbol{X}_0), \tag{2.101}$$

wherein $\Delta X_j = \left(\boldsymbol{X} - \boldsymbol{X}_0\right)_j$ denotes the j Cartesian component of the displacement vector.

By time differentiation of the above identity and using the fact G_t is a solution of the diffusion equation, it follows that

$$\begin{aligned}
\frac{\mathrm{d}}{\mathrm{d}t}\langle \Delta X_j(t) \Delta X_k(t)\rangle =& D_0 \int_\Omega \mathrm{d}^3\boldsymbol{X} \int_\Omega \mathrm{d}^3\boldsymbol{X}_0 \, \Delta X_j \, \Delta X_k \, \nabla^2_{\boldsymbol{X}} G_t(\boldsymbol{X}, \boldsymbol{X}_0) P(\boldsymbol{X}_0) \\
=& D_0 \int_\Omega \mathrm{d}^3\boldsymbol{X}_0 \, P(\boldsymbol{X}_0) \left[\int_\Omega \mathrm{d}^3\boldsymbol{X} \, 2\delta_{jk} \, G_t(\boldsymbol{X}, \boldsymbol{X}_0) \right. \\
&+ \int_{\partial\Omega} \mathrm{d}S \, \Delta X_j \, \Delta X_k \frac{\partial}{\partial \boldsymbol{n}} G_t(\boldsymbol{X}, \boldsymbol{X}_0) \\
&\left. - \int_{\partial\Omega} \mathrm{d}S \, G_t(\boldsymbol{X}, \boldsymbol{X}_0) \frac{\partial}{\partial \boldsymbol{n}} \left(\Delta X_j \, \Delta X_k\right) \right],
\end{aligned} \tag{2.102}$$

the last line resulting from Green's theorem and the fact $\nabla^2_{\boldsymbol{X}} \left(\Delta X_j \, \Delta X_k\right) = 2\delta_{jk}$.

If diffusion is purely reflected, then the above equation reduces to

$$\frac{\mathrm{d}}{\mathrm{d}t}\langle \Delta X_j(t) \Delta X_k(t)\rangle = 2D_0\delta_{jk} - 2\frac{D_0}{V_0} \,\mathrm{Sym}\left[\int_{\partial\Omega} \mathrm{d}S \, n_j(\boldsymbol{X}) \, \langle \Delta X_k(t)\rangle_{\boldsymbol{X}} \right]. \tag{2.103}$$

The function Sym [ ] returns the symmetrical part of the argument; $n_j(\boldsymbol{X})$ denotes a normal vector component at the surface point $\boldsymbol{X}$ and

$$\langle \Delta X_k(t)\rangle_{\boldsymbol{X}} = \int_\Omega \mathrm{d}^3\boldsymbol{X}_0 \, \Delta X_k G_t(\boldsymbol{X}, \boldsymbol{X}_0) H(\boldsymbol{X}_0) \tag{2.104}$$

corresponds to the mean displacement of the particles that reach the boundary point $\boldsymbol{X}$ at time t.

The important result implied by Eq.(2.103) is that the time-dependence of displacement correlations, in general, does not follow the simple Einstein-Smoluchowski

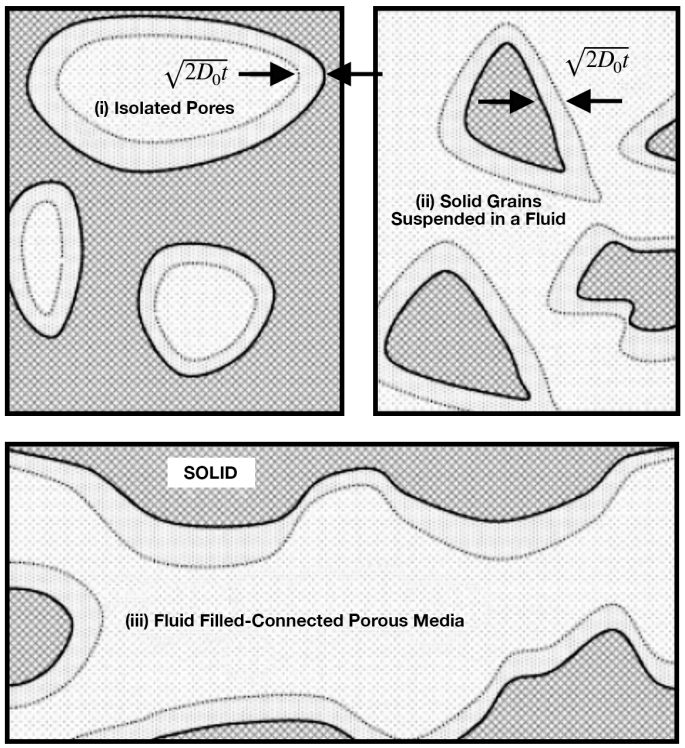

Figure 2.3: Three scenarios of short-time behavior: (i) isolated pores, (ii) a suspension and (iii) a well-connected pore structure (Extracted from Sen [92])

relation, that is, $\langle \Delta X_j(t) \Delta X_k(t) \rangle \neq 2D_0\, t\, \delta_{jk}$. Geometry enforces correlations between displacement components as a result of collisions with boundaries; furthermore, the behavior of these correlations is directly affected by how many of the diffusing particles can actually reach the confining walls over the time of observation, a notion to which Kac refers as **the principle of not feeling the boundary** [59].

The argument is quite simple. Notice that if t is small, the diffusion propagator must be sharply distributed about $\boldsymbol{X}$, a boundary point. The small dispersion means that just the particles really close to the boundary, say, within a radius proportional to $\sqrt{D_0 t}$ of $\boldsymbol{X}$, can effectively contribute in the integral defining $\langle \Delta X_k(t) \rangle_{\boldsymbol{X}}$, see Fig.2.3. Consequently, the mean particle displacement can only reflect local features of the nearest enclosing geometry, like the very presence of a wall, its curvature and so on. In fact, one may regard the diffusion propagator in Eq.(2.104) as a sort of time-dependent spatial filter that progressively accounts for more distant elements of the domain.

For example, let Ω have a smooth boundary and be bounded, so $H(\boldsymbol{X})$ can be

made equal to 1, and assume t is so short that the characteristic diffusion length scale, $\sqrt{D_0 t}$, is smaller than the typical radius of curvature of the confining walls. Over such time scale, the particles that are able to reach a boundary point do so unhampered by any geometric feature of the domain, as a result,

$$\langle \Delta X_k(t) \rangle_{\boldsymbol{X}} \sim -\sum_m (\boldsymbol{e}_m(\boldsymbol{X}) \cdot \boldsymbol{e}_k) \int_{x_3>0} \mathrm{d}^3 \boldsymbol{x}\, x_m\, g_t(\boldsymbol{x}, \boldsymbol{0}), \tag{2.105}$$

in which g_t denotes the diffusion propagator to the associated plane wall problem and $\{\boldsymbol{e}_m(\boldsymbol{X})\}$ comprise a unit vector system related to the local surface coordinate frame. The propagator for such a simple problem is found quite easily through the method of images[29] and, as it turns out, implies that

$$\begin{aligned} \langle \Delta X_k(t) \rangle_{\boldsymbol{X}} &\sim -(\boldsymbol{e}_3(\boldsymbol{X}) \cdot \boldsymbol{e}_k) \int_0^\infty \mathrm{d}x_3\, x_3\, \frac{1}{\sqrt{\pi D_0 t}} e^{-\frac{x_3^2}{4D_0 t}} \\ &= (\boldsymbol{n}(\boldsymbol{X}) \cdot \boldsymbol{e}_k) \sqrt{\frac{4D_0 t}{\pi}} \int_0^\infty \mathrm{d}y\, e^{-y}, \end{aligned} \tag{2.106}$$

since $\boldsymbol{n} = -\boldsymbol{e}_3$ by construction. Accordingly, for sufficiently small times, Eq.(2.103) implies

$$\frac{\langle \Delta X_j(t) \Delta X_k(t) \rangle}{2D_0 t} \sim \delta_{jk} - \frac{4}{3}\sqrt{\frac{D_0 t}{\pi}} \frac{1}{V_0} \int_{\partial\Omega} \mathrm{d}S\, n_j(\boldsymbol{X}) n_k(\boldsymbol{X}). \tag{2.107}$$

By taking the trace of the above, the short-time behavior of mean squared displacements is also derived (recall $\sum_j n_j^2 = 1$)

$$\frac{\langle |\Delta \boldsymbol{X}(t)^2| \rangle}{6D_0 t} \sim 1 - \frac{4}{9\sqrt{\pi}} \frac{S_0}{V_0} \sqrt{D_0 t}, \tag{2.108}$$

which shows deviation from unrestricted Gaussian behavior is apparent already at vanishingly small times.

It is possible to carry more advanced asymptotic analyses of displacement correlation functions. The next order correction introduces the effect of boundary local curvature on the calculation of mean particle displacements. The methodology is exactly the same, but calculations are much more involved because of the form of new approximate diffusion propagator which necessarily introduces correlations between displacement components. The result is derived by Mitra *et al.*[80] and presented here,

without proof, for completeness of exposition:

$$\frac{\langle|\Delta \boldsymbol{X}(t)^2|\rangle}{6D_0 t} \sim 1 - \frac{4}{9\sqrt{\pi}}\frac{S_0}{V_0}\sqrt{D_0 t} - \frac{\bar{H}}{6}\frac{S_0}{V_0}D_0 t, \tag{2.109}$$

in which

$$\bar{H} = \frac{1}{S_0}\int_{\partial\Omega} \mathrm{d}S\ \frac{\kappa_1 + \kappa_2}{2} \tag{2.110}$$

denotes the surface average of mean curvature of the boundary.

The practical importance of displacement correlation functions is now abundantly clear. Observation of these quantities allows estimation of several relevant geometric features of the confining structure: Surface-to-volume ratio (independently of surface relaxivity), mean boundary curvature, volumetric dispersion coefficient or diffusion tortuosity (in the limit $t \to \infty$ respectively for bounded and unbounded domains[92]) and geometry-induced anisotropy characteristics.

Finally, in the NMR literature, it is much more common to express MSD or displacement correlation functions in terms of **time-dependent diffusion coefficients** (TDC) which are simply defined as

$$D_{jk}(t) \equiv \frac{\langle \Delta X_j(t) \Delta X_k(t)\rangle}{2D_0 t}. \tag{2.111}$$

In contrast to ADC, which are sequence-dependent and really just useful provided the GPA is valid, TDC reproduce definite statistical characteristics of the reflected Brownian motion.

2.5 The narrow pulse approximation (NPA)

The presented *head-on* approach to the problem of characterizing NMR signal decay for arbitrary sequences is quite modern. Traditionally, the problem of solving the Bloch-Torrey equation was circumvented by devising sequences in which field inhomogeneities are applied over times so short that it is reasonable to neglect diffusion altogether during encoding blocks. This idea comprises today what is known as the **narrow pulse approximation** (NPA) and it was so important in early diffusion studies that it virtually made **pulsed field gradient** (PFG) techniques synonymous to NMR diffusion methods.

If diffusive transport is neglected in Eq.(2.14), it follows that the nuclear transverse

magnetization simply picks up a phase factor

$$M(\boldsymbol{X},t) = \exp\left[-i\gamma \int_{t_0}^{t} \mathrm{d}\, t' b_z(\boldsymbol{X},t')\right] M(\boldsymbol{X},t_0) \tag{2.112}$$

over the time the dephasing field is left on. Specifically in the context of uniform gradient techniques, the phase factor simplifies to

$$\exp\left[-i\gamma\Delta t\,(\boldsymbol{g}\cdot\boldsymbol{X})\right],$$

provided the external field inhomogeneity completely dominates the encoding.

Thus, the nuclear magnetization at the end of a piecewise constant encoding sequence, like most PFG, can determined explicitly if the NPA is valid on actual encoding blocks. This is the principal quantitative aspect of the NPA.

Consider, for example, the original Stejskal and Tanner PFG sequence[107], whose effective temporal profile is defined by

$$f(t) = \begin{cases} 1, & 0 < t < \delta \\ 0, & \delta < t < \tau + \delta \\ -1, & \tau + \delta < t < \tau + 2\delta \end{cases} \tag{2.113}$$

and assume δ is sufficiently small, so the NPA is valid. Then by the end of the sequence the nuclear magnetization will be

$$M(\boldsymbol{X},t) = e^{i\boldsymbol{q}\cdot\boldsymbol{X}} \int_{\Omega} \mathrm{d}^3\boldsymbol{X}_0\, G_\tau(\boldsymbol{X},\boldsymbol{X}_0) e^{-i\boldsymbol{q}\cdot\boldsymbol{X}_0} M(\boldsymbol{X}_0,0), \tag{2.114}$$

wherein $\boldsymbol{q} = \gamma\delta\boldsymbol{g}$, consequent to the fact diffusion proper can only happen over the medium block which has duration τ. Furthermore, as a result of rephasing, an echo is

formed precisely at $t = \tau + 2\delta$ if no other sources of field inhomogeneity are present[17]. The echo amplitude corresponds to the total magnetic moment at the instant of its formation, so

$$E_{\boldsymbol{q}}(t) = \frac{1}{V_0}\int_\Omega \mathrm{d}^3\boldsymbol{X} \int_\Omega \mathrm{d}^3\boldsymbol{X}_0\, G_t(\boldsymbol{X},\boldsymbol{X}_0) e^{i\boldsymbol{q}\cdot(\boldsymbol{X}-\boldsymbol{X}_0)} \tag{2.115}$$

after normalization (notice the difference between t and τ can be neglected provided δ is small).

The NPA implies that the Fourier transform of a diffusion propagator is experimentally accessible and, consequently, the diffusion propagator itself could be, in principle, observed through exhaustive experimentation. More immediately, displacement correlation functions and TDC can be obtained directly from the data, for

$$\langle \Delta X_j(t)\Delta X_k(t)\rangle = -\lim_{\boldsymbol{q}\to 0} \frac{\partial^2}{\partial q_i \partial q_j} \ln E_{\boldsymbol{q}}(t) \tag{2.116}$$

and structural form-factors can be measured from the long-time behavior, as

$$E_{\boldsymbol{q}}(t) \longrightarrow \left| \frac{1}{V_0}\int_\Omega \mathrm{d}^3\boldsymbol{X}\, e^{i\boldsymbol{q}\cdot\boldsymbol{X}} \right|^2 \tag{2.117}$$

is implied by $\lim_{t\to\infty} G_t(\boldsymbol{X},\boldsymbol{X}_0) = 1/V_0$.

It is important however to point out that all these results are only strictly valid in the formal limit of the NPA, namely, $\delta \to 0$ and $\boldsymbol{g} \to \infty$ in such a way that $\gamma\boldsymbol{g}\delta \to \boldsymbol{q}$, and that deviations from such an *ideal* behavior are commonplace in actual experimental procedure. Correcting for these is another area where the general methodology presented on this chapter can be of importance.

[17] Here, it is instructive to mark the distinction between stimulated and spin echo sequences. If, apart from excitation, the underlying field pulse protocol in a PFG sequence never switches between longitudinal and transverse magnetization, in other words, if nuclear magnetization remains on the transverse plane over the entire duration of the sequence, then, in practice, internal field inhomogeneities will also promote some spin encoding over the otherwise purely diffusive sequence block. Though most rephasing can occur at $t = \tau + 2\delta$, provided the external gradient dominates encoding, it will not be complete until $t = 2\tau$ when the decoding of internal field inhomogeneities is finished. As a result, for spin echo-based PFG, acquisition is programmed at longer times to account for this effect. But this means spin diffusion must be considered over the interval $\tau + 2\delta < t < 2\tau$ as well. These issues are avoided by slightly modifying Stejskal and Tanner's sequence. Nuclear magnetization can be, immediately after encoding, *stored* in the longitudinal axis, where field inhomogeneities play no part; spins are allowed to diffuse and are brought back to transverse plane for decoding and acquisition. Then, rephasing occurs precisely at the end of the sequence and it is said a stimulated echo is formed.

CHAPTER 3

Surface-induced relaxation

In this chapter, a theory to account for NMR relaxation of water protons in situations in which the fluid is confined to pore structures exhibiting a scarce distribution of paramagnetic centers on the internal surface is developed.

A paramagnetic center or site is considered generally to be any molecular configuration that is able to bear unpaired electrons. Common examples are adsorbed paramagnetic ions and superficial crystallographic defects, like those arising from substitution by a paramagnetic ion or forming electron traps. Although much of the stated and assumed here concerns the response of water, the model has sufficiently general features to explain **proton relaxation of other polar fluids** under similar conditions.

The predictions of the model are compared to experimental results. One of the main results presented here is the fact that the anisotropy introduced by the magnetic dipolar coupling in the relaxation rates of active surface elements induces a measurable orientation dependence in NMR signal decay of porous samples, provided their pore structure is not statistically isotropic; that is, pores typically exhibit some preferred directional trend. Many of these concepts are explained below. Measurements of T_1 proton relaxation on water saturating micrometrical capillary tubes are performed to reveal the effect. Finally, much of the content of this chapter was published as an article in *Physical Review E*, 99(4), 2019[83].

3.1 The general picture

There are many mechanisms by which solid walls can influence the NMR relaxation of a wetting fluid. Electron-nucleus **magnetic couplings**, introduced by the presence of just a few paramagnetic centers dilutely spread over the surface, are distinguished though for being relatively strong interactions that can effectively govern microscopic spin behavior and, thus, significantly enhance the macroscopically observed NMR decay[8,67,112].

Water under confinement is known to be characterized by two distinct *phases* in fast exchange of molecules: A surface-affected phase, whose thickness is determined by just a few molecular layers[31,36,38], and a bulk phase, in which fluid properties are virtually unchanged by the condition. The fact that surface-induced relaxation can be a macroscopically relevant process reveals the effectiveness of translational molecular diffusion as a transport phenomenon, as nuclear magnetization must be constantly restored at fast-relaxing regions to produce a noticeable effect.

The **intermolecular interaction** between centers and constituent fluid molecules may also be strong to the point that, within the surface-affected phase, coordination structures are retained[88], as in the case of an adsorbed metal-aquo complex, or newly formed[36]. This is in fact expected to be a general feature for polar fluids, whose molecules accordingly exhibit permanent **electric dipoles**, moving about the localized charge distributions of paramagnetic sites.

At these structures, the hyperfine interaction between electronic and nuclear magnetic moments is taken to be the dominant mechanism promoting nuclear relaxation. This follows from the fact large magnetic moments are introduced by the unpaired electrons of centers. Evidently such an influence is the strongest over molecules in direct coordination and falls rather fast with the distance from sites. Therefore, it is reasonable to assume that any relevant nuclear magnetization decay occurring at surface regions is attributable to the nuclear relaxation of these molecular assemblies. The more so, because experimental studies done on clean or cleaned structures, i.e., devoid of paramagnetic centers reveal a feeble increase on NMR relaxation rates[31,41].

In the context of NMR in porous media, this picture of nuclear spins *in coordination* was introduced by Kleinberg *et al.*[64] but it is instructive to point out that the same view is fundamental on the NMR relaxation theory of paramagnetic solutions[10,97].

3.1.1 The basic macroscopic framework

The model here considered fits in the somewhat phenomenological framework consolidated by Cohen and Mendelson[25]; accordingly, it is not required to assume **fast diffusion** at start. As a result, although molecular transport between surface and bulk phases is taken to be fast, its characteristic time scale is believed to be long compared to correlation times associated with the microscopic mechanisms that induce relaxation in either phase. Such hypothesis allows one to talk meaningfully of NMR relaxation in each phase and to consider it as separate process from molecular exchange. Bulk relaxation, therefore, is considered to be simple (satisfying a Bloch equation) as it is the case for water and many other polar fluids and, hence, all that is necessary to advance a comprehensive picture is a model for relaxation at surface-affected regions.

Recall from Chapter 2 that a balance of nuclear magnetization holds at every point of the domain, macroscopically associated with the pore space; namely,

$$\frac{\partial m_i}{\partial t} = -\frac{m_i}{\mathrm{T}_i} + D_0 \nabla^2 m_i \tag{3.1}$$

plus the boundary condition[25]

$$D_0 \frac{\partial m_i}{\partial \boldsymbol{n}} + \frac{\mathsf{h}}{\mathrm{T}_i^{(s)}} m + \mathsf{h} \frac{\partial m_i}{\partial t} = 0, \tag{3.2}$$

in which m_i again denotes the deviation from equilibrium value of either the (real) longitudinal magnetization or the (complex) transverse one; T_i and $\mathrm{T}_i^{(s)}$, the corresponding relaxation times of the bulk and surface phases; D_0 is the bulk self-diffusion coefficient of the fluid and $\boldsymbol{n}$, surface normal vector. The parameter h is a length scale associated with the extent of surface effects; it typically corresponds to the thickness of few molecular layers, thus lies in the order of the nanometer. For this reason, the last term in the boundary condition can be neglected whenever one is concerned exclusively with macroporous media and, then, the whole problem reduces to the class discussed in the works of Brownstein and Tarr[16,17], though their treatment presupposes an uniform surface relaxivity. .

The time scale of molecular exchange has been removed from the above model via a limiting process, but its order of magnitude is nevertheless important for establishing what microscopically must constitute a surface element. In particular, an assessment about the size of surface elements is indispensable for modeling surface-

induced relaxation from first principles; a point soon to be made clearer.

Estimations of the rate of molecular exchange, or equivalently, of the mean time of adherence of molecules to surfaces are difficult. Cohen and Mendelson [25] offer the number 10^{10} protons per second in the cited work, but fail to mention how one can reach such a figure, apart from suggesting it is probably based on non-equilibrium considerations. A rather strict estimate can be provided in the case of gases by resorting to the kinetic theory and it leads to the impressive number of 10^{13} particles per second[1]. Recently with the advent of molecular dynamic simulation, the exchange rates can determined numerically. Faux *et al.* [36] report values raging from 10^8 to 10^{10} water molecules per second, depending on surface affinity, in their study on model cementitious materials.

Lacking more accurate estimations, the nanosecond is assumed as the reference time scale and so it can be argued that if the mean adherence time of molecules to a surface element is in that order, then the time scale in which major changes of nuclear magnetization occur in the bulk phase, due to diffusive transport, must be of the same magnitude. Since a molecule in bulk covers a distance roughly proportional to $\sqrt{D_0 t}$ over a time t, it is possible to estimate the length scale of the finest nuclear magnetization heterogeneities in the bulk phase; roughly, something in the order of nanometers for liquid water.

To repeat the argument: Changes in magnetization that occur over a time in the order of a nanosecond can only be effectively homogenized by diffusion over nanometric distances. Therefore, surface elements must be approximately that long in lateral extent, provided they are simply defined as molecular systems which exchange nuclear spin with the bulk and can potentially answer for the smallest of scale of nuclear magnetization heterogeneities.

It is important to point out that **coordination structures** appear in the molecular dynamic simulations and their lateral span seems to be about 0.5 nm in the case of water molecules orbiting Ca^{2+} ions [36][2]. Simulations also confirm that diffusive transport **along** the surface is negligible when compared to molecular transfers with the bulk phase. This is perhaps to be expected from the experimental studies done on cleaned porous media, otherwise a truly minute distribution of paramagnetic centers could still greatly influence signal decay.

[1] The calculation was done by myself and it is based on effusion rates

[2] For reference, it is perhaps instructive to point out that both water molecules and calcium ions define particularly small particles, with diameters in the order of 1 angstrom.

For those reasons, it is here assumed that a mathematical surface element physically corresponds to nanometric regions which are either entirely comprised of a single paramagnetic center accompanied by a molecular **coordination complex**, in which case defining an **active element**, or which are completely devoid of such structures, thereby an inactive patch.

As it turns out, given the nature of the dominant mechanism for relaxation, NMR decay in active surface elements is proved to be simple; any exchange between surface elements can be neglected and so all requisites for Eq.(3.2) are met.

On the other hand, estimations of ion concentration at the surface of silicon based materials indicate that surface coverages[3] typically range from 10^{-4} to 10^{-2}. This suggests active patches can only respond to nearly one per cent of the entire available surface. As a result, surface relaxivity must be effectively regarded as function of boundary points that assumes relatively low values at inactive portions, which are nonetheless frequent, and spikes up upon crossing the comparatively scarce active surface elements.

Such intrinsic heterogeneity is the primary distinction of the considered model. Typically, surface relaxivities are assumed uniform, based on material homogeneity or on effective surface transport. As discussed, however, these hypotheses seem to be unrealistic in materials in which surface-induced relaxation is dominated by the presence of paramagnetic centers.

3.2 Surface relaxation rates

The relaxation rate of an active surface element can be modeled from first principles disregarding completely the effects of molecular exchange because of the separation of time scales.

Microscopically, every active element is associated to an ensemble of nuclear spins that hover about the paramagnetic center in such a way that particle motion is confined to a spherical cap. The imposed geometrical constraint is clearly an abstraction; nonetheless, one that is assumed to capture the most important geometrical features of molecular configurations at that scale.

[3]The ratio of occupied surface sites per total site number. It is important to remark that just as 3D crystalline structures, physical surfaces also display lattice arrangements wherein cells (from the point of view of the solid) or sites (from the standpoint of a fluid phase) can be identified. The typical concentration of surface sites in a solid wall is 10^{15} per cm^2.

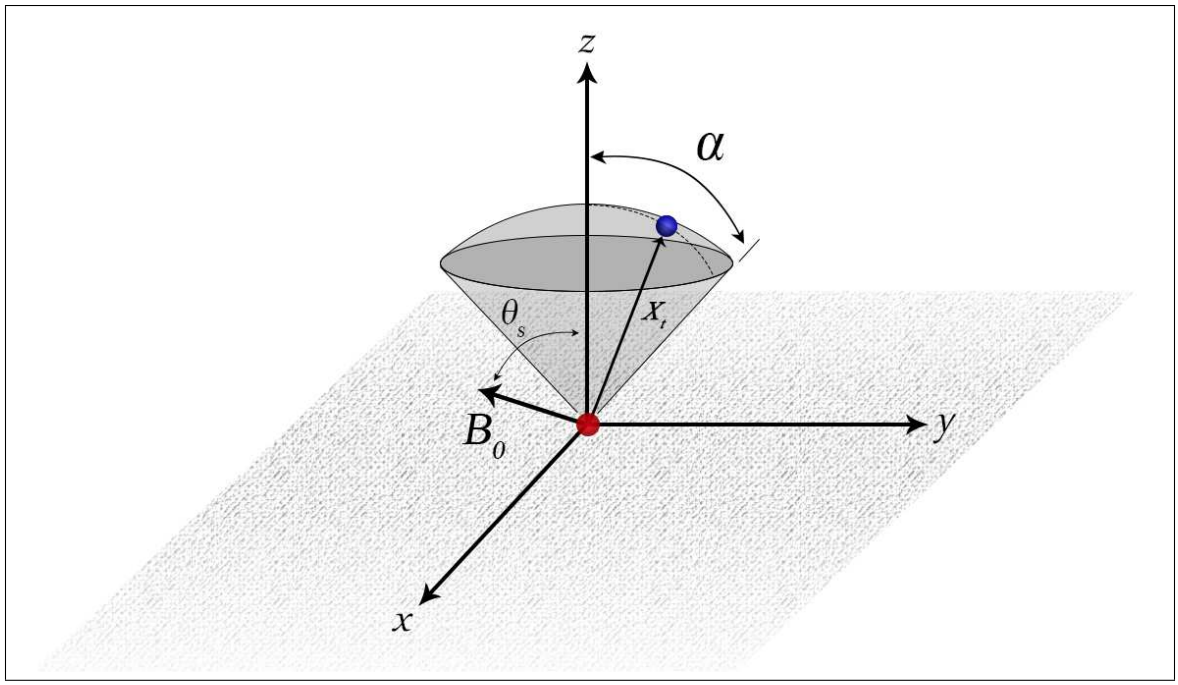

Figure 3.1: Schematic of constraints for the dynamic model. A considered nuclei is represented as a blue dot and is constrained to move along the spherical cap of aperture 2α. The red dot highlights a paramagnetic center embedded on a solid boundary whose inclination with respect to the externally applied magnetic field, B_0, is θ_s.

For simplicity, the axis of the cone subtended by the spherical cap is taken to be parallel to surface element (macroscopic) normal vector and all elements are assumed identical in this structure, which is illustrated in Fig.3.1.

Since molecular motion is constrained by the presence of solid walls, a reasonable requirement is that the aperture of the cap is less than 360 degrees; apertures larger than 180 degrees could in principle be evoked to account for sites constituted of adsorbed complexes.

To the desired level of description, it is not necessary to advance a more detailed definition of the molecular structures that actually comprise an active spin ensemble. Obviously, complexed molecules, if there are any, contribute with their nuclear spins and hence provide a good example of structural element. However, the model does not need to be exclusively associated with a single type of molecular configuration.

For instance, Faux et al.[36] report the occurrence of rings of water molecules flanking adsorbed Ca^{2+} ions just as close to the considered centers as formally complexed molecules. The authors attribute these structures to a cooperative movement of molecules controlled by the ion's influence. This suggests that, whatever the way

polar molecules assemble themselves around a paramagnetic center, the spherical cap model can reasonably well represent the actual region in which a considered nuclear species dwells.

The hyperfine interaction between nuclear spins and the magnetic moment of the paramagnetic center is taken to be the dominant mechanism promoting surface relaxation at active elements. Any magnetic interaction between nuclei can be neglected due to the fact electron magnetic moments are much larger than nuclear moments (recall that the gyromagnetic ratio of electrons is approximately 658 times larger than that of protons)[1]. The assumption is useful because it effectively uncouples nuclear spins within the ensemble and, incidentally, allows one to dismiss all two-particle correlations and to treat the motion of any single nucleus effectively.

As a result, though nuclear wobbling is consequent to complex intermolecular and intramolecular interactions, the actual nature of this motion is immaterial; all that is needed is a satisfactory representation of the motion itself. This is precisely where abstractions, such as the spherical cap model, become important.

Accordingly, the coupling potential of a nucleus to a paramagnetic center can compactly written as

$$V = -\gamma\hbar \boldsymbol{I} \cdot \mathbf{b} \tag{3.3}$$

wherein $\boldsymbol{I}$ is the nuclear spin operator and $\mathbf{b}$, the local field generated by the electronic moments at the position of the nucleus. The operators involved in the definition of $\mathbf{b}$ have a much faster dynamics than the nuclear spin operators and are effectively independent of nuclear spin history. Hence, the NMR relaxation at a surface element follows a Bloch equation and is characterized by local rates,[1,96]

$$\frac{1}{\mathrm{T}_1} = \frac{\gamma^2}{2} J_1(\omega_0) \tag{3.4}$$

and

$$\frac{1}{\mathrm{T}_2} = \frac{\gamma^2}{4} \left(J_0(0) + J_1(\omega_0) \right) \tag{3.5}$$

wherein the functions $J_q(\omega)$ represent the Fourier transforms of local field correlations:

$$\Gamma_q(t) = \left\langle \Delta b_q^\dagger(t) \Delta b_q(0) \right\rangle \tag{3.6}$$

and b_q denotes the **spherical component** of the local field operator relative to a system whose $\mathbf{e}_0$-axis coincides with the direction of the externally applied static field

$\boldsymbol{B}_0$, thus, the lab frame.

It must be remarked that the expectations above are fundamentally quantum equilibrium averages, that is, defined by a Boltzmann-Gibbs density operator. This consequently introduces the Hamiltonian of the nuclear spin environment, H_E, and the statistical temperature, β, associated with such system into the description. H_E typically depends on a vast set of variables, among which are the position of the nucleus and the electronic spin pertaining to the paramagnetic center.

The **deviation from equilibrium value** of the local field component is indicated by Δb_q. A local static field contribution, $\langle \mathbf{b} \rangle$, is to be expected from the stationary character of the spin environment and its anisotropic configuration. In fact, the dominant nuclear spin Hamiltonian to be associated with a surface element (to which ΔV is the perturbation inducing relaxation) is

$$\mathcal{H}_Z = -\gamma \hbar \boldsymbol{I} \cdot (\boldsymbol{B}_0 + \langle \mathbf{b} \rangle) \tag{3.7}$$

but, once again, (reference chapter I) as $|\langle \mathbf{b} \rangle|$ is typically small compared to B_0, only the parallel component $\langle b_0 \rangle$ needs to be considered. The presence of such a term corresponds to a first order frequency shift of magnitude $\gamma \langle b_0 \rangle$ that can affect transverse nuclear magnetization of surface elements. Consequently, when considering surface effects in NMR relaxation via Eq.(3.2), such a shift should be incorporated explicitly in the expression for surface relaxivity which is then defined by an expression like $h/\mathsf{T}_2^{(s)} + ih\gamma \langle b_0 \rangle$. Therefore, transverse surface relaxivities are not necessarily real[4].

3.2.1 The microscopic local field

Upon averaging out the effects of electronic motion, the local field at a nucleus position is assumed to be dominated by a dipolar coupling with the total spin, $\boldsymbol{S}$, of the paramagnetic center (see Appendix D). As a result,

$$\mathbf{b}(\boldsymbol{X}) = \frac{\mu_0}{4\pi} \frac{\gamma_e \hbar}{|\boldsymbol{X}|^3} \left(3 \frac{\boldsymbol{S} \cdot \boldsymbol{X}}{|\boldsymbol{X}|^2} \boldsymbol{X} - \boldsymbol{S} \right) \tag{3.8}$$

[4]Imaginary surface relaxivity components can introduce some interesting effects in the dynamics of nuclear magnetization by effectively coupling real and imaginary transverse magnetization components.

or, as it is convenient for calculation, by introducing a spherical basis that refers to the lab frame,

$$\mathsf{b}_q(\boldsymbol{X}) = \frac{\mu_0}{4\pi}\gamma_e\hbar\sum_{q'} C_{qq'}\mathsf{D}_{q-q'}(\boldsymbol{X})S_{q'} \tag{3.9}$$

in which $\mathsf{D}_q(\boldsymbol{X}) = \frac{Y_2^q(\boldsymbol{X})}{|\boldsymbol{X}|^3}$; $\boldsymbol{X}$ denotes the position of the nucleus and $Y_2^q(\boldsymbol{X})$ is the second rank spherical harmonic component associated with the nucleus position operator. The numerical matrix $C_{qq'}$ is introduced in order to normalize these spherical harmonic operators and its components are defined by the expression

$$C_{qq'} = (-1)^{q'}\sqrt{\frac{4\pi}{5}}\left(\delta_{0q}\delta_{0q'} + \sqrt{\frac{1}{2^{|q-q'|}}\frac{(2+|q-q'|)!}{(2-|q-q'|)!}}\right). \tag{3.10}$$

Thus,

$$\begin{aligned}\langle\mathsf{b}_q\rangle &= \frac{\mu_0}{4\pi}\gamma_e\hbar\sum_{q'} C_{qq'}\left\langle\mathsf{D}_{q-q'}(\boldsymbol{X})S_{q'}\right\rangle \\ &= \frac{\mu_0}{4\pi}\gamma_e\hbar\sum_{q'} C_{qq'}\left\langle\mathsf{D}_{q-q'}\right\rangle\left\langle S_{q'}\right\rangle\end{aligned} \tag{3.11}$$

for it is reasonable to assume that nucleus position is virtually uncoupled from the spin of the paramagnetic center, i.e., the physical processes that govern the evolution of each set of variables are assumed to be uncorrelated. As for the field correlation functions

$$\begin{aligned}\Gamma_q(t) &= \left\langle\Delta b_q^\dagger(t)\Delta b_q(0)\right\rangle = \left\langle b_q^\dagger(t)b_q(0)\right\rangle - \left\langle b_q^\dagger\right\rangle\left\langle b_q\right\rangle \\ &= \left(\frac{\mu_0}{4\pi}\gamma_e\hbar\right)^2\sum_{q'q''} C_{qq'}C_{qq''}\left\langle S_{q'}(t)^\dagger\mathsf{D}_{q-q'}^\dagger(\boldsymbol{X}_t)\mathsf{D}_{q-q''}(\boldsymbol{X}_0)S_{q''}(0)\right\rangle - \left\langle b_q^\dagger\right\rangle\left\langle b_q\right\rangle \\ &= \left(\frac{\mu_0}{4\pi}\gamma_e\hbar\right)^2\sum_{q'q''} C_{qq'}C_{qq''}\left\langle\mathsf{D}_{q-q'}^\dagger(\boldsymbol{X}_t)\mathsf{D}_{q-q''}(\boldsymbol{X}_0)\right\rangle\left\langle S_{q'}(t)^\dagger S_{q''}(0)\right\rangle - \left\langle b_q^\dagger\right\rangle\left\langle b_q\right\rangle.\end{aligned} \tag{3.12}$$

As already pointed out, all expectations involved in the above expressions are fundamentally quantum equilibrium averages. The neglect of electronic variables other than the total spin moment and decoupling from nucleus position operators greatly simplifies calculation. However, to actually calculate the correlations, knowledge of the Hamiltonians that describe the dynamics of each separate set of variables is still required. It is assumed that such a detailed characterization of microscopic mech-

anisms is too involved for an usable description, therefore the true correlations are approximated by expectations derived from simpler models.

Dipolar tensor correlations

The dipolar tensor correlations are here modeled through the adoption of a stochastic dynamics for the position vectors of the nuclei. Such a practice is common in chemical modeling.

Since only nuclear spins on the immediate vicinity of the paramagnetic centers are considered, a random motion constrained to a spherical cap of fixed aperture and centered at the paramagnetic site should retain the essential features of the actual dynamics. This very same model was first suggested by Kleinberg *et al.*[64] to explain NMR relaxation of fluids in porous media. Their theory, however, is somewhat distinct from the one here considered, is only semi-quantitative, presupposes fast diffusion and has been applied only to statistically isotropic pore structures, i.e., structures in which no preferred orientation is exhibited by surface elements. As it turns out, a detectable dependence on sample orientation in NMR relaxation rates, a phenomenon here referred to as anisotropy of response, can be explained, through a more detailed and quantitative analysis, by the orientation dependence introduced by the dipolar coupling on the relaxation rates of surface elements, provided the porous medium is not statistically isotropic.

The angular dependence of field correlations follows directly from the fact that the dipolar tensor components, D_q, transform under rotations as spherical tensor components of second rank and, furthermore, because the correlations which are important for the NMR relaxation at surface elements are those referring in fact to the lab frame.

It is natural and easier, however, to consider similar correlations on the frame of symmetry of the surface element, that is, a frame whose $\mathbf{e}_0$-axis coincides with the surface normal at its position. The inclination of the surface normal with respect to the direction of the externally applied field, θ_S, becomes as a relevant parameter since[66]

$$\left\langle \mathsf{D}_q^\dagger(\boldsymbol{X}_t)\mathsf{D}_q(\boldsymbol{X}_0)\right\rangle = \sum_m |\mathsf{d}^{(2)}_{m,q}(\theta_S)|^2 \left\langle \bar{\mathsf{D}}_m^\dagger(\boldsymbol{X}_t)\bar{\mathsf{D}}_m(\boldsymbol{X}_0)\right\rangle \tag{3.13}$$

wherein the $\mathsf{d}^{(2)}_{m,q}$ denotes the Wigner d-matrix elements for the second rank and the bar implies spherical components refer to the surface element frame. The absence of correlations of the type $\left\langle \bar{\mathsf{D}}_m^\dagger(\boldsymbol{X}_t)\bar{\mathsf{D}}_{m'}(\boldsymbol{X}_0)\right\rangle$ with $m' \neq m$ is a consequence of

(assumed) rotational invariance of the nuclear system about the axis of the surface element[53]. This result in fact follows from symmetry assumptions on the actual nuclear motion: Eq.(3.13) is expected to hold for the correlations appearing in Eq.(3.12) regardless of dynamic modeling approximations, provided the Hamiltonian of the nuclear system has such an axial rotational invariance.

The mathematical problem of solving the rotational diffusion equation restricted to a spherical cap has already been throughly treated by other authors. The results here used are derived by Wang and Pecora[114]. Simply, the dipolar correlation functions in the frame of the surface are

$$\begin{aligned}
\left\langle \bar{\mathsf{D}}_0^\dagger(\boldsymbol{X}_t)\bar{\mathsf{D}}_0(\boldsymbol{X}_0)\right\rangle &= \frac{5}{4\pi R^6}\left(\Upsilon_0^{(0)}(\alpha)+\Upsilon_1^{(0)}(\alpha)e^{-\nu_0(\nu_0+1)\mathcal{D}_R|t|}\right),\\
\left\langle \bar{\mathsf{D}}_1^\dagger(\boldsymbol{X}_t)\bar{\mathsf{D}}_1(\boldsymbol{X}_0)\right\rangle &= \left\langle \bar{\mathsf{D}}_{-1}^\dagger(\boldsymbol{X}_t)\bar{\mathsf{D}}_{-1}(\boldsymbol{X}_0)\right\rangle = \frac{5}{4\pi R^6}\Upsilon_1^{(1)}(\alpha)e^{-\nu_1(\nu_1+1)\mathcal{D}_R|t|},\\
\left\langle \bar{\mathsf{D}}_2^\dagger(\boldsymbol{X}_t)\bar{\mathsf{D}}_2(\boldsymbol{X}_0)\right\rangle &= \left\langle \bar{\mathsf{D}}_{-2}^\dagger(\boldsymbol{X}_t)\bar{\mathsf{D}}_{-2}(\boldsymbol{X}_0)\right\rangle = \frac{5}{4\pi R^6}\Upsilon_1^{(2)}(\alpha)e^{-\nu_0(\nu_0+1)\mathcal{D}_R|t|},
\end{aligned} \tag{3.14}$$

these are in fact only good approximations for the actual non-exponential correlations that result from the model and hold provided the conical aperture, α, is not greater than 150 degrees. R denotes the mean distance between the paramagnetic center and the orbiting nuclei; $\mathcal{D}_R$ is the rotational diffusion coefficient, or equivalently, the reciprocal of the correlation time of this type of motion. The various ν_q that appear are eigenvalues of the underlying problem and, unfortunately, non-trivial functions of the aperture with no general closed form. Gengeliczki et al.[39] offer the numerical approximations

$$\begin{aligned}
\nu_0(\alpha) &= 3.133\alpha^{-1.122} \quad \text{and}\\
\nu_1(\alpha) &= 1.725\alpha^{-1.122}
\end{aligned} \tag{3.15}$$

with α defined in radians. On the other hand, the other aperture dependent functions are analytically determined by the expressions

$$\begin{aligned}
\Upsilon_0^{(0)}(\alpha) &= \frac{1}{4}\cos(\alpha)^2(1+\cos(\alpha))^2,\\
\Upsilon_1^{(0)}(\alpha) &= \frac{1}{5}-\frac{1}{20}\cos(\alpha)-\frac{3}{10}\cos(\alpha)^2-\frac{1}{20}\cos(\alpha)^3+\frac{1}{5}\cos(\alpha)^4,\\
\Upsilon_1^{(1)}(\alpha) &= \frac{1}{5}+\frac{1}{5}\cos(\alpha)+\frac{1}{5}\cos(\alpha)^2-\frac{3}{10}\cos(\alpha)^3-\frac{3}{10}\cos(\alpha)^4,\\
\Upsilon_1^{(2)}(\alpha) &= \frac{1}{5}-\frac{7}{40}\cos(\alpha)-\frac{7}{40}\cos(\alpha)^2+\frac{3}{40}\cos(\alpha)^3+\frac{3}{40}\cos(\alpha)^4.
\end{aligned} \tag{3.16}$$

Electron spin correlations

Having considered dipolar contributions fully, it remains to characterize total spin correlations, also introduced in Eq.(3.12). In this respect, notice that any Hamiltonian governing spin equilibrium under a magnetic field must be comprised essentially of the Zeeman potential and other spin operators that result from the crystalline (electrostatic) field at the solid surface. Then, first assume the simplest possible case in which the former contribution is completely dominant. This is clearly a valid regime whenever external fields are sufficiently high or when paramagnetic centers are not so strongly bound to the pore surface.

Because the total spin moment is in canonical equilibrium under an externally applied field, the roaming nuclei experience a local field due to a magnetic moment which is consistent with any of the possible spin states encompassed by such equilibrium. Accordingly, the spin correlation at $t = 0$ (full correlation) is determined by the equilibrium statistics. As time progresses, these correlations (consequently, field correlations as well) are lost due to thermal fluctuations of the spin itself, in a way particular to the electron system considered and its environment.

Now, provided the decay of correlations happens within a specific time-scale, then it is phenomenologically valid to represent all spin correlations by the simple decays. Namely,

$$\left\langle S_q(t)^\dagger S_q(0)\right\rangle - \left\langle S_q^\dagger\right\rangle \left\langle S_q\right\rangle = \left\langle \Delta S_q^\dagger \Delta S_q\right\rangle e^{-\frac{|t|}{\tau_q}} e^{-iq\omega_e t}, \tag{3.17}$$

wherein τ_q denotes the electronic correlation time associated with the pair of components designated by q and ω_e is the Larmor frequency of an electron.

The expectation on the right-hand side of Eq.(3.17) is a thermal equilibrium average. All $\left\langle S_q(t)^\dagger S_{q'}(0)\right\rangle$, with $q' \neq q$, are taken to be zero in consequence of assuming initially uncorrelated variables remain uncorrelated (a Zeeman Hamiltonian implies $\left\langle S_q^\dagger S_{q'}\right\rangle = 0$ for $q' \neq q$ in equilibrium). Furthermore, notice that in this notation $q = 0$ corresponds to longitudinal correlation, whereas transverse correlation functions are indicated by labels ± 1.

In view of the high temperature approximation[5], which is also excellent for electronic systems in the temperature and field conditions experiments are usually carried, the average total spin, $\langle S_0\rangle$, is in the first order of $\beta\hbar\omega_e$. Since this quantity enters the definition of the first order frequency shift (see Eq.(3.11)) and the latter may be rele-

[5]The high temperature approximation is simply the neglect of high order terms in $\beta\hbar\omega$ and reflects the fact that magnetic spin energies are usually small compared to $k_B T = \beta^{-1}$ unless T is very low (about mK)[1,28].

vant in the case of transverse relaxation, spin correlations need to be expanded up to the first order of $\beta\hbar\omega_e$ to keep relaxation rates and frequency shifts in the same order of magnitude. As a result, both the product of average spin components, appearing in Eq.(3.17), and the product of average fields in Eq.(3.12) can be neglected, for these terms necessarily introduce second order corrections. Finally, under the considered approximations, equilibrium spin correlations reduce to

$$\left\langle \Delta S_q^\dagger \Delta S_q \right\rangle = \frac{S(S+1)}{3}\left(1 - \frac{q\beta\hbar\omega_e}{2}\right). \tag{3.18}$$

Local field spectral densities

Substitution of Eqs.(3.13, 3.17, 3.14) on Eq.(3.12) yields a form which is essentially a linear combination of exponential decays. Instead of analyzing the full expression, notice that upon Fourier transformation each of these terms contribute to the total spectral density with a Lorenztian distribution. The general form of these distributions are

$$2\tau_{q'}\left[\frac{1+\nu_m(\nu_m+1)\mathcal{D}_R\tau_{q'}}{\left(1+\nu_m(\nu_m+1)\mathcal{D}_R\tau_{q'}\right)^2+\left(\omega-q'\omega_e\right)^2\tau_{q'}^2}\right], \tag{3.19}$$

which puts on evidence the role of the electronic correlation times. Then, a quick evaluation of the parameters involved is beneficial.

Reported determinations of τ_0 in the conditions of the presented problem are sporadic in the NMR literature. A reasonable order of magnitude is in the tenths of the nanosecond[37,64]; the actual value depends on many factors like the nature, oxidation state and possibly chemical environment of the paramagnetic center. An old reference[10] states that the longitudinal relaxation time of electrons belonging to paramagnetic ions in solution can be of even lower order. Incidentally, τ_1, the corresponding time scale of transverse effects (electron spin coherence), is anticipated to be much shorter, perhaps in the order of picoseconds. For bulk water, the rotational diffusion coefficient is usually obtained via an Einstein-Smoluchowski type of equation which gives an order of $10^{10}\mathrm{s}^{-1}$ at normal temperature[28]. It is not clear whether, for the restricted wobble here considered, the order should be maintained or reduced, assuming surface effects tend to make nearby molecular behavior more solid-like. If the bulk value is assumed, the mean squared angular displacement of nuclei, $\mathcal{D}_R\tau_0$, may be close to unit, provided the rest of the estimates are sound.

Furthermore, if $q' \neq 0$, the frequency term is dominated by the electronic Larmor frequency, which, for fields in the proton range of MHz, should be in the range

of hundreds of MHz to hundreds of GHz, but, since τ_1 is assumed very small, the whole expression between brackets is nearly equal to 1 over this entire frequency range. Therefore, for $q' \neq 0$, the spectral contributions are in practice uniform and determined by twice the value of τ_1, which, however, is hypothetically negligible compared to τ_0. This implies that only the contributions associated with the index $q' = 0$ are relevant for the presented model[6].

Similarly, for the case of $q' = 0$, the frequency term is almost unimportant over the entire working range. Even in the case of very high field spectrometers ($\geq$ 100 MHz), the product $\omega_0\tau_0 \approx 0.1$. As argued above, $\mathcal{D}_R\tau_0$ is about unit, so it is possible to neglect the frequency dependence on Eq.(3.19) altogether.

Finally, the spectral densities reduce to

$$J_q(\theta_S) = j_1 \frac{4-|q|}{3} \left[\Upsilon_0^{(0)}(\alpha) |\mathsf{d}_{0,q}^{(2)}(\theta_S)|^2 + \frac{\Upsilon_1^{(0)}(\alpha)}{1+\nu_0(\nu_0+1)\mathcal{D}_R\tau_0} |\mathsf{d}_{0,q}^{(2)}(\theta_S)|^2 + \frac{\Upsilon_1^{(1)}(\alpha)}{1+\nu_1(\nu_1+1)\mathcal{D}_R\tau_0} \left(|\mathsf{d}_{1,q}^{(2)}(\theta_S)|^2 + |\mathsf{d}_{-1,q}^{(2)}(\theta_S)|^2 \right) + \frac{\Upsilon_1^{(2)}(\alpha)}{1+\nu_0(\nu_0+1)\mathcal{D}_R\tau_0} \left(|\mathsf{d}_{2,q}^{(2)}(\theta_S)|^2 + |\mathsf{d}_{-2,q}^{(2)}(\theta_S)|^2 \right) \right] \tag{3.20}$$

wherein the constant factor j_1 is given by

$$j_1 = 2 \left(\frac{\mu_0}{4\pi} \frac{\gamma_e \hbar}{R^3} \right)^2 S(S+1)\tau_0. \tag{3.21}$$

One special merit of the above formulas is that they specify the order of magnitude of surface relaxivities. Though both τ_0 and R are somewhat phenomenological parameters introduced by the model, there are reasonable estimates for their values. As argued above, $\tau_0 \approx 0.1$ ns and, for R, the typical order of covalent separation of atoms in molecules is a reasonable figure. Thus, $R \approx 1$Å. Hence,

$$\frac{\gamma^2 j_1}{2} = 1.217 \times S(S+1) \frac{[\tau_0(ns)]}{[R^6(\text{Å})]} \times 10^8, \tag{3.22}$$

wherein the brackets denote only the numerical values of the corresponding quantities

[6] Physically, this means that only energy fluctuations of the electron spin system have any effect of nuclear relaxation.

on the indicated units. Using $S = 5/2$, which is the spin associated with common paramagnetic centers comprised of Fe^{3+} or Mn^{2+}, and $R = 2.75$Å, the diameter of a water molecule, the formula yields surface relaxation rates in the order of $10^5 s^{-1}$ and, consequently, surface relaxivities not larger than $100\,\mu$m/s.

The first order frequency shift

Finally, the first order frequency shift presented on Eq.(3.11) is determined by

$$\begin{aligned}\langle \mathsf{b}_0 \rangle &= \frac{\mu_0}{4\pi}\gamma_e \hbar C_{00} \langle \mathsf{D}_0 \rangle \langle S_0 \rangle = \frac{\mu_0}{4\pi}\gamma_e \hbar \left(2\sqrt{\frac{4\pi}{5}}\right) \mathsf{d}^{(2)}_{0,0}(\theta_S) \left\langle \bar{\mathsf{D}}_0 \right\rangle \langle S_0 \rangle \\ &= \frac{\mu_0}{4\pi}\frac{(\gamma_e \hbar)^2}{R^3}\frac{S(S+1)}{3}\cos(\alpha)(1+\cos(\alpha))\mathsf{d}^{(2)}_{0,0}(\theta_S)\beta B_0,\end{aligned} \tag{3.23}$$

following again the results of Wang and Pecora[114] and making explicit use of the high temperature approximation in the spin expectation. It is interesting to see that the typical order of magnitude of the fractional shift, excluding the aperture and inclination factors, is 10^{-4}. This is relatively high value. Measured magnetic susceptibilities in porous ceramics containing significant iron content are in same order only when concentrations of iron oxide reach about 8%[81], a figure too great for most natural materials. Hence, there may be systems in which first order frequency shifts contribute as much to nuclear spin dephasing as internal susceptibility contrasts.

3.2.2 Field dependence

The model underlying Eq.(3.20) is based on the complete dominance of the external Zeeman interaction and so should be valid on high field conditions. The lack of frequency dependence, nevertheless, needs to be addressed, for it is known, particularly from studies on microporous materials, that NMR relaxation of water and other polar compounds, like acetone, presents a noticeable field dependence[36,41,65,66].

According to the model, such behavior cannot arise from the Lorenztian character of the spectral densities, because, if estimates are right, electron spin correlation times are simply too short to allow any noticeable effect other than extreme narrowing on the frequency range of most typical spectrometers. As a result, some of the approximations made need to be revisited; particularly, the neglect of other electron spin couplings as surface crystalline fields should gain relevance on electron spin behavior as external magnetic fields are weakened.

It is clear that, in general, both types of interaction are important. Crystalline surface couplings must in fact dominate the electron spin system at sufficiently low external magnetic fields. Hence, it is reasonable to advance the hypothesis that the **frequency dependence** detected on NMR dispersion (NMRD) studies may be only apparent, for it is properly a **field dependence** caused by a relative shift in dominance of electron spin interactions.

Within the range in which frequency effects, in true sense, are negligible, two plateaus can therefore be expected to appear in the NMRD curves, which typically plot acquired longitudinal relaxation rates versus probing frequency: A first at **low frequencies**, corresponding to the dominance of surface crystalline effects, and another at relatively **high frequencies**, as the Zeeman interaction effective starts to govern electron spin behavior. This qualitative description in fact agrees with the published data[65].

Crystalline fields work by basically lifting multiplet degeneracies that would otherwise occur in a given unpaired electron system not bound to the surface. In many systems of interest, the crystalline field-induced splittings can be explained by means of a effective spin Hamiltonian, H_S, which must reflect symmetries of the crystalline environment, as well restrictions imposed by spin number. The important aspect here, however, is that even in the absence of external magnetic fields, crystalline fields, which are of electrostatic origin, may give rise to spin phenomena like fixation of the **zero field magnetic moment** of the electron spin system along preferred directions or like the development of anisotropic Zeeman coupling with an external field[2].

Presently, it is desired to characterize the electron spin dynamics insofar as it is necessary to grasp the most relevant features of surface-induced relaxation mechanisms. Thus, for the sake of simplicity, no anisotropy in the electron Zeeman interaction is assumed and the sole contribution of crystalline effects to H_S is taken to be determined by a term that tends to align the electron spin with the local surface normal, which is then assumed to define the **easy axis** of the considered spin system.

Notwithstanding the heuristic character of these considerations, a word about the latter coupling is still necessary. In most situations in which a spin Hamiltonian is evoked to explain the influence of crystal structure, H_S is defined through a power series of spin operators that satisfy basic local rotational symmetries. This typically means only even-powered spin operators are retained in the end, because symmetry under reflection onto mirror planes of a crystal must be satisfied as well. However,

a spin system attached to a site on the boundary of a solid wall should not exhibit reflection symmetry and, consequently, odd-powered terms in the spin Hamiltonian are in principle allowed.

On these terms, the simplest characterization of surface crystalline effects that reproduces the aforementioned properties is advanced by zero field linear spin Hamiltonian, which for convenience is written as

$$\mathsf{H}_S^{(0)} = \gamma_e \hbar A \boldsymbol{n} \cdot \boldsymbol{S}. \tag{3.24}$$

Again, $\boldsymbol{n}$ denotes the local surface normal and the electron gyromagnetic ratio as well as Planck constant are introduced only to make the surface crystal parameter, A, get dimensions of magnetic field, even though the whole term is of **electrostatic nature**. Notice that such a term has complete rotational symmetry about the easy axis and implies a non-zero spin magnetic moment parallel to it at equilibrium .

At non-zero field strengths, a Zeeman interaction must added to the zero field Hamiltonian. This ultimately makes H_S effectively a Zeeman Hamiltonian as well and introduces an **effective magnetic field**, whose magnitude and inclination with respect to the lab frame's $\mathbf{e}_0$-axis are respectively determined by

$$\begin{aligned} B_0' &= B_0 \sqrt{1 + 2\lambda \cos\theta_S + \lambda^2}, \\ \cos\theta_S' &= \frac{1 + \lambda \cos\theta_S}{\sqrt{1 + 2\lambda \cos\theta_S + \lambda^2}}, \end{aligned} \tag{3.25}$$

wherein the parameter $\lambda = A/B_0$ defines the scaled strength of the crystalline field. Low (magnetic) field conditions imply large λ, whereas the parameter tends to zero at high fields.

These assumptions are economical in a conceptual sense, since they allow the description of surface effects by virtually a single parameter, and fortunate from a theoretical standpoint, for they also allow the very same reasoning that lead to Eq.(3.17) to be applied in a most general scenario.

The fact that H_S is also defined by a Zeeman-type coupling implies that, functionally, Eq.(3.17) applies to correlations of spin components in the **effective field frame**. But, then, to write spin correlations in the lab frame of reference, as it is required by Eq.(3.12), one only needs to note that the S_q components are spherical

tensors of first rank and must transform upon rotations accordingly. As a result,

$$\left\langle S^{\dagger}_{q'}(t)S_{q''}(0)\right\rangle = \sum_{n} \mathsf{d}^{(1)}_{n,q'}(\theta'_S)\mathsf{d}^{(1)}_{n,q''}(\theta'_S)e^{-i(q''-q')\phi'_S}\left\langle S'^{\dagger}_{n}(t)S'_{n}(0)\right\rangle, \tag{3.26}$$

wherein ϕ'_S is the polar angle of the *effective field* of the element as defined in the lab frame.

By substitution of the above equation on Eq.(3.12),

$$\begin{aligned}\Gamma_q(t) = \left(\frac{\mu_0}{4\pi}\gamma_e\hbar\right)^2 \frac{S(S+1)}{3} \sum_{q'q''mn} \Big[C_{qq'}C_{qq''} \left(\mathsf{d}^{(2)}_{m,q-q'}(\theta_S)\mathsf{d}^{(2)}_{m,q-q''}(\theta_S)\mathsf{d}^{(1)}_{n,q'}(\theta'_S)\mathsf{d}^{(1)}_{n,q''}(\theta'_S)\right) \\ \times \left\langle \bar{\mathsf{D}}^{\dagger}_{m}(\boldsymbol{X}_t)\bar{\mathsf{D}}_{m}(\boldsymbol{X}_0)\right\rangle \exp^{-i(q'-q'')(\phi_S-\phi'_S)} \left(1-\frac{n\beta\hbar\omega_e}{2}\right) e^{-\frac{|t|}{\tau_n}} e^{-in\omega'_e t}\Big]\end{aligned} \tag{3.27}$$

up to the first order on $\beta\hbar\omega_e$, high-temperature being assumed on electron spin correlations once more.

Then, the same chain of arguments that lead to Eq.(3.20) can be repeated; consequently, only the terms referring to the index $n = 0$ need to be considered and, by making use of the fact that $\phi_S = \phi'_S$[7], it follows that

$$\Gamma_q(t) = \left(\frac{\mu_0}{4\pi}\gamma_e\hbar\right)^2 \frac{S(S+1)}{3} \sum_{m} F_{m,q}(\theta_S,\lambda)\left\langle \bar{\mathsf{D}}^{\dagger}_{m}(\boldsymbol{X}_t)\bar{\mathsf{D}}_{m}(\boldsymbol{X}_0)\right\rangle e^{-\frac{|t|}{\tau_0}} \tag{3.28}$$

in which, now,

$$F_{m,q}(\theta_S,\lambda) = \left|\sum_{q'} C_{qq'}\mathsf{d}^{(2)}_{m,q-q'}(\theta_S)\mathsf{d}^{(1)}_{0,q'}(\theta'_S)\right|^2. \tag{3.29}$$

It is not difficult to check that upon the high field limit ($\lambda \to 0$) the above expression reduces to the one treated before as $\theta'_S = 0$ and $\mathsf{d}^{(1)}_{0,q'}(0) = \delta_{0q'}$.

Finally, after identical considerations concerning the suitability of extreme nar-

[7] It is important to choose an one-parameter family of coordinate axes such that, starting from the lab (or high field) frame, one can reach the surface element (or low field) frame in the limit $\lambda \to \infty$. Notice, nonetheless, that two parameters are generally needed to characterize a rotation between any two given frames. This difficulty can be circumvented once it is realized that two lab frames differing only by a rotation about the $\boldsymbol{e}_0$-axis are completely equivalent. Hence, instead of attaching one limit of the family to the chosen lab frame, it is best to associate the limit with the equivalent frame which yields the surface element frame upon rotation of θ_S (or of θ'_S) about its $\boldsymbol{e}_y$-axis. Because of the co-planarity of the *field* vectors, namely, $\boldsymbol{B}_0$, $A\boldsymbol{n}$ and $\boldsymbol{B}'_0$, the polar angle of the entire family then becomes independent of λ.

rowing, the spectral densities are determined by

$$\begin{aligned} J_q(\theta_S,\lambda) =& j_1 \left[\Upsilon_0^{(0)}(\alpha) F_{0,q}(\theta_S,\lambda) + \frac{\Upsilon_1^{(0)}(\alpha)}{1+\nu_0(\nu_0+1)\mathcal{D}_R\tau_0} F_{0,q}(\theta_S,\lambda) \right. \\ &+ \frac{\Upsilon_1^{(1)}(\alpha)}{1+\nu_1(\nu_1+1)\mathcal{D}_R\tau_0} \left(F_{1,q}(\theta_S,\lambda) + F_{-1,q}(\theta_S,\lambda)\right) \\ &\left. + \frac{\Upsilon_1^{(2)}(\alpha)}{1+\nu_0(\nu_0+1)\mathcal{D}_R\tau_0} \left(F_{2,q}(\theta_S,\lambda) + F_{-2,q}(\theta_S,\lambda)\right) \right], \end{aligned} \tag{3.30}$$

the field-dependence being revealed through the parameter λ.

Ultimately, the above formula encompasses all the basic features that should affect surface relaxation rates. The obvious setback is that it introduces a rather big set of parameters. About that, it is possible that conical semiapertures may be estimated from microscopy results or through MD simulations, or, even better, constrained by some a priori knowledge of the molecular structures formed at the surface level. In the next section, the manner with which the inclination of surface elements is removed from characterization is discussed. Yet, values of $\mathcal{D}_R\tau_0$ and λ seem to be only accessible via the model itself but, due to an unexpected remarkable sensitivity to the former parameter (see Figs.(3.2, 3.3)), the evaluation of these parameter may require an unfeasibly good characterization of surface configuration and distribution of paramagnetic centers. Fortunately, it is the qualitative aspects of the proposed theory, in spite of its inherent quantitative cumbersomeness, that which is believed worth of consideration.

3.3 NMR signal decay

Recall from Eq.(2.35) that the initial rate of saturation in recovery signals is determined exclusively by the bulk relaxation rate, the surface-to-volume ratio of the structure and the mean surface relaxivity. Namely,

$$\frac{\mathrm{d}}{\mathrm{d}t} \ln E(0) = \frac{1}{\mathrm{T}_1} + \frac{\bar{\rho}_1 S_0}{V_0} \tag{3.31}$$

wherein

$$\bar{\rho}_1 = \frac{1}{\mathrm{S}_0} \int_{\partial\Omega} \mathrm{d}S\, \rho_1(\boldsymbol{X}). \tag{3.32}$$

As it is amply discussed in Chapter 2, surface-induced relaxation is typically a

relatively weak process compared to diffusive transport. It amounts to, in many cases, being sufficiently well characterized by a mono-exponential decay modulating the entire signal. This situation is especially frequent in sequences that employ longitudinal magnetization storage because of the smaller relaxivities associated with surface longitudinal relaxation and the characteristic insensitivity to magnetic field heterogeneities. Therefore, the mean surface relaxivity can be generally regarded as the macroscopic signature of surface-induced relaxation.

In most thorough NMR studies, all other quantities introduced by Eq.(3.31) are separately accessible and so the evaluation of saturation or decay rates (depending on the employed sequence) yields an almost direct measurement of the mean surface relaxivity. With a proper estimate of interface thickness, h, and a suitable model for surface relaxation rates (recall $\rho_i = \mathsf{h}/\mathrm{T}_i^{(s)}$), such measurements in principle can provide information, on the microscopic level, about physical and chemical processes that occur in the fluid-solid interface of a porous medium, or even, as it is attempted below with the developed model, hint on specific topological characteristics of the pore structure like favored directions for pore communication.

Accordingly, consider Eq.(3.32). The focus on longitudinal rates of decay is due to the fact they are theoretically simpler and, from an experimental standpoint, more directly accessible. Furthermore, the treatment of transverse decay rates are entirely analogous provided the effects of field inhomogeneities on signal decay are compensated by the chosen sequence.

The relaxation time of active surface elements depends on the inclination of the local surface normal in respect to the external field. As pointed out, active elements typically cover but a small fraction of the boundary of a porous medium and, expectedly, are randomly distributed over it. Therefore, it is reasonable to represent the surface field $\rho_1(\boldsymbol{X})$ as the product of a surface indicator function $p_a(\boldsymbol{X})$, which is equal 1 on points representing active elements and zero otherwise, and the local relaxation rate of an active element, accordingly, a function dependent only of the local inclination, as determined by Eqs.(3.4,3.5,3.30). The relaxivities of inactive elements may be taken equal zero, as both bulk and other surface mechanisms contribute negligibly compared to the process considered in the model[31].

Consequently,

$$\begin{aligned}\bar{\rho}_1 &= \frac{\mathsf{h}}{\mathrm{S}_0}\int_{\partial\Omega}\mathrm{d}\,\mathrm{S}\frac{1}{\mathsf{T}_1^{(s)}(\boldsymbol{X})} = \frac{\mathsf{h}}{\mathrm{S}_0}\int_{\partial\Omega}\mathrm{d}S\,\frac{p_a(\boldsymbol{X})}{\mathsf{T}_1\left[\theta(\boldsymbol{X})\right]}\\ &= \frac{\mathsf{h}}{\mathrm{S}_0}\int_{\partial\Omega_a}\mathrm{d}\,\mathrm{S}_a\frac{1}{\mathsf{T}_1\left[\theta(\boldsymbol{X})\right]} = \frac{S_a}{\mathrm{S}_0}\bar{\rho}_a\end{aligned} \tag{3.33}$$

Notice an entirely equivalent relation can be written in terms of surface relaxation rates by just dividing it by h. Due to the proportionality of quantities, the terms are used interchangeably.

The fraction S_a/S is simply the coverage of active elements; it can be recast in terms of surface density of paramagnetic centers once the mean area of a surface site is defined. Namely,

$$\mathrm{S}_a = N_a\mathrm{a}_s = (\sigma_S\mathrm{a}_s)\,\mathrm{S} \tag{3.34}$$

wherein N_a denotes the number of active elements in the considered pore structure, a_s is the mean area of a surface site ($\approx 10^{-15}\mathrm{cm}^2$) and σ_S is the areal density of paramagnetic centers.

If some geometric knowledge about the porous structure is a priori available, the mean surface relaxation rate can be determined by direct calculation, though this method is likely to be feasible for simple geometrical shapes only. An alternative, more flexible approach consists of adopting a **distribution of inclinations** for the pore structure. For instance, if the porous medium can be assumed statistically isotropic, there must exist surface elements virtually pointing on all directions and out of those a fraction S_a/S will be active. An uniform isotropic distribution of inclinations is therefore a reasonable model for that statistically isotropic pore structure and consequently,

$$\bar{\rho}_a \equiv \frac{1}{4\pi}\int\mathrm{d}\Omega\,\rho_1(\theta) = \frac{1}{2}\int_0^\pi\mathrm{d}\theta\sin\theta\rho_1(\theta), \tag{3.35}$$

in particular, the longitudinal relaxation in the high field limit simplifies into

$$\bar{\rho}_a = \frac{\mathsf{h}\gamma^2 j_1}{10}\left[\Upsilon_0^{(0)}(\alpha) + \frac{\Upsilon_1^{(0)}(\alpha)}{1+\nu_0(\nu_0+1)\mathcal{D}_R\tau_0} + \frac{2\Upsilon_1^{(1)}(\alpha)}{1+\nu_1(\nu_1+1)\mathcal{D}_R\tau_0} + \frac{2\Upsilon_1^{(2)}(\alpha)}{1+\nu_0(\nu_0+1)\mathcal{D}_R\tau_0}\right]. \tag{3.36}$$

The nondimensional longitudinal mean surface rate for isotropic media, normalized by $\gamma^2 j_1/10$, is presented in Fig.3.2 as a function of the semiaperture in the two limits associated with high and low field configurations, that is, $\lambda = 0$ and $\lambda \to \infty$.

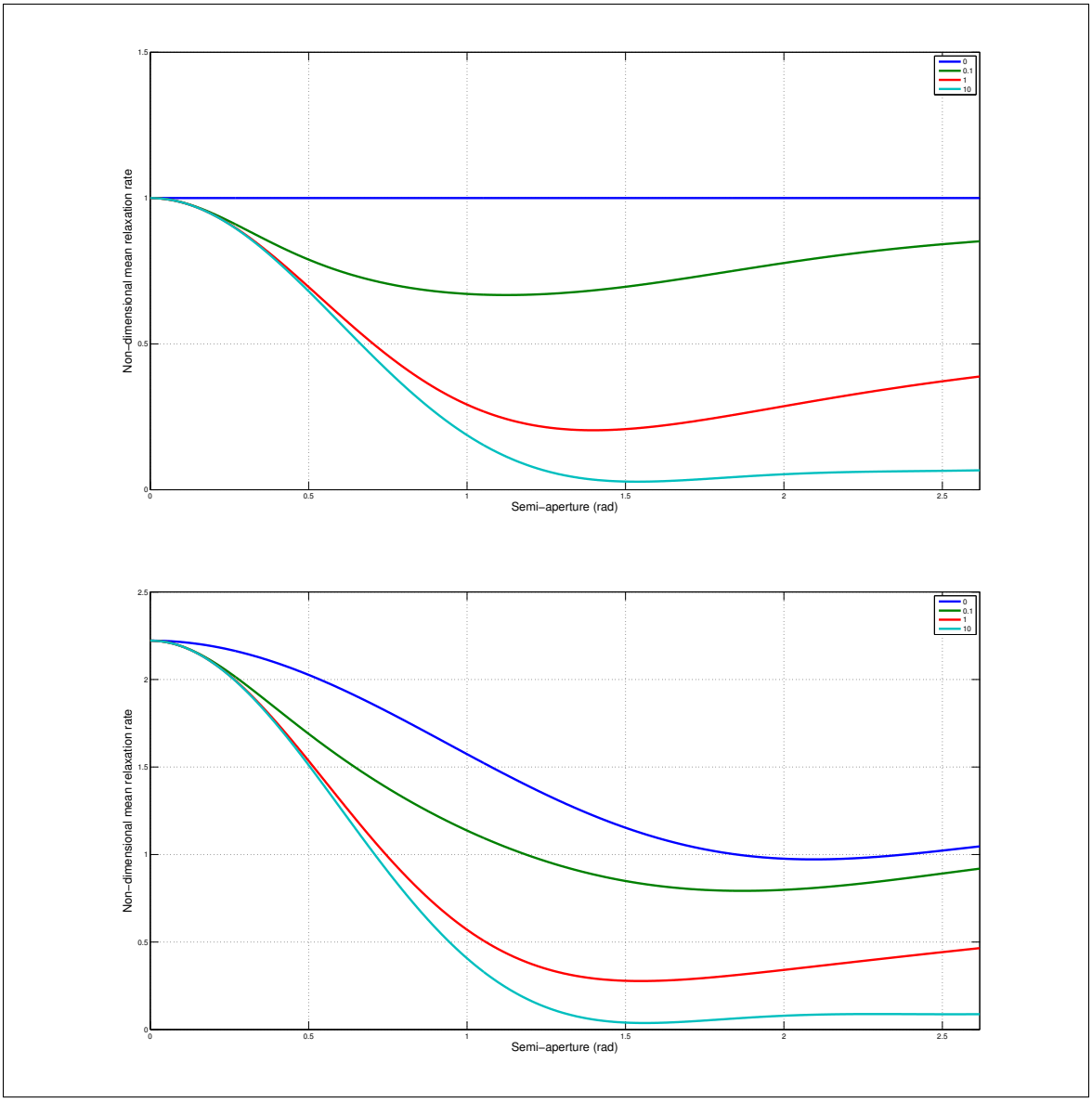

Figure 3.2: Top: high field behavior ($\lambda = 0$) of mean surface rates for isotropic media as a function of semiaperture. Bottom: low field behavior ($\lambda \longrightarrow \infty$) of mean surface rates for isotropic media as a function of semiaperture. The distinct curves in each graph correspond to different values of the dynamical group $\mathcal{D}_R\tau_0$. Labels are printed in the figures.

As it is readily seen, larger values of $\mathcal{D}_R\tau_0$ imply lower rates for a given aperture regardless of field conditions (field dependence is monotonic for semiapertures smaller than 90° as shown below). Physically, this means that, if the electron spin correlation time is too long compared to the characteristic time scale of molecular wobbling, surface-induced NMR relaxation is a relatively weak mechanism provided the semiaperture of coordinated structures is not too small. In other words, a very fast molecular wobbling actually reduces the rates of relaxation for it overshadows the dominant process promoting NMR relaxation at active surface elements: The loss of electron spin correlations. One should keep in mind that this reasoning holds for normalized rates only; large absolute rates of decay are expected whenever τ_0 is long.

It is particularly interesting to see that at high fields the aperture dependence is completely lost whenever $\mathcal{D}_R\tau_0$ becomes vanishingly small, i.e., wobbling is relatively slow. One possible interpretation for such behavior is that molecular dynamic features become irrelevant in situations which the paramagnetic site loses spin correlation simply too quickly. Then, modulations of the dipolar interaction come entirely from fluctuations in the electron spin magnetic moment. Although such view is intuitively reasonable, it is challenged by the behavior of low field rates under similar conditions. A viable conciliation may come from the fact that on such limit the spin moment is preferably oriented towards the local easy axis, which coincides with the model cone axis. Consequently, the distribution of nuclei over the spherical cap becomes an important factor because of the directional character of the interaction.

Yet, the most striking prediction, concerning isotropic pore structures, advanced by the model is the logarithmic field dependence exhibited by mean relaxivities. It follows directly from Eq.(3.30) by integration over the distribution of inclinations. Unfortunately, the algebra involved is rather long and tedious, but it is nevertheless

possible to show that the averaging, implied by Eq.(3.35), reduces the expressions to[8]

$$\begin{aligned}
\langle F_{0,1}\rangle &= \frac{9-21\lambda^2+35\lambda^4+\lambda^6}{96\lambda^4} - \frac{(3-4\lambda^2+\lambda^4)^2}{192\lambda^5}\operatorname{arctanh}\left(\frac{2\lambda}{1+\lambda^2}\right),\\
\langle F_{1,1}+F_{-1,1}\rangle &= \frac{-3+2\lambda^2+13\lambda^4}{24\lambda^4} + \frac{(1+\lambda^2)(1-\lambda^2)^2}{16\lambda^5}\operatorname{arctanh}\left(\frac{2\lambda}{1+\lambda^2}\right),\\
\langle F_{2,1}+F_{-2,1}\rangle &= \frac{3+13\lambda^2+13\lambda^4+3\lambda^6}{96\lambda^4} - \frac{(1+6\lambda^2+\lambda^4)(1-\lambda^2)^2}{64\lambda^5}\operatorname{arctanh}\left(\frac{2\lambda}{1+\lambda^2}\right).
\end{aligned} \tag{3.37}$$

It is instructive to analyze such behavior graphically by varying the conical aperture and the dynamical group, $\mathcal{D}_R\tau_0$. The plots are shown in Fig.3.3.

Qualitatively, the curves for apertures smaller than 180 degrees resemble the behavior implied by the NMRD data presented by Korb[65] on hydrated plaster (Fig.8(a) *op. cit.*). Though the referred work actually presents the signal decay rate rather than the mean surface relaxivity of structure, comparison is bona-fide since the two quantities ideally differ only by the addition of a constant and a rescale (see Eq.(3.31)). Quantitatively, however, the model seems incapable to answer for the great disparity between low and high field rates revealed by the data (notice how low field rates are 10 times larger than high field rates).

Assuming the basic premises of the model are correct, an *underestimation* of the low field plateau may likely evidence that the underlying electron spin Hamiltonian employed and, consequently, the spin correlations that follow from it cannot be as

[8]The steps of the calculation behind Eq.(3.37) are here indicated.

Recall the presented functions are averages of sums introduced by Eq.(3.29) over all possible inclinations. Those sums, in turn, involve terms which are products of Wigner d-matrices elements of the first and second ranks. The first rank elements are particularly important, because they are determined rather by the inclination of the effective field, θ'_S, which is a function of both θ_S, the inclination of the surface element, and the parameter λ. The elements needed for the calculation, furthermore, are essentially sines and cosines of the θ'_S as any table of d-matrix elements will reveal.

Hence, because of Eq.(3.25), the product of first rank elements introduces rational expressions in terms of the parameters $\cos\theta_S$ and λ, whose common denominator is $1+2\lambda\cos\theta_S+\lambda^2$. Once a substitution of variables is made, such as $u=\cos\theta_S$, and the defining expressions of remaining d-matrix elements are employed, the resultant integrand becomes a large improper rational function of u.

From that point on, the derivation is a tedious exercise of calculus. One starts by obtaining quotient and remainder polynomials defined by the rational function and rewrites it as the sum of the former plus the proper rational function determined by the latter. The first part is easily integrated since it is a polynomial; for the second part, however, one still needs to use the method of partial fractions to yield a result. Recall the integration variable is only u.

Finally, rearrange all non-logarithmic terms of λ under a common denominator and express logarithmic behavior more compactly through arctanh( ) functions to obtain the result.

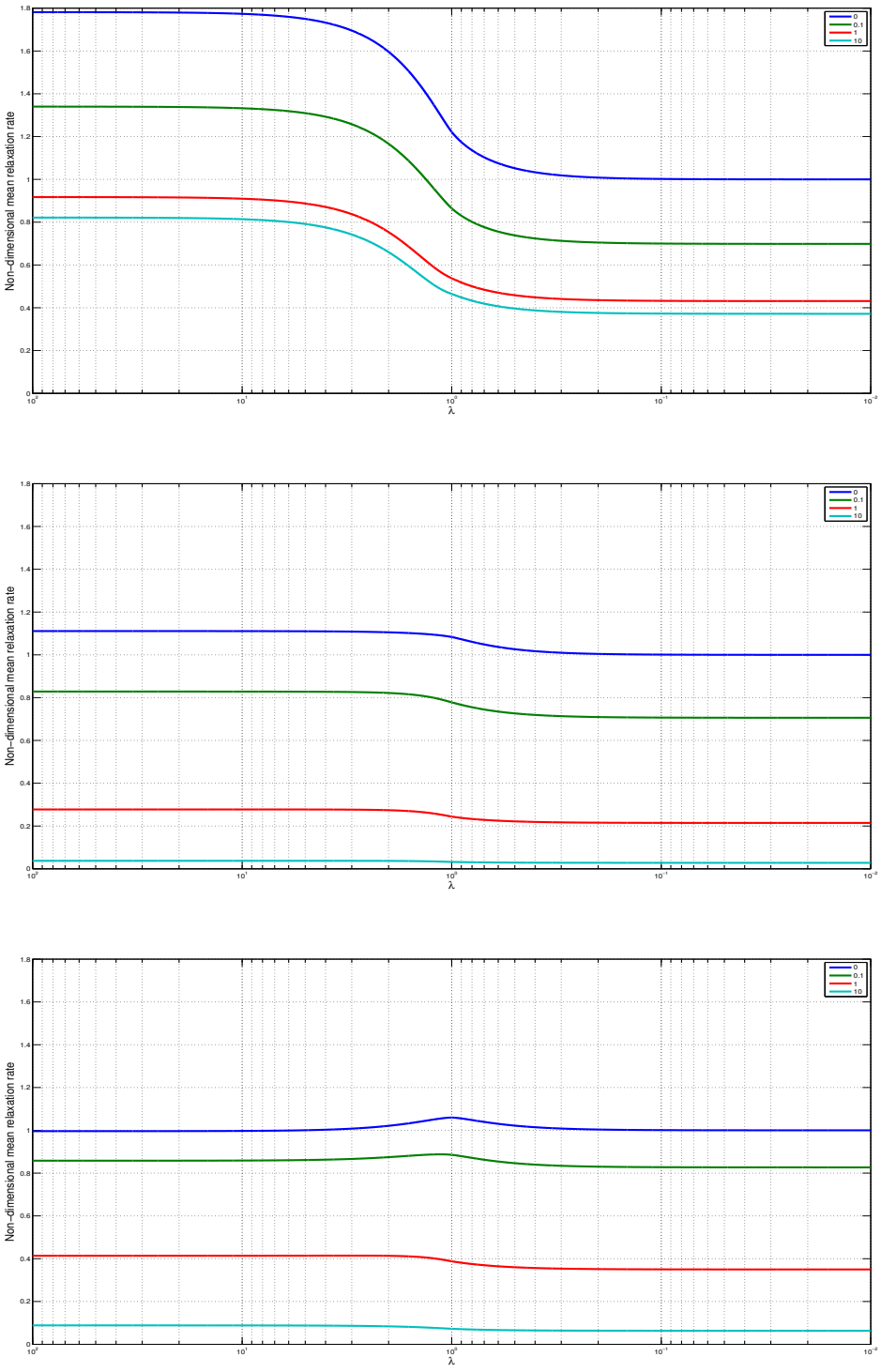

Figure 3.3: The field dependence of the nondimensional mean surface rate for three values of semiaperture, respectively, 45, 90 and 135 degrees. The distinct curves in each graph correspond to different values of the dynamical group $\mathcal{D}_R\tau_0$. The labels are printed in the figures.

simple as supposed. Higher order crystalline field terms, like the typical quadratic form, DS_z^2, encountered in electron spin magnetic resonance studies, may necessarily have to enter the description. Such corrections, however, are not pursued here. The presented model, in spite of its simplicity, illustrates well enough the general theory.

3.3.1 Simple structures

Clearly, the enhanced signal decay observed on an isotropic pore structure cannot depend on the direction of the applied magnetic field. But sufficient anisotropy in the internal geometry of a porous medium, in principle, can deliver signal decays that do have a definite dependence on sample orientation. This sensibility then could be used to identify directional trends in the configuration of plant tissues, like xylem and phloem[9], or rock formations that have undergone sufficient fracture or dissolution. In fact, the idea is more clearly illustrated once simple pore geometries are considered.

Slit pore geometry

A structure that is commonly used as a model geometry for microporous materials is that of a slit pore, that is, the gap between two plane boundaries. Considering a single slit, it is sufficiently clear that whatever is the direction of the external magnetic field in respect to the normal of one of the planes, only two inclinations can be associated with any active element, θ_0 and $\pi - \theta_0$. Consequently,

$$\bar{\rho}_a = \frac{\mathsf{h}}{2}\left(\frac{1}{\mathsf{T}_1[\theta_0]} + \frac{1}{\mathsf{T}_1[\pi - \theta_0]}\right) = \frac{\mathsf{h}}{\mathsf{T}_1[\theta_0]}. \tag{3.38}$$

The result can be easily applied to a pore system modeled as an assembly of similar slits with distinct orientations by just averaging it over a distribution which characterizes the assembly. Distinct signal decays should be observed by varying the orientation of the sample in respect to the applied field insofar as the anisotropy character of the distribution is distinguished.

Notice that, whereas the mean surface relaxivity of a pore does not depend on the size of its gap, the signal decay for the entire structure, expressed by Eq.(3.31), surely does, as the volume of the porous domain depends directly on slit separation.

[9] I must mention however that I have no clue about what mechanisms actually induce surface relaxation in these and other organic systems but, provided they fit the conditions of the model, the proposed effect could be in principle observed.

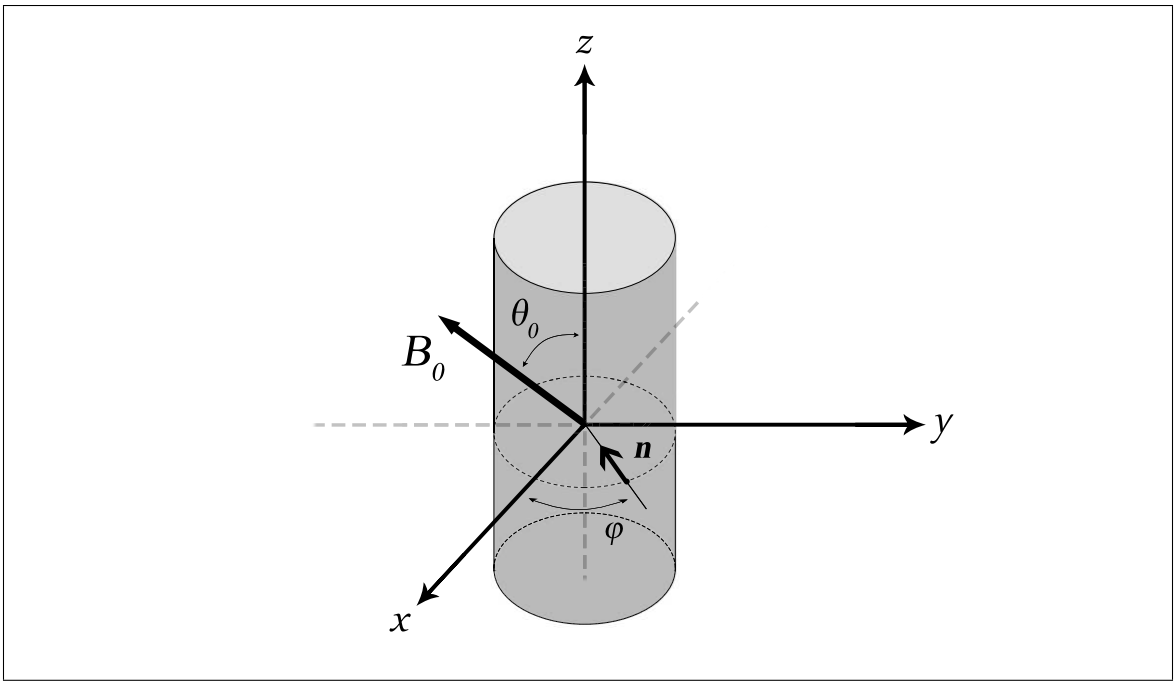

Figure 3.4: Diagram of a cylindrical pore. The chosen coordinate system is depicted. The normal vector of an arbitrary surface element is denoted by $\boldsymbol{n}$. The frame is orientated in such a way that the applied magnetic field lies in the xz-plane. The inclination of the structure in respect to the field is determined by the parameter θ_0.

This must be kept in mind whenever averaging over an assembly of slits with variable gaps. A similar issue persists in all other simple geometric models.

Capillary pore structures

As many biologically important porous media are vascular, it is fortunate that the analysis above can be carried without too much difficulty over the case of a single capillary pore, i.e., a tube-like structure.

First, adopt a coordinate system whose z-axis coincides with the tube axis and on which $\boldsymbol{B}_0$ lies on the xz-plane. Then, (see Fig.3.4) the normal of any surface element is fully characterized by the polar angle, ϕ, and the direction of the applied field by an azimuthal angle, θ_0. To wit,

$$\begin{aligned} \boldsymbol{n}(\phi) &= -\cos\phi \boldsymbol{e}_x - \sin\phi \boldsymbol{e}_y; \\ \boldsymbol{B}_0 &= B_0 \left(\sin\theta_0 \boldsymbol{e}_x + \cos\theta_0 \boldsymbol{e}_z\right). \end{aligned} \tag{3.39}$$

The inclination of a surface element in respect to $\boldsymbol{B}_0$ is determined by the equation

$$\cos\theta_{\boldsymbol{x}} = -\sin\theta_0\cos\phi, \tag{3.40}$$

which has two particularly simple closed-form solutions: For $\theta_0 = 0$, that is, the tube axis parallel to the field, $\theta_{\boldsymbol{x}} = \pi/2$ for all surface elements; for $\theta_0 = \pi/2$, $\boldsymbol{B}_0$ perpendicular to the axis, $\theta_{\boldsymbol{x}} = \phi$. In any case, Eq.(3.40) determines the inclination of any surface element uniquely as a function of the inclination of the structure and the polar angle. Therefore,

$$\begin{aligned}\bar{\rho}_a &= \frac{\mathsf{h}}{\mathrm{S}_a}\int_{\partial\Omega}\mathrm{d}S\,\frac{1}{\mathsf{T}_1[\theta_{\boldsymbol{X}}]}p_a(\boldsymbol{X}) = \frac{1}{\mathrm{S}_a}\int_0^{2\pi}\int_{-\ell/2}^{\ell/2}\mathrm{d}z\,\mathrm{d}\phi\,r\,\frac{p_a(\phi,z)}{\mathsf{T}_1[\theta_{\boldsymbol{X}}(\phi)]}\\ &= \frac{S}{\mathrm{S}_a}\frac{1}{2\pi}\int_0^{2\pi}\mathrm{d}\phi\,\frac{1}{\mathsf{T}_1[\theta_{\boldsymbol{X}}(\phi)]}\left(\frac{1}{\ell}\int_{-\ell/2}^{\ell/2}\mathrm{d}z\,p_a(\phi,z)\right).\end{aligned} \tag{3.41}$$

Now, under the assumption ℓ is sufficiently large and the areal distribution of paramagnetic centers is statistically uniform, the middle integral is precisely equal S_a/S, thus independent of ϕ, as it defines the fraction of active elements along a single line of surface elements on the boundary. Hence,

$$\bar{\rho}_a = \frac{\mathsf{h}}{2\pi}\int_0^{2\pi}\frac{1}{\mathsf{T}_s(\theta_{\boldsymbol{x}}(\phi))}\mathrm{d}\phi \tag{3.42}$$

with $\theta_{\boldsymbol{x}}$ being given as in Eq.(3.40). Notice the relaxivity is still a function of θ_0. Much like the same manner of the slit pore case, this can be used to model signal decays on vascular pore structure through the introduction of a suitable assembly of capillaries. In Fig.3.5, the effect of averaging on surface relaxivity is presented for three sample inclinations.

Spherical pores

Spherical cavities correspond to a third simple geometry model. Nearly spherical pores can be found on vesicular porous media.

Obviously, if pores are sufficiently large, an isotropic areal distribution of surface element orientation is entailed and the mean relaxivity of each cavity is given by Eq.(3.35). If, on the other hand, pore radius is too small, it is possible that each cavity contributes to signal decay with a distinct rate that may even show a dependence on field direction, due to the fact that there are simply too few centers scattered over

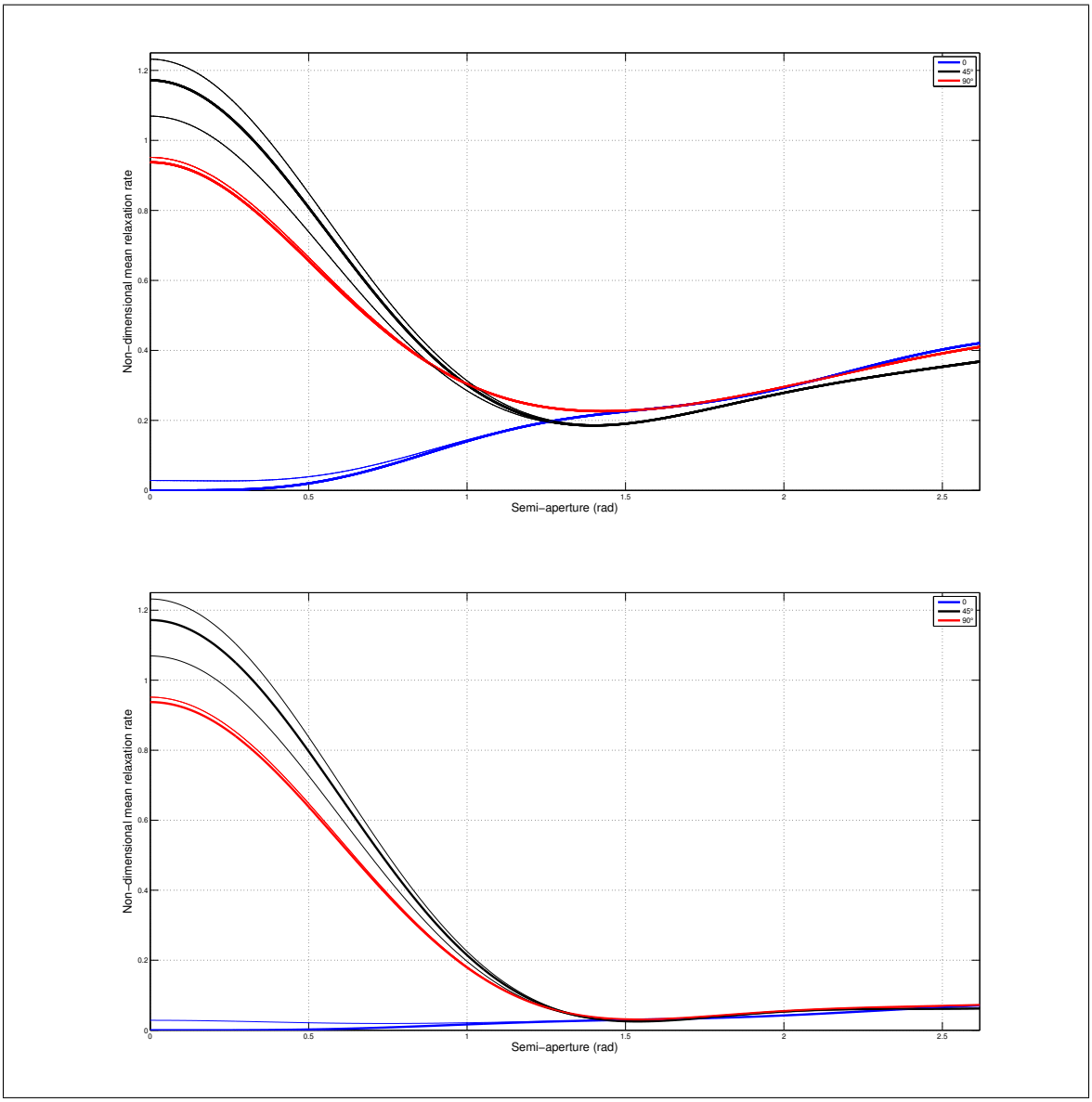

Figure 3.5: Mean surface longitudinal relaxation rates as function of semiaperture for the indicated inclination of a cylindrical pore structure. The thin lines represent the behavior for inclinations deviated by $\pm 5°$ from the intermediate indicated values. The top curves correspond to $\mathcal{D}_R\tau_0 = 1$, whereas the bottom ones to $\mathcal{D}_R\tau_0 = 10$. There is a continuous transition of the curves as the dynamical group is varied between the two showed values.

its boundary. However, such directional character should be lost upon averaging over the entire pore structure and again signal decay is explained by Eq.(3.35). Hence, no anisotropic response is expected from this sort of systems.

Pore-network models

The effect can be, at least qualitatively analyzed, in more general systems by clinging to the naive picture of a pore structure as a network of pores (vesicle-like regions) connect by throats (tubes) or cut through by fracture planes (slits). Provided the latter features are just as predominant as the former in terms of S/V ratio, a anisotropic response could hint about the directional character of pore topology in structure.

3.4 Experimental tests

Two types of systems with cylindrical pore geometry, a synthetic and a natural one, were tested for anisotropy response in the NMR signal decay. First studies were performed on arrays of silica capillaries acquired from Flexilicate (University of Malaya). Solid bundles were fabricated containing approximately 1950 silica capillaries with 50mm in length and no interstitial space between the cylindrical pores. Two bundles were used for the experiments, with 10 and 57μm pore diameters, respectively, as informed by the manufacturer. Pore structures are quite similar and sufficiently regular at the pore scale as seen in Fig.3.6. Both samples were saturated with distilled water. In the case of 57μm samples, saturation was achieved by capillary imbibition. For the 10μm ones, a syringe plunger was used to force water into the pores. The procedure consisted of attaching a bundle of approximately 20mm in length to the tip of a syringe and pressing the plunger until water was seen to come out through the other end. Then, 8mm fully saturated samples were cut out to be used in the experiments.

In order to also test for the effect in biological tissues, sections of bean sprout stem were selected as a natural vascular pore system. A bean seed (*phaseolus vulgaris*) was planted and cultivated on a cotton substrate with distilled water until the plant reached about 20cm in height. Segments of approximately 8mm in length were extracted from different positions along the stem for the experiments. No artificial saturation of these structures was induced, in other words, all water present in the studied tissue was absorbed by the plants themselves.

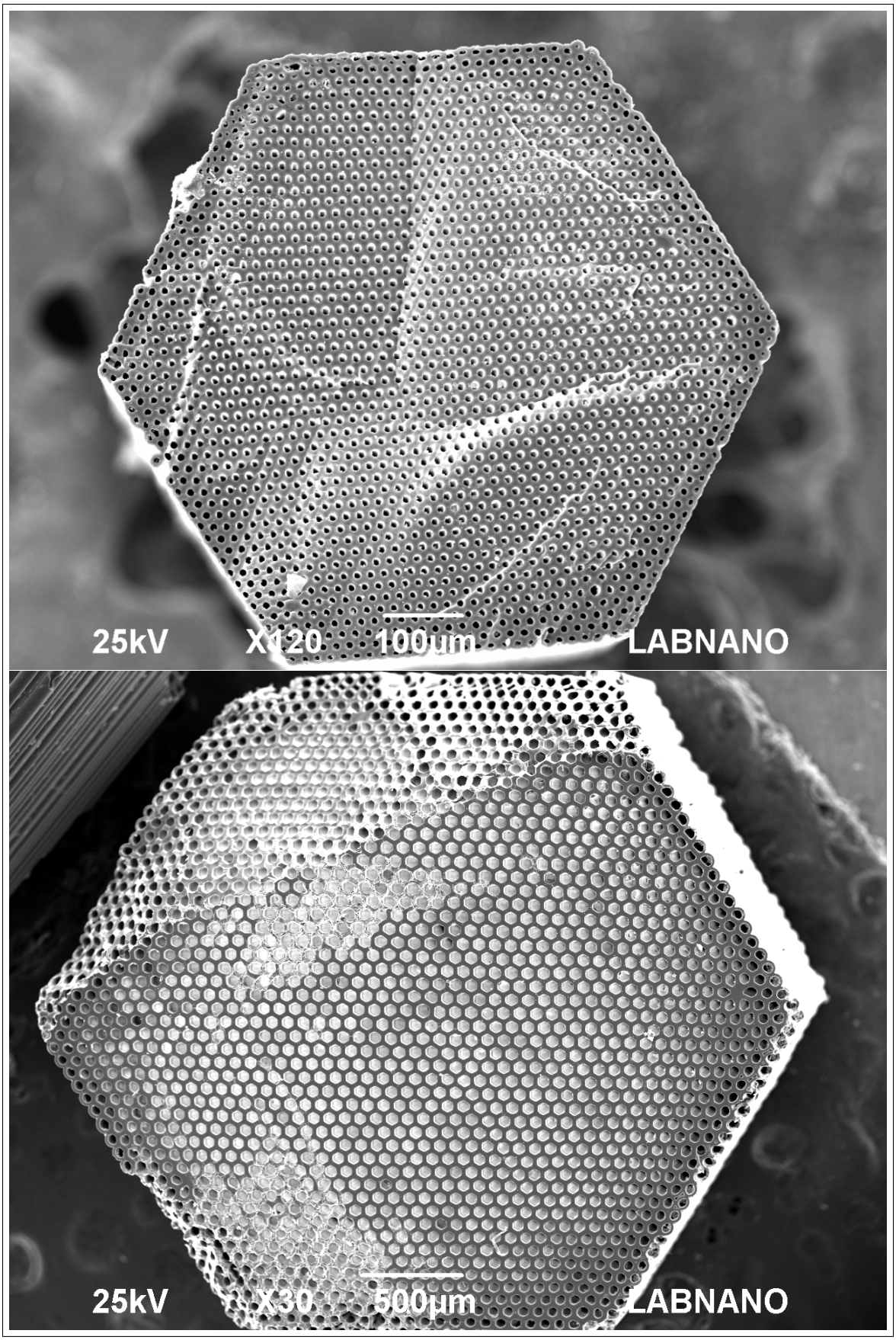

Figure 3.6: MEV scans of capillary bundles used in experiments: 10 and 57μm samples in the top and bottom respectively.

Longitudinal relaxation measurements (T_1) were performed on a high-field spectrometer (VARIAN 500MHz), using an inversion recovery sequence in a 10mm probe. Each sample was measured multiple times varying the angle θ_0 between the sample's axis and the static magnetic field B_0. To avoid desaturation effects and optimize signal-to-noise ratio during the measurements, all samples were previously submitted to a NMR-monitored drying experiment on laboratory conditions for calibration of sequence's total time, ensuring a loss of water not greater than 1% in all the cases. Thread seal tape was used to wrap and orient samples inside the NMR holder at different θ_0 values, orientation being set by means of a protractor. Naturally, the malleability of the tape and the process of handling down the sample through the holder are expected sources of error, but by visual examination it is estimated that samples were deviated from the intended orientation less than 5° after settling.

Figures 3.7 and 3.8 show the results obtained for longitudinal relaxation curves over three values of θ_0 for the 10 and 57μm capillary array and the bean stem sample respectively. Experimental points are marked and the black solid lines represent single exponential fits for each data set. Decay constants resulting from such fits are presented on Table 3.1.

The anisotropic response is not remarkable due to the face surface relaxivities being small, but it is observed in all considered structures. The working assumption is that the two synthetic samples used bear virtually identical characteristics regarding distribution and configuration of paramagnetic centers, so the increased sensibility revealed by decays in more confined samples would be entirely due to increase in S/V. Measured surface relaxivities, thus, are presented on Table 3.2 and are remarkably compatible and within the expected order of magnitude. The fact they are decreasing in the order 45°, 90°, 0 suggests semiapertures are of approximately 1 radian, provided $\mathcal{D}_R\tau_0$ is of order unity. This can be checked directly from the profiles depicted on Fig.3.5.

Unfortunately, the experimental resources to estimate concentration and nature of paramagnetic centers in the samples used were lacking. This would allow a further benchmarking of the proposed model. Sampling surface relaxivity on more inclinations would also be not only desirable but useful, specifically, for the estimation of microscopic parameters. However, it soon became apparent that the method devised for sample setting is simply too unrefined for the precise measurement that these estimates entail.

Finally, an anisotropic response was also observed in bean stem sections and the

Longitudinal decay rates in s^{-1}			
	0°	45°	90°
10μm	0.57 ± 0.04	0.67 ± 0.03	0.63 ± 0.02
57μm	0.372 ± 0.005	0.42 ± 0.02	0.40 ± 0.01
bean stem	0.59 ± 0.02	0.64 ± 0.03	0.67 ± 0.02

Table 3.1: Signal decay rates obtained from mono-exponential fits on the experimentally acquired data for each of the referred pore systems and sample inclination. Rates are in s^{-1}.For comparison, the measured bulk relaxation rate of water, used in the synthetic samples, was 0.3478 ± 0.0005.

Longitudinal surface relaxivities in μm/s			
	0°	45°	90°
10μm	0.5 ± 0.1	0.67 ± 0.08	0.59 ± 0.06
57μm	0.34 ± 0.08	1.0 ± 0.3	0.7 ± 0.2

Table 3.2: Longitudinal surface relaxivities for the two capillary bundles used. The numbers are expressed in μm/s.

results of one study is presented here only for the reader's appreciation. In order to explain the effect in such samples, it is conjectured that paramagnetic centers may be either formed by adsorption of paramagnetic ions at internal cell walls or the result of dangling bonds in the presumably intricate molecular structure of tissue boundaries.

3.5 Concluding Remarks

Some of the major ideas underlying the physics of enhanced NMR relaxation in fluids saturating porous media have been reviewed. The role of paramagnetic centers dilutely scattered along the solid surface has always been stressed as significant, however, the usual assumption that surface relaxivity is an uniform property is seen to oversimplify the problem for it neglects that the very influence of these centers must necessarily be local and dependent on the chemical structure of sites. Fast diffusion theories have successfully bypassed this issue due to the fact they are fully concerned with signal decay, thus making experimentally impossible to distinguish whether observed enhanced relaxation rates allude to a mean surface property or to an uniform quantity.

By assuming dominance of the electron-nucleus magnetic dipolar coupling over all other interactions that may induce nuclear relaxation and by taking into account the fact that the constraints imposed by solid boundaries, albeit likely equivalent, are not

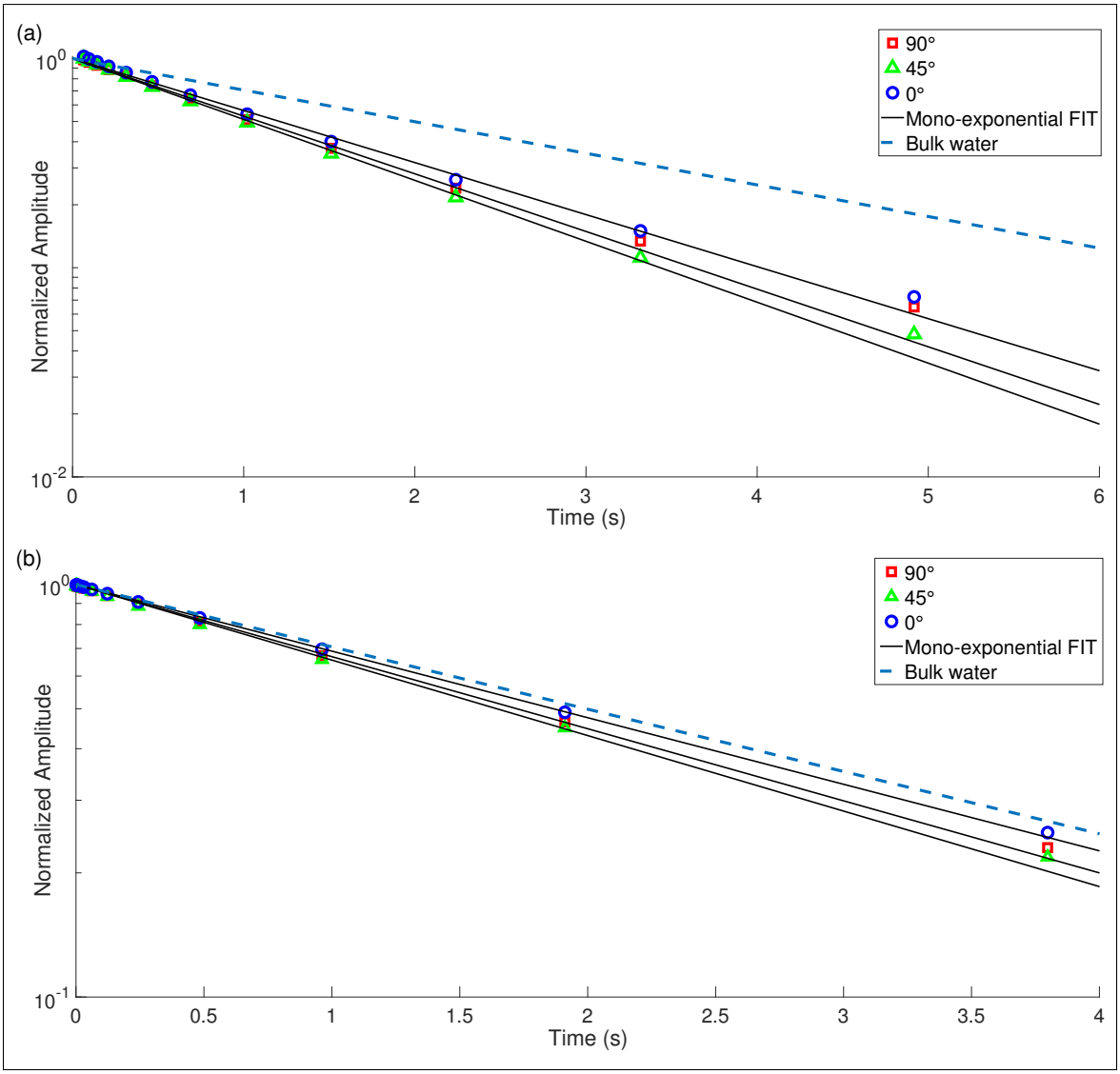

Figure 3.7: Longitudinal relaxation curves obtained for silica capillary array at different θ_0 values: (a) 10μm bundle, (b) 57μm. The magnetization has been normalized to best illustrate the single exponential character of the curves. The black solid lines are mono-exponential fits. The measured relaxation of bulk water is shown for comparison.

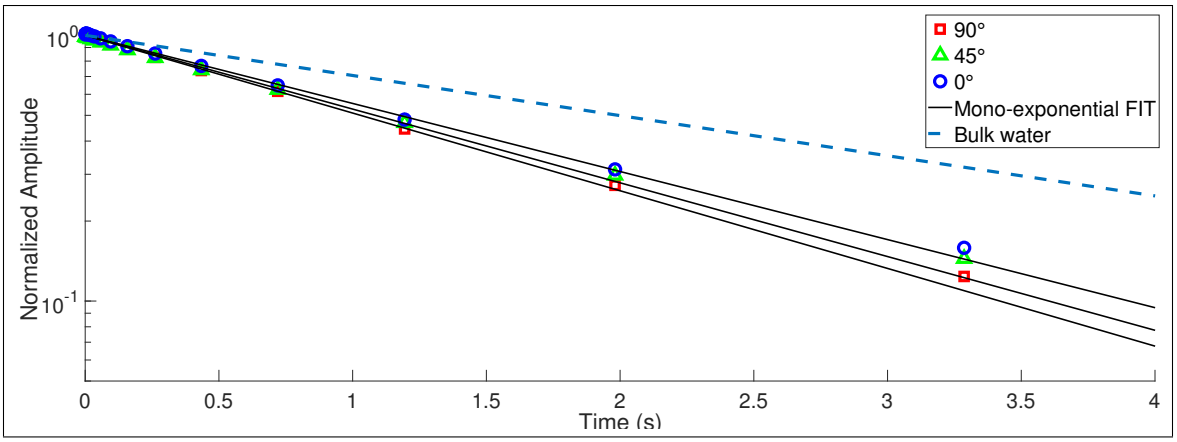

Figure 3.8: Longitudinal relaxation curves obtained for the bean stem sample at different θ_0 values. The magnetization has been normalized to best illustrate the single exponential character of the curves. Anisotropic response on signal decay was best observed on stem samples extracted from about 3cm above the roots. The black solid lines are mono-exponential fits. The measured relaxation of bulk water is shown for comparison.

in general identical for a naturally complex porous structure, it has been possible to put forward the thesis that, from the standpoint of the whole medium, NMR relaxation at surface-affected regions is a highly heterogeneous phenomenon, determined not only by the presence of paramagnetic centers, their nature and chemical state, but also by their orientation in relation to the external magnetic field.

Although discussions on the possibility and impact of heterogeneous surface-induced relaxation are not absent in the literature[89,90], they seem to be rather focused on the mathematical aspects of the underlying nuclear spin diffusion problem and motivated by the potentially frequent situation in which paramagnetic sites are not all chemically equivalent or evenly distributed along a boundary. The model here develop seems to be the first attempt to describe a fundamental mechanism pointing towards necessarily heterogeneous surface-induced relaxation, even though this intrinsic heterogeneity may have been recognized by other researchers since the paper of Kleinberg *et al.*[64].

The spectral densities pertaining to active surface elements regrettably are defined in terms of quite formidable expressions, which may hinder the quantitative applicability of the proposed theory notwithstanding the simplicity of the dynamical models employed. Other setback is the number of parameters introduced by the model that are already somewhat phenomenological on the microscopic scale. Surface relaxivities are also typically small in many materials, which is not particularly helpful when

trying to eliminate conceptual ambiguities via experimentation.

All of this indicates a need for improvement on the characterization of molecular motion nearby paramagnetic sites and, perhaps, on the development of proper electronic spin theories for surface structures. The former could definitely resolve some pertinent and long-standing questions as, for example, how relevant really is contact interaction or to what extent the constrained motion of few molecules is capable to represent well an effect that strictly concerns all molecules confined to a pore. It is recalled that at least two successful theories in explaining surface-induced signal decay in nano- and mesoporous structures do so without *binding* molecules to paramagnetic sites, as the presented model does. In turn, either molecular motion in the entire pore or over the whole surface is deemed relevant for successfully accounting for enhanced NMR relaxation[36,65]. Notwithstanding these issues, the proposed model yields sound results.

An anisotropic response depending on the morphology of the pore structure is an interesting prediction that it is experimentally confirmed, even though the effect has not been consistent or prominent in all considered samples. Another important feature is the logarithmic field-dependence on statistically isotropic structures. It is remarkable that such behavior arises naturally from the assumptions of the model and, in this case, has nothing to do with the long-time characteristic of local field correlations upon which the behavior has been previously justified[65]. As discussed, the dependence agrees qualitatively with that suggested by H^1-NMRD data on cementitious materials and it is speculated that agreement could be improved quantitatively through the use of more detailed electron spin models.

Finally, it is important to point out the fact that in the considered approach the matter of surface roughness has been deliberately avoided. On the treatment of simple pore structures, the assumption of ideally smooth boundaries is tacit. The *macroscopic* effects of roughness though could be incorporated to the theory without much difficulty by introducing a distribution of inclinations for surface elements that accounts for microscopic boundary irregularities. However, it is not clear whether surface texture does not also bring about its own set of complications, like asymmetry or bias in molecular wobbling (picture the cap of lopsided cone defining the dynamical region) or a non-uniformity of conical apertures along the surface. This last feature, in fact, can be easily modeled within the presented framework, provided one knows the details of molecular coordination around paramagnetic sites in the considered system. The first, on the other hand, requires a new calculation of dipolar correlations; the

underlying problem is quite involved but has been given attention by Gengeliczki *et al.*[39]. Nevertheless, such refinements do not seem to be very rewarding in the sense that, due to the typical weak character of surface-induced relaxation, the NMR signal decay is probably not a very good probe to surface-affected molecular behavior.

CHAPTER 4

Internal field encoding

In this chapter, a method is proposed to observe experimentally internal field characteristics, specifically, the autocorrelation function introduced in Chapter 2. The technique can be seen as a new take on the DDIF method [100,102] since the NMR protocols used are still based on the stimulated echo sequence template. In fact, all internal field encoding sequences here introduced are implemented identically to a PFG-SE sequence, being distinguished by the fact that no external source of field heterogeneity is ever used.

A thorough discussion of all various DDIF protocols is presented within the framework of Laplace eigenstructures. This turns out to be possible due to the fact that a closed expression for the NMR signal can be given, much like in the same way the PFG signal is explicitly determined when the NPA holds, provided field modulations are narrow in the sense defined below.

4.1 Narrow modulation

Consider the template of a stimulated echo sequence (SE):

$$\underbrace{\frac{\pi}{2}\text{---}t_e\text{---}}_{\text{I}}\underbrace{\frac{\pi}{2}\text{---------}t\text{---------}}_{\text{II}}\underbrace{\frac{\pi}{2}\text{---}t_d\text{---}\ \text{Acq.}}_{\text{III}}$$

As already discussed, encoding and decoding are performed respectively in the first and third stages; the storage (intermediate) stage is where nuclear magnetization undergoes diffusion uninfluenced by field heterogeneities.

The basic idea behind this structure is that the spin phase encoded in the first block is propagated over the second one along trajectories (realizations) that are characteristic of the underlying diffusion process to which particles are subjected. Notice that if diffusive transport were negligible during storage, then the dephasing promoted by the encoding stage would be perfectly corrected at decoding and so no echo attenuation would follow. SE sequences therefore advance a scheme through which the dephasing effect of diffusion can be (ideally) isolated and observed.

In a PFG-SE sequence, a gradient pulse is applied to encode and decode spin positions. However, a similar effect can also be established by simply leaving the system idle for a certain amount of time in the presence of internal field heterogeneities. Any method that exploits this effect can therefore be termed an internal field encoding technique, regardless of the temporal profile being used[1]. The considered SE template is interesting because of its simplicity.

Having thus decided on the basic temporal profile, it is possible to analyze what information can be acquired from a particular sequence. In fact, a closed expression for the echo amplitude can be given provided diffusion can be neglected over encoding and decoding periods. This requirement is similar to the NPA, used extensively in the analysis of PFG sequences, but it must be observed that, with the particular use of internal field heterogeneities, such a condition may be too stringent.

Recall that the NPA is valid only over time scales in which spins diffuse, on average, less than the scale of field heterogeneity. For gradient pulses, the latter scale is usually macroscopic, say in the order of the millimeter, which means pulses can be as long as in the hundreds of milliseconds and still satisfactorily satisfy the conditions for the NPA. Internal fields, on the other hand, are presumed to change over micrometric distances in typical porous samples. Therefore, modulations imposed at encoding and decoding intervals have to be at least three order of magnitude shorter than the typical duration of gradient pulses. This requirement by itself is not too problematic from a control standpoint but does introduce a problem of sensitivity which is best understood once it is considered what such narrow modulations imply.

If t_e is sufficiently short, then, right at the end of encoding, the nuclear magnetization has picked up a phase factor determined by $\exp(-i\gamma b(\boldsymbol{X})t_e)$, as it follows

[1]For example, a Hahn echo sequence obviously defines a internal encoding method as well

directly from the Bloch-Torrey equation with the neglect of diffusion. If the internal field, $b(\boldsymbol{X})$, is a product of susceptibility contrasts, it must be proportional to the susceptibility difference[2] and to B_0. Hence, it is reasonable to assume that the encoded phase has its magnitude governed by the parametric group $\Delta\chi\omega_0 t_e$, which must be ranged in between in 10^{-3} to 10^{-1} rad for Larmor frequencies in the interval of 1 to 100 MHz, provided it is assumed $\Delta\chi \approx 10^{-4}$ [81] and t_e, as discussed, is in the order of tens of microseconds. As a result, narrow modulation typically implies small encoded phases, a regime called *weak encoding*. However, if encoding is indeed too weak, it might simply become too difficult to distinguish the resultant signal from what can be called a T_1 decay, i.e., the NMR signal of a sequence with no encoding whatsoever. Because of this sensibility issue internal field encoding methods should generally work best under high field conditions.

Alternatively, the GPA could be used to interpret results from low field set-ups when narrow modulation requirements cannot be met. This approach will be considered elsewhere. In the following material, narrow modulation is always assumed.

4.1.1 The general sequence

Let $\varphi(\boldsymbol{X}) \equiv \gamma b(\boldsymbol{X}) t_e$ be encoded spin phase and at first assume $t_d = t_e$. A general expression can be given for the signal produced by an arbitrary sequence defined over the SE template. Here, the notation and results presented in Appendix A regarding the effect of RF pulsed are used.

Encoding

Nuclear magnetization by the end of encoding is determined by

$$m(\boldsymbol{X}, t_e^-) = m_0 e^{i\left(\phi_1 - \frac{\pi}{2}\right)} e^{-i\varphi(\boldsymbol{X})} \tag{4.1}$$

wherein $\phi_1 = n_1\pi/2$, $n_1 = \{0, 1, 2, 3\}$, is the RF pulse phase.

Storage

A single component of the transverse magnetization can be stored on the longitudinal axis per implementation. Over the storage time, t, spins experience NMR

[2] Strictly, the relative permeability of two media is the parameter that governs field distributions. However, when both media have small susceptibilities compared to unity, the field heterogeneity, that is, the component that adds to the external field is proportional to the susceptibility difference.

relaxation and undergo diffusion. Once again, let $G_t(\boldsymbol{X}, \boldsymbol{X}_0)$ denote the diffusion propagator for the underlying diffusion problem. It is then straightforward to show that (see Eq.(A.1) and Eq.(2.28)) the nuclear magnetization by end of storage is given by

$$\begin{aligned} M_z(\boldsymbol{X}, t) = m_0 \left(1 - e^{-\frac{t}{\mathrm{T}_1}} \int_\Omega \mathrm{d}^3\boldsymbol{X}_0\, G_t(\boldsymbol{X}, \boldsymbol{X}_0)\right) \\ - M_0 e^{-\frac{t}{\mathrm{T}_1}} \int_\Omega \mathrm{d}^3\boldsymbol{X}_0\, G_t(\boldsymbol{X}, \boldsymbol{X}_0) \cos\left(\varphi(\boldsymbol{X}_0) + \phi_2 - \phi_1\right) \end{aligned} \tag{4.2}$$

in which $\phi_2 = n_2\pi/2$ is the phase of the second RF pulse.

Decoding

Decoding has the same structure of encoding because respective time intervals are of the same duration. Therefore, at acquisition, the magnetization of the system is

$$m(\boldsymbol{X}, t_d) = M(\boldsymbol{X}, t) e^{i\left(\phi_3 - \frac{\pi}{2}\right)} e^{-i\varphi(\boldsymbol{X})}. \tag{4.3}$$

once again $\phi_3 = n_3\pi/2$ is the RF pulse phase.

The signal

Finally, the echo amplitude is determined by

$$E(t) = \left[S_{sat}(t) - M_0 e^{-\frac{t}{\mathrm{T}_1}} \int_\Omega \mathrm{d}^3\boldsymbol{X} \int_\Omega \mathrm{d}^3\boldsymbol{X}_0\, e^{-i\varphi(\boldsymbol{X})} G_t(\boldsymbol{X}, \boldsymbol{X}_0) \cos\left(\varphi(\boldsymbol{X}_0) + \phi_2 - \phi_1\right)\right] e^{i\left(\phi_3 - \frac{\pi}{2}\right)}. \tag{4.4}$$

The contribution $S_{sat}(t)$ is precisely the signal of a saturation recovery at time t. Notice that this term is independent of the first two RF pulse phases. Thus, once ϕ_3 is fixed, this contribution can be effectively removed from the resultant signal by an appropriate phase cycling.

4.1.2 DDIF protocols

Although the effects of internal fields have always been to some extent considered in NMR relaxation and diffusion methods, the first internal field encoding method proposed with the intention of probing pore geometry characteristics appears to be the DDIF sequence[73,101,102]. The protocols are entirely based on the SE template

and, due to the extra degree of control introduced by phase cycling, it is possible to distinguish three DDIF methods.

	n_1	n_2	n_3	Acq
Sine DDIF	1	0	0	+
	3	0	0	-
	1	2	0	-
	3	2	0	+
Cosine DDIF	1	0	0	+
	3	0	0	-
	1	2	0	-
	3	2	0	+

Table 4.1: Phase cycling for DDIF sequences

The sine method

Consider the phase cycling for the sine sequences presented at Table 4.1. The signals produced by each implementation are

$$\begin{aligned} E_{1,4}(t) &= -iS_{sat}(t) + iM_0 e^{-\frac{t}{\mathrm{T_1}}} \int_\Omega \mathrm{d}^3\boldsymbol{X} \int_\Omega \mathrm{d}^3\boldsymbol{X}_0\, e^{-i\varphi(\boldsymbol{X})} G_t(\boldsymbol{X},\boldsymbol{X}_0) \sin\varphi(\boldsymbol{X}_0), \\ E_{2,3}(t) &= -iS_{sat}(t) - iM_0 e^{-\frac{t}{\mathrm{T_1}}} \int_\Omega \mathrm{d}^3\boldsymbol{X} \int_\Omega \mathrm{d}^3\boldsymbol{X}_0\, e^{-i\varphi(\boldsymbol{X})} G_t(\boldsymbol{X},\boldsymbol{X}_0) \sin\varphi(\boldsymbol{X}_0). \end{aligned} \tag{4.5}$$

Stacking ($E = E_1 - E_2 - E_3 + E_4$) and normalization of the resultant signal yields

$$\begin{aligned} E_{sin}(t) &= i\frac{e^{-\frac{t}{\mathrm{T_1}}}}{V} \int_\Omega \mathrm{d}^3\boldsymbol{X} \int_\Omega \mathrm{d}^3\boldsymbol{X}_0\, e^{-i\varphi(\boldsymbol{X})} G_t(\boldsymbol{X},\boldsymbol{X}_0) \sin\varphi(\boldsymbol{X}_0) \\ &\equiv ie^{-\frac{t}{\mathrm{T_1}}} \left\langle e^{-i\varphi(\boldsymbol{X}_t)} \sin\varphi(\boldsymbol{X}_0) \right\rangle, \end{aligned} \tag{4.6}$$

where once again the bracket notation for expectations is introduced to evidence the statistical interpretation of the diffusion propagator.

The cosine method

Similarly, implementing the cycling for the cosine sequences, also presented at Table 4.1, produces a signal given by

$$\begin{aligned} E_{cos}(t) &= i\frac{e^{-\frac{t}{\mathrm{T_1}}}}{V}\int_\Omega \mathrm{d}^3\boldsymbol{X}\int_\Omega \mathrm{d}^3\boldsymbol{X}_0\, e^{-i\varphi(\boldsymbol{X})}G_t(\boldsymbol{X},\boldsymbol{X}_0)\cos\varphi(\boldsymbol{X}_0) \\ &\equiv ie^{-\frac{t}{\mathrm{T_1}}}\left\langle e^{-i\varphi(\boldsymbol{X}_t)}\cos\varphi(\boldsymbol{X}_0)\right\rangle \end{aligned} \tag{4.7}$$

after normalization.

The Modulated Internal Field (MIF) method

The basic distinction of sine and cosine DDIF protocols is what component of the encoded magnetization is stored. As it turns out, it is just as easy to produce a protocol that stores transverse magnetization completely. An example is shown at Table 4.2 and such a choice defines what is here called the MIF sequence. For encoding and decoding stages of equal duration, the signal after normalization is determined by

$$\begin{aligned} E_{MIF}(t) &= \frac{e^{-\frac{t}{\mathrm{T_1}}}}{V}\int_\Omega \mathrm{d}^3\boldsymbol{X}\int_\Omega \mathrm{d}^3\boldsymbol{X}_0\, e^{-i\varphi(\boldsymbol{X})}G_t(\boldsymbol{X},\boldsymbol{X}_0)e^{i\varphi(\boldsymbol{X}_0)} \\ &\equiv e^{-\frac{t}{\mathrm{T_1}}}\left\langle e^{-i(\varphi(\boldsymbol{X}_t)-\varphi(\boldsymbol{X}_0))}\right\rangle. \end{aligned} \tag{4.8}$$

For arbitrary but sufficiently small t_e and t_d, however, the MIF signal is determined by the two-point characteristic function of the internal field variable, that is, the random process associated with the magnetic field inhomogeneity within the pore space that is induced by the Brownian motion of nuclei. Let $u_e = \gamma t_e$ and $u_d = \gamma t_d$, so to write

$$E_{MIF}(t) = e^{-\frac{t}{\mathrm{T_1}}}\left\langle e^{-iu_d b_t}e^{iu_e b_0}\right\rangle \equiv e^{-\frac{t}{\mathrm{T_1}}}\Phi_b(-u_d,u_e). \tag{4.9}$$

Because all two-point statistical information regarding the process is contained in the latter function (see Appendix B), knowledge of internal field autocorrelation and field scattering kernel is, in principle, experimentally accessible. Namely,

$$\begin{aligned} \langle b_t b_0\rangle &= \frac{\partial^2\Phi_b(0,0)}{\partial u_d\partial u_e}, \\ \left\langle \Delta b^2(t)\right\rangle &= -\left.\frac{\mathrm{d}^2\Phi_b(-u_e,u_e)}{\mathrm{d}u_e^2}\right|_{u_e=0}. \end{aligned} \tag{4.10}$$

This perspective is the main advantage of the MIF protocol over the other DDIF methods and seems to have not been explored before the present work even though the sequence behind Eq.(4.8) was the first DDIF sequence proposed[100].

There is, however, a practical issue: Because the desired information is contained in fact on the derivatives of Φ, to determine internal field correlations experiments need to be carried over a two-dimensional array of u_e and u_d values and results need to be appropriately grouped and interpolated. The whole procedure is, unfortunately, easier said than done as it can be too demanding, from experimental and numerical perspectives, to acquire consistent data from internal encoding sequences at times not in general fulfilling the rephasing condition and process it.

An alternative and more viable approach is here formulated by exploiting the fact that if encoding is sufficiently weak, the encoded phase is typically defined by a small number.

	n_1	n_2	n_3	Acq
MIF	1	0	0	+
	3	0	0	-
	1	2	0	-
	3	2	0	+
	1	0	3	+
	3	0	3	-
	1	2	3	-
	3	2	3	+

Table 4.2: Phase cycling for the MIF sequence

4.1.3 Weak encoding

Weak encoding refers to the assumption $\varphi(\boldsymbol{X}) \ll 1$ everywhere. The regime is of practical importance for it reduces echo amplitude to a combination of the first statistical moments of the encoded phase variable. Namely, for $t_e = t_d$,

$$\begin{aligned}
\tilde{E}_{sin}(t) &= i\,\langle\varphi(\boldsymbol{X}_0)\rangle + \langle\varphi(\boldsymbol{X}_t)\varphi(\boldsymbol{X}_0)\rangle + \mathcal{O}(\varphi^3),\\
\tilde{E}_{cos}(t) &= i\,\langle 1\rangle + \langle\varphi(\boldsymbol{X}_t)\rangle - i\,\langle\varphi(\boldsymbol{X}_t)^2 + \varphi(\boldsymbol{X}_0)^2\rangle + \mathcal{O}(\varphi^3),\\
\tilde{E}_{MIF}(t) &= \langle 1\rangle - i\,\langle\varphi(\boldsymbol{X}_t) - \varphi(\boldsymbol{X}_0)\rangle - \frac{1}{2}\left\langle(\varphi(\boldsymbol{X}_t) - \varphi(\boldsymbol{X}_0))^2\right\rangle + \mathcal{O}(\varphi^3),
\end{aligned} \tag{4.11}$$

in which $\tilde{E}(t) \equiv E(t)e^{t/\mathrm{T_1}}$.

Assuming the diffusion propagator is symmetric under interchange of position arguments, it is possible to simplify the expressions even further:

$$\begin{aligned}\tilde{E}_{sin}(t) &= \langle\varphi(\boldsymbol{X}_t)\varphi(\boldsymbol{X}_0)\rangle + i\,\langle\varphi(\boldsymbol{X}_0)\rangle\,,\\ \tilde{E}_{cos}(t) &= \langle\varphi(\boldsymbol{X}_0)\rangle + i\,\left(\langle 1\rangle - 2\left\langle\varphi(\boldsymbol{X}_0)^2\right\rangle\right),\\ \tilde{E}_{MIF}(t) &= \langle 1\rangle - \frac{1}{2}\left\langle(\varphi(\boldsymbol{X}_t) - \varphi(\boldsymbol{X}_0))^2\right\rangle,\end{aligned} \tag{4.12}$$

wherein higher order contributions are neglected.

It is seen that weak encoding, in principle, allows a more straightforward experimental determination of internal field characteristics. The autocorrelation and mean function appear respectively as the real and imaginary part of a Sine DIFF echo and the field scattering kernel is contained in the MIF signal and can be easily isolated once the T_1 decay signal is determined.

4.2 Probing confinement length scales

As discussed in Chapter 2, the Neumann Laplace eigenstructure provides genuine geometric information about a domain. Particularly, Neumann eigenvalues relate to the length scale of variation of corresponding eigenfunctions, which must be somehow associated with the relevant length scales and topology of the underlying geometry. Due to its fundamental nature, it is instructive to consider first the meaning of the statistical moments of the encoded phase in the absence of surface relaxivity. Then, because

$$\int_\Omega \mathrm{d}^3\boldsymbol{X}\, G_t(\boldsymbol{X},\boldsymbol{X}_0) = 1 \quad \forall \boldsymbol{X}_0 \in \Omega, \tag{4.13}$$

$$\begin{aligned}\langle 1\rangle = 1 \quad \text{and} \quad \left\langle\varphi(\boldsymbol{X}_0)^k\right\rangle &= \frac{1}{V}\int_\Omega \mathrm{d}^3\boldsymbol{X}\int_\Omega \mathrm{d}^3\boldsymbol{X}_0\, G_t(\boldsymbol{X},\boldsymbol{X}_0)\varphi(\boldsymbol{X}_0)^k\\ &= \frac{1}{V}\int_\Omega \mathrm{d}^3\boldsymbol{X}_0\,\varphi(\boldsymbol{X}_0)^k = \bar{\varphi^k}.\end{aligned} \tag{4.14}$$

Thus, on weak encoding, the signals produced by all three methods here considered are governed exclusively by the field autocorrelation function if $\rho_1(\boldsymbol{X}) = 0$ and,

accordingly,

$$\begin{aligned}\langle\varphi(\boldsymbol{X}_t)\varphi(\boldsymbol{X}_0)\rangle &= \frac{1}{V}\int_\Omega \mathrm{d}^3\boldsymbol{X}\int_\Omega \mathrm{d}^3\boldsymbol{X}_0\,\varphi(\boldsymbol{X})\left(\sum_{m=0}^{\infty} e^{-D_0\lambda_m^2 t}u_m(\boldsymbol{X})u_m^*(\boldsymbol{X}_0)\right)\varphi(\boldsymbol{X}_0)\\ &= \sum_{m=0}^{\infty} e^{-D_0\lambda_m^2 t}\left(\frac{1}{\sqrt{V}}\int_\Omega \mathrm{d}^3\boldsymbol{X}\,\varphi(\boldsymbol{X})u_m(X)\right)\left(\frac{1}{\sqrt{V}}\int_\Omega \mathrm{d}^3\boldsymbol{X}_0\,u_m^*(X_0)\varphi(\boldsymbol{X}_0)\right)\\ &= \frac{1}{V}\sum_{m=0}^{\infty} e^{-D_0\lambda_m^2 t}|\,\langle m|\varphi\rangle\,|^2.\end{aligned} \tag{4.15}$$

Also,

$$\begin{aligned}\left\langle\Delta\varphi^2(t)\right\rangle = \frac{1}{2}\left\langle(\varphi(\boldsymbol{X}_t)-\varphi(\boldsymbol{X}_0))^2\right\rangle &= \left\langle\varphi(\boldsymbol{X}_0)^2\right\rangle - \langle\varphi(\boldsymbol{X}_t)\varphi(\boldsymbol{X}_0)\rangle\\ &= \bar{\varphi^2} - \frac{1}{V}\sum_{m=0}^{\infty} e^{-D_0\lambda_m^2 t}|\,\langle m|\varphi\rangle\,|^2\\ &= \frac{1}{V}\sum_{m=1}^{\infty}|\,\langle m|\varphi\rangle\,|^2\left(1-e^{-D_0\lambda_m^2 t}\right).\end{aligned} \tag{4.16}$$

Substitution on Eq.(4.12) implies that the Sine DDIF sequence produces a fast decay from $\bar{\varphi^2}$ to the level defined by $\bar{\varphi}^2$. The difference $\bar{\varphi^2}-\bar{\varphi}^2$ determines the **spatial variance of the encoded phase**, precisely, the spin phase dispersion present in the system by the end of encoding. The Cosine DDIF signal, on the other hand, does not vanish any faster than the bulk decay, up to the considered order of approximation. For the signal produced by the MIF sequence, in its turn, it is best to subtract entirely the contribution from the T_1 decay. From this simple procedure, the variance of the encoded phase (i.e., the field scattering kernel) can be observed as a function of time. Of course, by a similar manipulation, the same curve could be, in theory, produced by the components of a Sine DDIF signal. In practice, however, probing second moment information directly from signal decay can become unfeasible under weak encoding and it is generally non-trivial to assure that the encoding regime holds.

Encoded phase variance and autocorrelation

The encoded phase variance indicates how much dephasing is imposed on nuclear spins by diffusive transport alone. It starts from zero, as no dephasing can occur if there is no motion, and monotonically tends to the cap defined by the spatial variance

as nuclei move beyond the correlation distance of the internal field. The shape of the curve depends directly on which superior diffusion modes are activated by the internal field.

If a single mode is excited, the build up has a characteristic sigmoid form. Again, it is instructive to think of $\sqrt{D_0 t}$ as the diffusion length scale even in the case of restricted diffusion. Then, it can be said that the contribution of each mode saturates as soon as particles diffuse over a distance comparable to the characteristic length scale of the mode.

Now, if multiple modes are relevant, individual mode saturation could become visible in the form of short shoulderlike segments below full saturation level, provided length scales are sufficiently distinct. This in principle allows for **time domain** identification of diffusion length scales and, because the degree by which modes are activated depends on how much *resemblance* field heterogeneities bear to them, the phase variance is not only useful in characterizing length scales pertaining to internal fields but also characteristic lengths of the pore structure itself[101].

Finally, since the variance and the autocorrelation function of the encoded are complementary functions, knowledge of one determines the other completely. In practice, however, such a correspondence is only strictly valid in the absence of surface relaxation.

4.2.1 The effect of surface relaxation

Surface-induced relaxation is unavoidable in most porous systems. A non-zero surface relaxivity produces a diffusion propagator that is no longer *normalized* in the sense of Eq.(4.13). As a result, all moments of the encoded phase now show a time decay. This is readily verified through the eigendecomposition of the Robin propagator. Namely,

$$\begin{aligned}\langle 1\rangle &= \frac{1}{V}\int_\Omega \mathrm{d}^3\boldsymbol{X}\int_\Omega \mathrm{d}^3\boldsymbol{X}_0\left(\sum_{m=0}^{\infty} e^{-D_0\mu_m^2 t} v_m(\boldsymbol{X}) v_m^*(\boldsymbol{X}_0)\right)\\ &= \sum_{m=0}^{\infty} e^{-D_0\mu_m^2 t}\left(\frac{1}{\sqrt{V}}\int_\Omega \mathrm{d}^3\boldsymbol{X}\, v_m(X)\right)\left(\frac{1}{\sqrt{V}}\int_\Omega \mathrm{d}^3\boldsymbol{X}_0\, v_m^*(X_0)\right)\\ &= \sum_{m=0}^{\infty} e^{-D_0\mu_m^2 t}|\,\langle 0|v_m\rangle\,|^2,\end{aligned} \tag{4.17}$$

$$\left\langle \varphi(\boldsymbol{X}_0)^k \right\rangle = \frac{1}{\sqrt{V}} \sum_{m=0}^{\infty} e^{-D_0 \mu_m^2 t} \langle 0|v_m\rangle \left\langle v_m|\varphi^k \right\rangle , \tag{4.18}$$

$$\langle \varphi(\boldsymbol{X}_t)\varphi(\boldsymbol{X}_0)\rangle = \frac{1}{V} \sum_{m=0}^{\infty} e^{-D_0 \mu_m^2 t} \langle \varphi|v_m\rangle \langle v_m|\varphi\rangle . \tag{4.19}$$

Once again the notation $|m\rangle$ is reserved to Neumann eigenfunctions; the meaning of the above expressions is therefore clear. For any $\rho \neq 0$, the lowest eigenvalue μ_0^2 is no longer identically zero, so all functions in fact vanish as $t \longrightarrow \infty$.

Although any surface relaxation produces a dramatic effect on the time dependence of statistical moments, frequently, it only slightly perturbs the spatial features of Neumann diffusion modes. **Fast diffusion** is experimentally manifested by a nearly mono-exponential T_1 decay. For this to occur, it is clear from Eq.(4.17) that the projection of superior Robin eigenmodes onto the fundamental Neumann mode must be negligible. Actually, in fast diffusion, each Robin eigenmode remains nearly parallel to its Neumann counterpart (see Appendix.C). If Neumann eigenmodes for a given pore structure are non-degenerate, it is possible to show that up to the first order of perturbation, Eq.C.14,

$$\langle 1\rangle = e^{-\bar{\rho} S t/V} \tag{4.20}$$

$$\left\langle \varphi(\boldsymbol{X}_0)^k \right\rangle = \frac{e^{-\bar{\rho} S t/V}}{\sqrt{V}} \left(\langle 0|\varphi^k\rangle - \sum_{n=1}^{\infty} \frac{R_{0n}}{D_0 \lambda_n^2} \left\langle n|\varphi^k \right\rangle \right) + \frac{1}{\sqrt{V}} \sum_{n=1}^{\infty} e^{-\left(D_0 \lambda_n^2 + R_{nn}\right) t} \frac{R_{n0}}{D_0 \lambda_n^2} \left\langle n|\varphi^k \right\rangle , \tag{4.21}$$

$$\begin{aligned} \langle \varphi(\boldsymbol{X}_t)\varphi(\boldsymbol{X}_0)\rangle = \frac{1}{V} \sum_{m=0}^{\infty} & e^{-\left(D_0 \lambda_m^2 + R_{mm}\right) t} \langle \varphi|m\rangle \langle m|\varphi\rangle \\ & + \frac{2}{V} \sum_{m,n \neq m} e^{-\left(D_0 \lambda_m^2 + R_{mm}\right) t} \frac{R_{mn}}{D_0 \left(\lambda_m^2 - \lambda_n^2\right)} \langle \varphi|m\rangle \langle n|\varphi\rangle \end{aligned} \tag{4.22}$$

wherein $\bar{\rho}$ denotes the mean surface relaxivity and the matrix elements R_{mn} are defined by Eq.(C.7).

The mean encoded phase

The fact that superior eigenmodes already play a part in the evolution of the mean encoded phase was used by Lisitza and Song[73] when proposing the Sine DDIF method as an alternative to traditional NMR relaxation approaches for probing confinement length scales. To put it in the terminology of this chapter, their idea consists simply of using the long time behavior in the T_1 decay signal (called the reference

signal by the authors) to remove the contribution of the fundamental diffusion mode from the mean encoded phase, thus producing a processed decay curve determined only by superior diffusion modes.

Song[101] then argues, based on computer simulations, that internal field heterogeneities typically appear within, rather than across, the pores of a complex structure. This idea suggests internal field encoding is most effective in activating diffusion modes whose characteristic length scales are compatible to pore sizes. Hence, revealing the possibility for a direct assessment of these quantities through exponential analysis of the resultant signal. In this respect, Lisitza and Song's protocol is advantageous in comparison to the traditional NMR relaxometric approach, because the conversion factor between rates and length scales in the former method is a quantity that can be determined irrespective of the porous medium, namely, the molecular diffusion coefficient, D_0, whereas in the latter an isolated measurement of $\bar{\rho}$ is required for every porous system studied.

Though the DDIF method indeed represents a considerable improvement in the logic behind NMR pore size characterization, it remains attached to the data processing procedure of traditional approaches. Non-negative Laplace inversions of recovery and CPMG signals are commonplace in NMR-based studies of porous media. The positivity constraint there, vital not only for producing reasonable pore size distributions but also for improving the resolution of inversions themselves, is guaranteed by relations like Eq.(4.17) in which the *weight* of each mode is necessarily positive. On the other hand, there is no *a priori* justification for adopting such a constraint in the processing of Sine DDIF data, as Eq.(4.18) suggests.

To stress this and some other issues of the formulation, consider a situation in which Eq.(4.21) applies. Assume, for example, that the considered pore structure is a collection of isolated or nearly isolated pore systems of similar geometrical features and the conditions for validity of Eq.(4.21) are met in every substructure. Then, each of them introduces in the observed signal a decay given by

$$\sum_{n=1}^{\infty} e^{-\left(D_0\lambda_n^2+R_{nn}\right)t}\frac{R_{n0}}{D_0\lambda_n^2}\left\langle n|\varphi\right\rangle . \tag{4.23}$$

Frequently, the slowest activated mode not only survives for longer but virtually determines the sum. For definiteness, denote this mode by $\hat{n}$. Accordingly, the resultant DDIF signal can be interpreted as the Laplace transform of a distribution

whose non-zero values relate to coefficients

$$\frac{R_{\hat{n}0}\,\langle \hat{n}|\varphi\rangle}{D_0\lambda_{\hat{n}}^2} \tag{4.24}$$

that pertain to each porous substructure. It is clear that the above expression is not necessarily positive and, interestingly, not exclusively determined by the encoded phase. Consequently, imposing a positivity constraint on Laplace inversions of Sine DDIF signals is generally unwarranted. A conclusion that in fact does not change by assuming the porous medium is, conversely, well communicated, so the DDIF signal itself is expressed by Eq.(4.23). This is, really, a major shortcoming of the Sine DDIF method. But, perhaps, it serves to point out that the information provided by the mean encoded phase is not quite the most adequate for pore size characterization.

Finally, Lisitza and Song's protocol is not particularly suited to deal with multi-scaled porous media as well. This is most easily seen by assuming the pore structures in each scale are isolated from one another. Then, the long time behavior of the T_1 decay is dictated by the slowest fundamental mode; typically, that corresponds to the least confined structure in the medium. Therefore, in order to produce a decay determined only by superior modes, successive elimination of fundamental modes must be performed, which is not ideal as that already requires a prior exponential analysis of T_1 decays[102].

Autocorrelation and variance

In retrospect, Eq.(4.19) reveals the autocorrelation function is more appropriate for the whole analytical procedure to which, rather, the mean encoded phase is subjected in the Sine DDIF method. Plainly, removal of the fundamental mode contribution can be done in the same manner and the moment can be normalized into a convex combination of exponential decays, hence the positivity constraint necessarily applies upon inversion.

There can be, however, a detectability problem with the direct acquisition of second order terms in the Sine DDIF methods. Recall the method produces an echo that appears predominantly in the imaginary component of the signal. Because of weak encoding, it can be difficult to acquire consistently the second order contribution in the real part. High fields could prove beneficial in alleviating this issue as signal-to-noise ratios improve at higher Larmor frequencies. But, in any case, it is best to look for approaches in which the desired information is delivered as the dominant

component of the observed signal.

The encoded phase variance, for example, can provide information on characteristic lengths of the pore domain. Taking surface relaxation into consideration,

$$\begin{aligned}\left\langle \Delta\varphi^2(t)\right\rangle &= \frac{1}{\sqrt{V}}\sum_{m=0}^{\infty} e^{-D_0\mu_m^2 t}\left\langle 0|v_m\right\rangle\left\langle v_m|\varphi^2\right\rangle - \frac{1}{V}\sum_{m=0}^{\infty} e^{-D_0\mu_m^2 t}|\left\langle\varphi|v_m\right\rangle|^2 \\ &= \frac{1}{\sqrt{V}}\sum_{m=0}^{\infty} e^{-D_0\mu_m^2 t}\left\langle 0|v_m\right\rangle\left\langle v_m|\varphi^2\right\rangle - \frac{e^{-D_0\mu_0^2 t}}{V}\sum_{m=0}^{\infty}|\left\langle\varphi|v_m\right\rangle|^2 \\ &\qquad + \frac{1}{V}\sum_{m=1}^{\infty}|\left\langle\varphi|v_m\right\rangle|^2\left(e^{-D_0\mu_0^2 t} - e^{-D_0\mu_m^2 t}\right) \\ &= \frac{1}{V}\sum_{m=1}^{\infty}\left(|\left\langle\varphi|v_m\right\rangle|^2 - \sqrt{V}\left\langle 0|v_m\right\rangle\left\langle v_m|\varphi^2\right\rangle\right)\left(e^{-D_0\mu_0^2 t} - e^{-D_0\mu_m^2 t}\right),\end{aligned} \tag{4.25}$$

the last step following from the completeness of Robin eigenfunctions.

Notice that $e^{-D_0\mu_0^2 t} - e^{-D_0\mu_m^2 t}$ is always non-negative for any m because μ_0^2 is the smallest eigenvalue of the Laplace operator. The functions therefore have a single maximum occurring at

$$t_m = \frac{1}{D_0\left(\mu_m^2 - \mu_0^2\right)}\ln\left(\frac{\mu_m^2}{\mu_0^2}\right), \tag{4.26}$$

which implies contributions from higher modes peak at progressively shorter times but, because of all share the same slow rate of decay, the variance curve can still exhibit shoulderlike features, akin to momentary saturation levels, before the global maximum is reached. Consequently, length scales may become identifiable much in the same way discussed in absence of surface relaxation notwithstanding the fact that ultimately the variance does not saturate but decays.

The variance function in these cases, however, is not particularly convenient for Laplace inversion or for determination of internal field characteristics since such information could only be provided in the long time behavior that surface-induced relaxation leaves unobservable. Another particularly curious issue lies in the sign of coefficients in Eq.(4.25). Although the sum of all mode contributions must at all times be non-negative, it appears some contributions could pick a negative sign. This is, however, unlikely if surface-induced relaxation is weak compared to diffusion. Assuming the domain exhibits a non-degenerate Neumann eigenstructure, first order

perturbation theory implies

$$|\langle\varphi|v_m\rangle|^2 - \sqrt{V}\langle 0|v_m\rangle\langle v_m|\varphi^2\rangle = |\langle m|\varphi\rangle|^2 + 2\sum_{n\neq m}\frac{\langle\varphi|m\rangle R_{mn}\langle n|\varphi\rangle}{D_0(\lambda_m^2-\lambda_n^2)} \tag{4.27}$$

for all $m > 0$.

All these considerations suggest the internal field autocorrelation function is the most suitable probe of confinement length scales that can be accessed by the presented protocols.

4.2.2 Beyond the rephasing condition

Since knowledge of the two-point characteristic function of the internal field presupposes independent variation of encoding and decoding times, it is only natural to consider what can be done by acquiring echo information beyond the rephasing condition. With that in mind, assume a sequence could produce a signal decay determined by

$$\begin{aligned}\tilde{E}_{aux}(t) &= \left\langle\left(e^{-i\gamma t_d b_t}-1\right)\left(e^{i\gamma t_e b_0}-1\right)\right\rangle \\ &= \left\langle e^{-i\gamma t_d b_t}e^{i\gamma t_e b_0}\right\rangle - \left\langle e^{-i\gamma t_d b_t}\right\rangle - \left\langle e^{i\gamma t_e b_0}\right\rangle + \langle 1\rangle\end{aligned} \tag{4.28}$$

Then, upon weak encoding,

$$\tilde{E}_{aux}(t) = \gamma^2 t_e^2\langle b_t b_0\rangle + \mathcal{O}\left(\varphi^3\right) \tag{4.29}$$

by setting ultimately $t_d = t_e$.

As it turns out, the auxiliary signal can be generated by the MIF sequence by just superimposing the result of four implementations: An acquisition with equal encoding and decoding times, t_e (an echo maximum); a second with a vanishingly small encoding time, 0^+, and decoding time t_e; a third in which the previous situation is reversed and finally a T_1 decay. By stacking these results according to Eq.(4.28), the auxiliary signal can be observed.

Another nice feature of Eq.(4.28) is that it also allows one to visually check the encoding regime, for $0 \leq \tilde{E}_{aux}(0) \leq 2$ for all t_e and weak encoding can only be satisfied provided $\tilde{E}_{aux}(0) < 1$. The former inequality follows directly from Eq.(4.28) since the right hand side vanishes entirely in the limit encoding times become too small, whereas for sufficiently large encoding times only the middle terms tend to

zero since they correspond to FID amplitudes.

Autocorrelation short-time asymptotics

If the bounding surface of the pore structure is assumed smooth, then it is possible to use the short-time asymptotic analysis developed in Section 2.4 to deduce the short-time behavior of internal field autocorrelations.

The argument is basically the same. For the desired order of approximation, surface-induced relaxation can be neglected and by Eq.(2.91)

$$\langle b_t b_0 \rangle = \overline{b^2} - \frac{1}{2} \left\langle \left(b(\boldsymbol{X}_t) - b(\boldsymbol{X}_0) \right)^2 \right\rangle , \tag{4.30}$$

which implies

$$\begin{aligned} \frac{\mathrm{d}}{\mathrm{d}t} \langle b_t b_0 \rangle &= -\frac{D_0}{2V_0} \int_\Omega \mathrm{d}^3\boldsymbol{X} \int_\Omega \mathrm{d}^3\boldsymbol{X}_0 \, \left(b(\boldsymbol{X}) - b(\boldsymbol{X}_0) \right)^2 \nabla^2_{\boldsymbol{X}} G_t(\boldsymbol{X}, \boldsymbol{X_0}) \\ &= -\frac{D_0}{2V_0} \int_\Omega \mathrm{d}^3\boldsymbol{X}_0 \left[\int_\Omega \mathrm{d}^3\boldsymbol{X} \, \nabla^2_{\boldsymbol{X}} \left[\left(b(\boldsymbol{X}) - b(\boldsymbol{X}_0) \right)^2 \right] G_t(\boldsymbol{X}, \boldsymbol{X_0}) \right. \\ &\quad \left. - \int_{\partial\Omega} \mathrm{d}S \, G_t(\boldsymbol{X}, \boldsymbol{X_0}) \frac{\partial}{\partial \boldsymbol{n}} \left(b(\boldsymbol{X}) - b(\boldsymbol{X}_0) \right)^2 \right] , \end{aligned} \tag{4.31}$$

using the fact G_t is a solution of the diffusion equation that satisfy Neumann boundary conditions and Green's theorem.

Now, the internal field satisfies Laplace equation within the pore domain; as a result

$$\frac{\partial}{\partial \boldsymbol{n}} \left(b(\boldsymbol{X}) - b(\boldsymbol{X}_0) \right)^2 = 2 \left(b(\boldsymbol{X}) - b(\boldsymbol{X}_0) \right) \frac{\partial}{\partial \boldsymbol{n}} b(\boldsymbol{X}), \tag{4.32a}$$

$$\nabla^2_{\boldsymbol{X}} \left(b(\boldsymbol{X}) - b(\boldsymbol{X}_0) \right)^2 = 2 \left| \nabla_{\boldsymbol{X}} b(\boldsymbol{X}) \right|^2 . \tag{4.32b}$$

So,

$$\frac{\mathrm{d}}{\mathrm{d}t} \langle b_t b_0 \rangle = -D_0 \overline{|\nabla b|^2} + \frac{D_0}{V_0} \int_{\partial\Omega} \mathrm{d}S \, \frac{\partial b}{\partial \boldsymbol{n}} \int_\Omega \mathrm{d}^3\boldsymbol{X}_0 \, G_t(\boldsymbol{X}, \boldsymbol{X_0}) \left(b(\boldsymbol{X}) - b(\boldsymbol{X}_0) \right) . \tag{4.33}$$

For sufficiently short t, the diffusion propagator is concentrated about $\boldsymbol{X}_0$, which means the difference $b(\boldsymbol{X}) - b(\boldsymbol{X}_0)$ can be reasonably well determined by its first

order approximation. Hence, by Eq.(2.106)

$$\begin{aligned}\int_\Omega \mathrm{d}^3\boldsymbol{X}_0\, G_t(\boldsymbol{X},\boldsymbol{X_0})\,(b(\boldsymbol{X})-b(\boldsymbol{X}_0)) &\approx \sum_k \frac{\partial b}{\partial X_k}\int_\Omega \mathrm{d}^3\boldsymbol{X}_0\, G_t(\boldsymbol{X},\boldsymbol{X_0})\Delta X_k \\ &= \sqrt{\frac{4D_0t}{\pi}}\frac{\partial b}{\partial \boldsymbol{n}}\end{aligned} \tag{4.34}$$

and so, by integrating Eq.(4.33)

$$\langle b_t b_0\rangle \sim \overline{b^2} - \overline{|\nabla b|^2} D_0 t + \frac{4}{3\sqrt{\pi}}\frac{S_0}{V_0}\overline{\left|\frac{\partial b}{\partial \boldsymbol{n}}\right|^2}(D_0t)^{\frac{3}{2}} \tag{4.35}$$

wherein

$$\overline{\left|\frac{\partial b}{\partial \boldsymbol{n}}\right|^2} = \frac{1}{S_0}\int_{\partial\Omega}\mathrm{d}S\,\left|\frac{\partial b}{\partial \boldsymbol{n}}\right|^2. \tag{4.36}$$

There are two length scales that result from the above approximation that may be interesting to characterize confinement. The first concerns the scale of variation of the internal field and can be defined by

$$L_{\boldsymbol{G}} = \frac{\overline{b^2}}{\overline{|\nabla b|^2}}. \tag{4.37}$$

Under the assumption internal fields vary over intrapore scales, this number is useful to either confirm the hypothesis in cases wherein the characteristic pore size is known or indicate the order of the intended scale. The second length scale is a measurement of the specific surface of the structure apart from the ratio of near-surface and volumetric mean gradients. Namely,

$$\left(\frac{S_0}{V_0}\right)_{\boldsymbol{G}} = \frac{1}{\overline{|\nabla b|^2}}\overline{\left|\frac{\partial b}{\partial \boldsymbol{n}}\right|^2}\frac{S_0}{V_0}. \tag{4.38}$$

Intuitively, it is expected that such a ratio of mean field gradients is larger than unity since magnetic field inhomogeneities should be largest close to and across the solid boundary. The near-surface mean gradient, therefore, is an average over the region in which magnetic fields typically exhibit the largest variation. Yet, provided variations are considerably more relevant over a sort of boundary layer, the volumetric mean average should be dominated by gradients within such a layer and, consequently, the ratio would be close to unity, making $\left(\frac{S_0}{V_0}\right)_{\boldsymbol{G}}$ a good estimate of the surface-to-volume

ratio of the structure.

4.3 Experimental tests

An experiment was designed in order to assess the feasibility of the MIF method and to verify its major ideas. Two model porous media were created by pouring spherical soda-lime glass beads (Cospheric; Santa Barbara, CA), with diameters varying in between the respective ranges $45-53\mu m$ and $425-500\mu m$, into $5mm$ NMR tubes and saturating each system with distilled water (100%). All tests were carried in a Varian/Agilent 11.7 T spectrometer equipped with a 5mm ^{1}H probe ($\omega_0/2\pi = 500$MHz), at room temperature (298.15 K). Longitudinal relaxation (T_1) measurements using an inversion recovery sequence were performed so recycling delays could be determined for each sample.

The MIF protocol was programmed and run for the array of encoding times:

$$t_e = \{1, 5, 20, 50, 100, 200, 400, 600\}\ \mu\text{s}.$$

In all measurements, the storage or diffusion time, t, was varied exponentially from $100\mu s$ to $16s$ in a 30-point array. Finally, the acquisition window was set to open right after the end of the last RF pulse in every experiment. This not only allowed for visualization of echo formation but also meant decoding times were varied in each run. Accordingly, the echo amplitude was recorded at the 8 decoding time values determined by the encoding array for each encoding duration considered. Acquisition points therefore can be refereed as $E_t(t_e, t_d)$.

The signal $E_t(1, 1)$ was considered a suitable representation for T_1 decay signal, i.e., $\langle 1 \rangle$. This was verified by comparing it directly with the saturation curve produced by the inversion experiments. Each data set corresponding to a given t_e was normalized by the zero-time amplitude of the signal $E_t(t_e, t_e)$ which was determined via a two-exponential non-linear least squares (NLS) fit on data points for which $t < 1$s. The effect of encoding times in the stimulated echo amplitudes is shown for both systems in Fig.4.1.

It is evident that larger encoding times are able to activate more and more superior diffusion modes since decay is progressively and noticeably enhanced. From a physical standpoint, this means that the spatial distribution of spin phases becomes heterogeneous to the point that even typically short particle displacements can lead

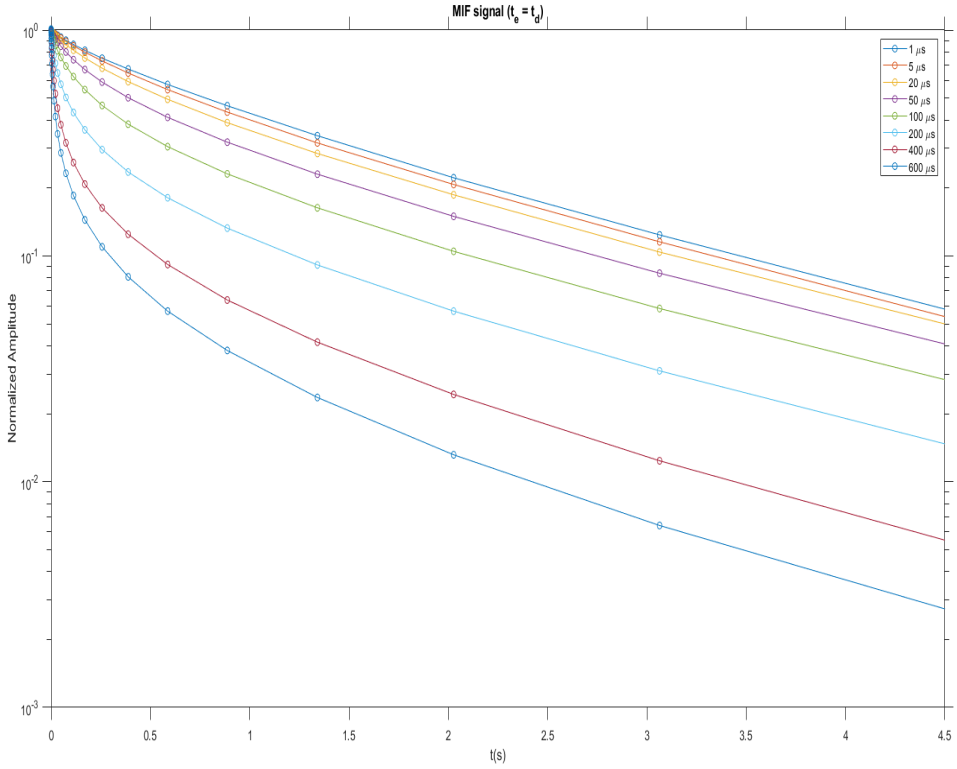

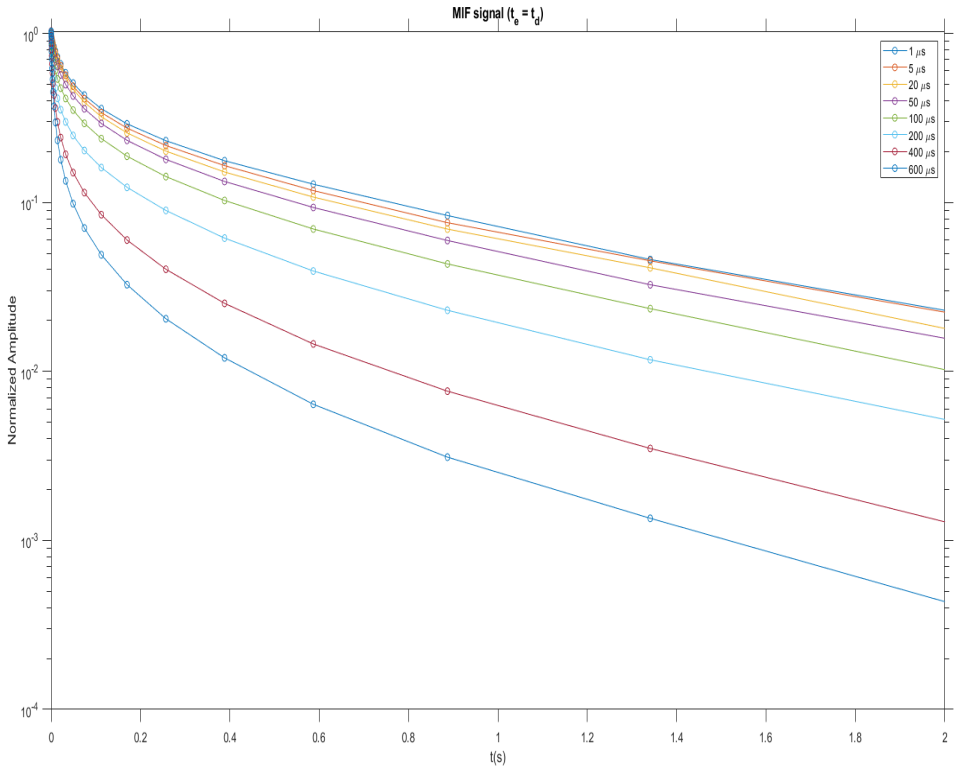

Figure 4.1: Echo attenuation as a function of diffusion times, $E_t(t_e, t_e)$, for distinct values of encoding times for the pack of spherical glass beads of diameters $425-500\mu m$ (Top) and $45-53\mu m$ (Bottom)

to substantial dephasing. The effect is not necessarily more pronounced in the more confined system. Notice that, in this case, the T_1 decay is already multiexponential which points to the fact that, likely, surface-induced relaxation cannot be considered a small effect and that superior modes contribute to the observed decay. Decays are also faster because characteristic length scales associated with diffusion modes are comparatively shorter. On the other hand, it is hard to tell whether internal field encoding itself is more pronounced in the more confined system. Finally, the long time behavior of all curves pertaining to each system is nearly identical and denotes the prevalence of the fundamental mode.

The auxiliary signals are generated by data processing through the combination

$$S_t(t_e) = E_t(t_e, t_e) - E_t(1, t_e) - E_t(t_e, 1) + E_t(1, 1). \tag{4.39}$$

The results are plotted in Fig.4.2 and show that encoding times larger than 100μs are way beyond the weak encoding regime in both systems. In fact, for the less confined structure, the 50μs encoding time already seems to be too large even though the typical encoded spin phase is still smaller than 1. This was really confirmed via a parabolic fit of initial amplitudes versus encoding times for $t_e = 5, 20, 50$. The last point becomes too deviated from the parabola for the large bead pack. Hence, only the 20μs encoding curve is used for this system on the analysis of the internal field autocorrelation since the 5μs encoding produces an auxiliary signal of negligible amplitude. On the other hand, both 20μs and 50μs encoding times in the small bead pack fit reasonably well to the said approach to be considered weak encoding times. This is fortunate because the whole analytical procedure can be carried on both sets of data and results can be compared

The internal field autocorrelation functions are presented in Fig.4.3 wherein the corresponding auxiliary decays have been normalized by the squared number of precession cycles within the encoding stage, namely, $(\omega_0 t_e/2\pi)^2$. This normalization is convenient because it yields an estimate of the mean susceptibility contrast of the sample which is useful both for characterization and validation of results. All results lead to an absolute susceptibility contrast in the order of 10^{-5} which is precisely what

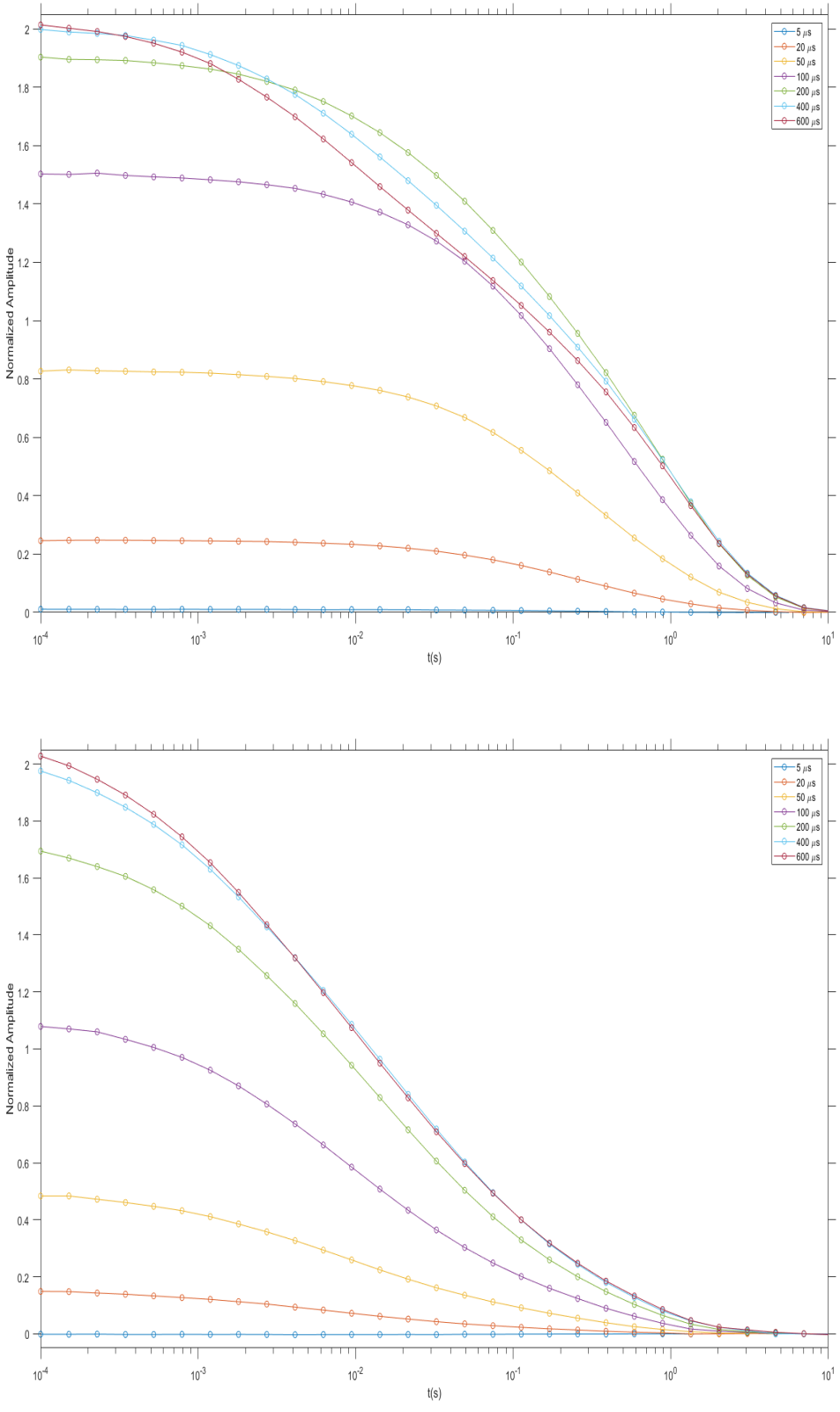

Figure 4.2: Auxiliary signals as a function of diffusion times for every encoding time considered. Data referring to the pack of spherical glass beads of diameters $425 - 500\mu m$ and $45 - 53\mu m$ are respectively shown at top and bottom.

Rates (s^{-1})/Proportions (%) for Autocorrelations			
	1st	2nd	3rd
$425-500\mu$m	0.90/40	1.21/49	30.9/11
$45-53\mu$m (20μs)	3.87/24	65.3/47	697/29
$45-53\mu$m (50μs)	3.02/26	48.8/44	468/30

Table 4.3: Decay rates and normalized coefficients for the internal field autocorrelation functions resulting from three exponential NLS fits on respective auxiliary signal decays. All fits have coefficients of determination, R^2, superior to 96%.

is expected for a water saturated soda lime glass structure[3].

The autocorrelations were also subjected to a mode analysis similar to the one employed traditionally in DDIF methods. Namely, the contribution of the fundamental mode is removed; the resultant data is normalized by the amplitude at $t = 0$ and inverted by a suitable discrete non-negative Laplace inversion method. To remove the contribution of the fundamental mode, a three exponential NLS fit was performed on corresponding auxiliary decays. The normalization constants come such from fits. The rates of decay and normalized coefficients are presented on Table 4.3. The fit for the less confined sample shows a nearly mono-exponential decay of rate close to $1s^{-1}$ although mono-exponential or even bi-exponential models could not satisfactorily fit the whole time range within the chosen tolerance of 4% in residual error. The rates and mode proportions pertaining to the more confined system are clearly more distinguished and there is a noticeable consistency of results when comparing the fit models produced by each data set. This corroborates the idea that weak encoding is the valid regime for both the 20μs and 50μs data sets, an interpretation that is reinforced by the performed inversions as well (See Fig.4.4).

Discrete inverse Laplace transforms were computed for each autocorrelation function under a non-negative constraint with and without the fundamental mode contribution. A constrained truncated singular value decomposition (TSVD) method was chosen as the inversion algorithm [30] due to the fact that regularization is a much more straightforward procedure for this particular class of methods. The number of stable (unconstrained) singular value components not removed from the solution defines the

[3] Water is paramagnetic and has a reported susceptibility value of 9.04×10^{-6} in the SI convention. I could not find any reference for magnetic susceptibility values of soda lime glass. The manufacturer only provides the information that the glass is diamagnetic and that χ is small compared to unity. However, it is possible to infer the actual value of the property due to the fact that the mineral composition of the glass is known. Soda lime is predominantly composed of silicon, sodium and calcium oxides. All these compounds are diamagnetic and have $|\chi| \sim 10^{-5}$. Hence, susceptibility contrasts must also be in that same order.

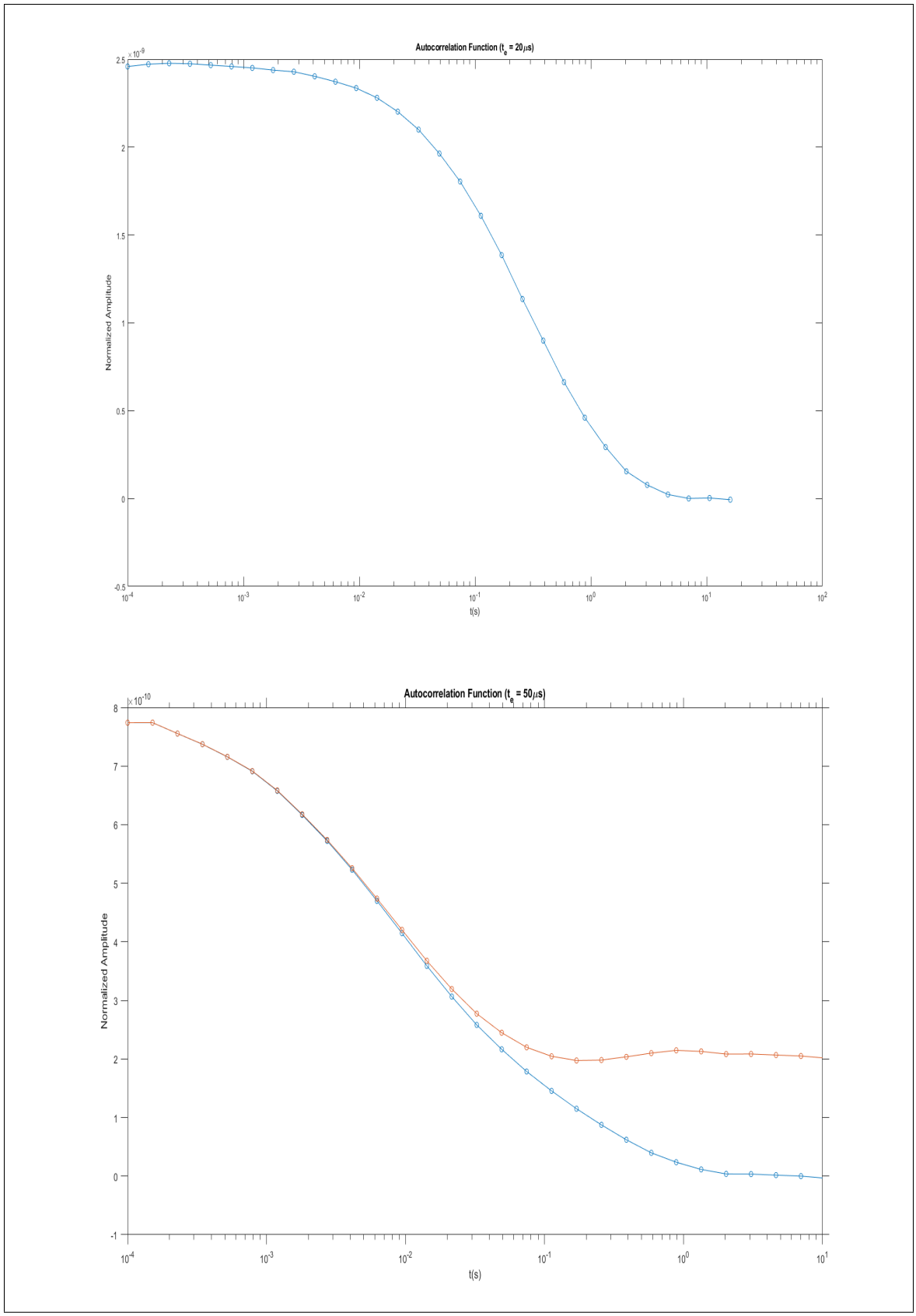

Figure 4.3: Internal field autocorrelation function, normalized by $(\omega_0 t_e/2\pi)^2$, for the pack of spherical glass beads of diameters $425-500\mu m$ (top) and $45-53\mu m$ (bottom). For the last plot, the autocorrelation after removal of fundamental mode decay is shown in red.

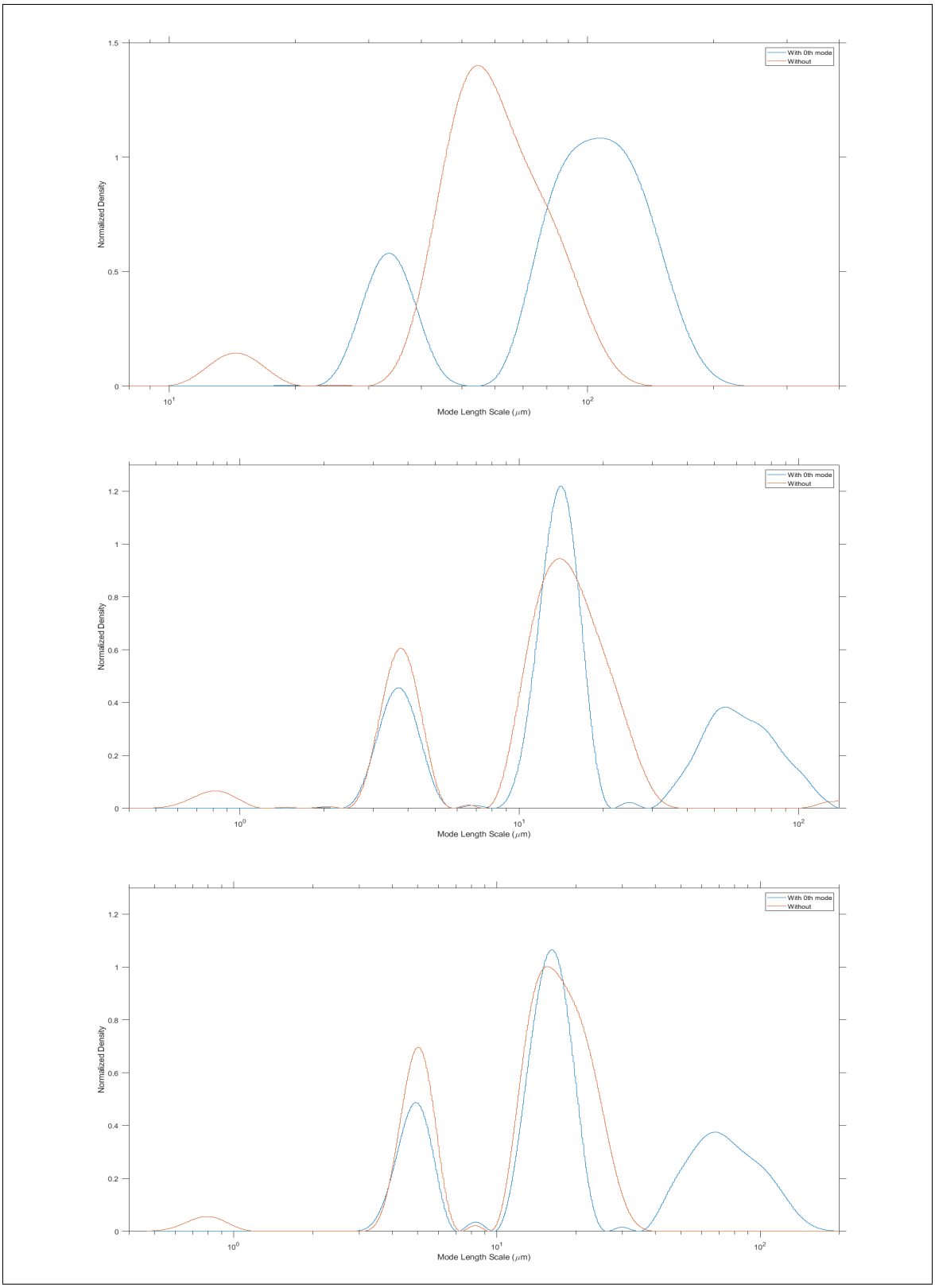

Figure 4.4: Distribution of characteristic sizes computed from autocorrelation with (blue) and without (red) fundamental mode contribution for the pack of spherical glass beads of diameters $425 - 500\mu m$ (top) and $45 - 53\mu m$ (medium and bottom).

Length scale(μm)/Contribution (%) of diffusion modes						
	$425-500\mu$m		$45-53\mu$m (20μs)		$45-53\mu$m (50μs)	
	with	without	with	without	with	without
1st	106/78	55/95	55/30	13.8/73	67.1/32	15.52/72
2nd	33/22	14.3/5	14.1/51	3.75/24	16.2/49	5.00/26
3rd	-	-	3.70/19	0.82/3	4.93/19	0.8/2

Table 4.4: Mode length scales of major peaks and subtended areas for the distributions presented on Fig.4.4.

amount of regularization on the solution and can be simply determined through a Picard plot[52]. The **decay rate distributions** that result from the procedure can then be converted into distributions of length scales pertaining to diffusion modes via the relation $L_i = \pi/\lambda_i = \pi\sqrt{D_0/s_i}$, in which s_i denotes the rate of decay of each mode. These are shown in Fig.4.4. It should be pointed out that for the sake of visualization distributions are properly scaled so that the apparent areas below the curve give precisely the contribution of each mode in spite of the fact graphs are plotted over a logarithmically scaled abscissa[35]. The characteristic length scale associated with each peak and corresponding areas are listed on Table 4.4.

There is a remarkable consistency in all results pertaining to the more confined structure. For both encoding times, a sizable contribution, roughly 30% of the signal, is associated with a mode whose characteristic size correlates well with the mean grain size, that is, the average diameter of beads. The majority of the signal however is associated with a mode which peaks at nearly 15 μm, which could be interpreted as the intra-granular length scale of internal field variations. Notice that removal of the fundamental mode emphasizes the contribution of said mode and that all mode length scales are effectively reproduced. The level of agreement is really remarkable, considering all the sources for ambiguity and error that are systematically introduced by the data processing procedure employed. On the other hand, values associated with the distribution of the less confined pore structure suggest interpretation in general is not so straightforward. The predominant signal contribution peaks at roughly 100 μm and, although it is associated with a broad distribution, there is no prevalence of length scales larger than 200 μm. So, it appears no inter-granular scale can be identified. Furthermore, there is no consistency of length scales before and after removal of such contribution, assuming it could be identified with the fundamental

mode. It is possible that the considered pore structure in this case is already too open (as opposed to confined) to exhibit enough separation between decay rates, a vital feature for a consistent exponential analysis.

Intuitively, it is expected that the internal field spatial profile scales with grain size. Accordingly, particle displacements would need to be typically 10 times larger in less confined system in order for spins to experience the same degree of dephasing they show in the more confined structure; if diffusion were unrestricted, this would require storage times approximately 3 times larger for the same degree of attenuation to be observed comparatively. On the other hand, Fig.4.3 shows that decay time scales are discrepant in orders of magnitude between both systems. It is thus possible that diffusion regimes are very different in the two systems studied, making it hard to benchmark the results of one upon the other's.

More reliable estimates are provided by the short time behavior of autocorrelations. Each function was fit by polynomial model of the type $f(x) = p_0 - p_2x^2 + p_3x^3$, in which $x = \sqrt{D_0 t}$, over a restricted data set of points chosen iteratively in order to maximize the coefficient of determination of fits, R^2. The results are plotted on Fig.4.5 and the interpreted results are exhibited on Table 4.5.

It is difficult to analyze how reasonable are the estimates for root mean square field and field gradients. To the best of knowledge, it is the first time these quantities are determined for a pore structure. Amazingly, the typical magnitude of field gradients is quite high. As reference, the values here reported are one to two orders of magnitude higher than common gradient strengths used in PFG experiments, which in turn already surpass tenfold the magnitude of gradients employed in MRI. On the other hand, these large internal field gradients must operate over microscopic distances, which is confirmed by the calculated values of $L_{\boldsymbol{G}}$. It is interesting to see how the length scale of variation of internal fields compares to the size of beads. For both samples the lengths are one order of magnitude below that of bead diameters, confirming that internal fields, at least for the samples used, typically vary over intrapore distances rather than across pores. The estimates of surface-to-volume ratios are in a remarkable agreement to the reference values pertaining to each structure. It is easy to show that for a mono-disperse pack of non-overlapping spheres

$$\frac{S_0}{V_0} = \frac{1-\phi}{\phi}\frac{6}{d} \tag{4.40}$$

in which ϕ denotes the porosity of the arrangement. For a random packing of spheres:

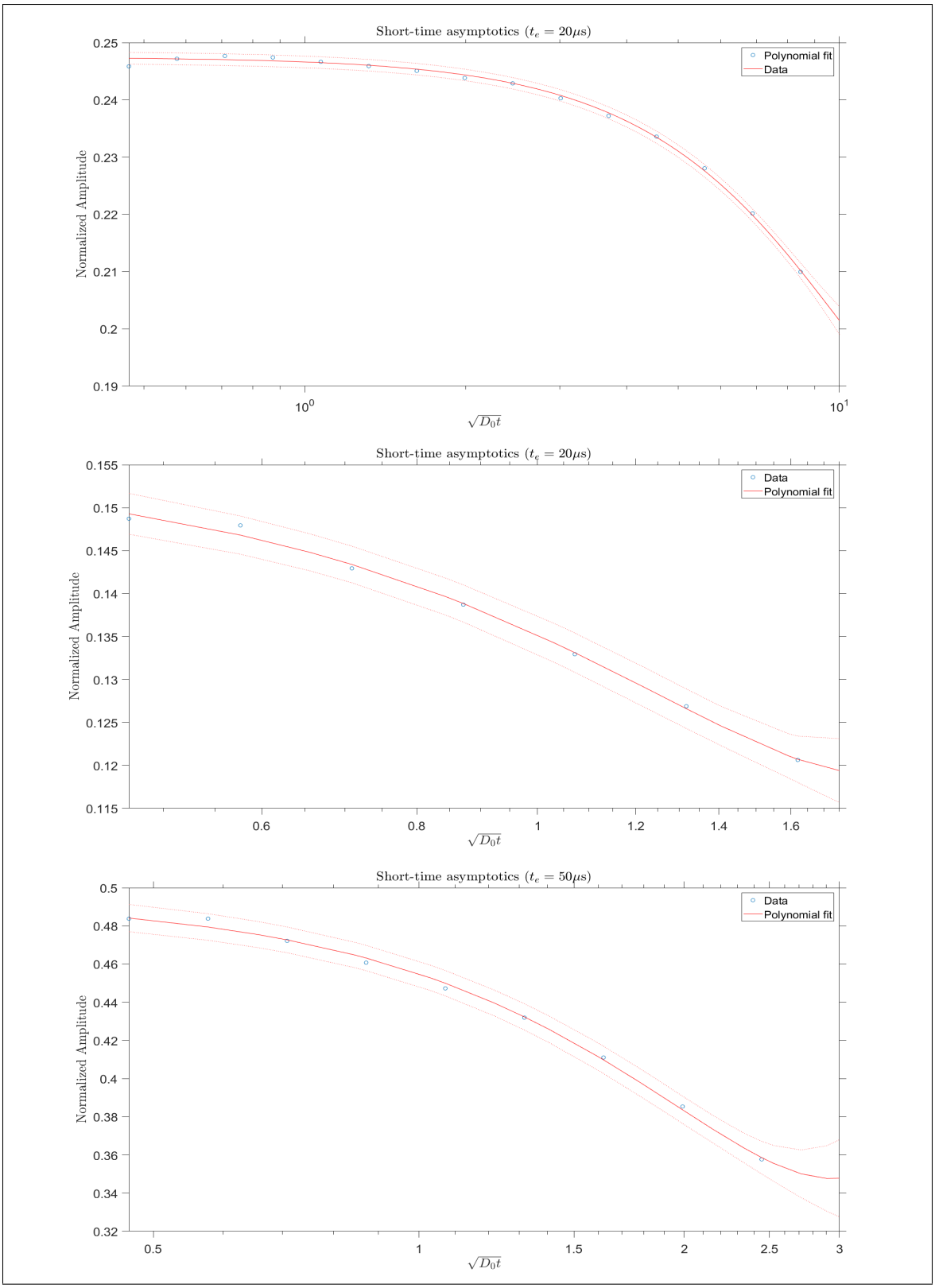

Figure 4.5: Short-time behavior of field autocorrelations for the pack of spherical glass beads of diameters $425 - 500\mu m$ (top) and $45 - 53\mu m$ (medium and bottom). Solid lines correspond to fits of Eq.(4.35) on the reduced set of experimental points, exhibit as circles. Dashed lines denote the 95% confidence interval of fits.

Internal field mean characteristics				
	$425-500\mu$m	$45-53\mu$m (20μs)	$45-53\mu$m (50μs)	
$\sqrt{\overline{B^2}}$	930.1±0.7	736±5	525±2	(mG)
$\sqrt{\overline{\lvert\nabla B\rvert^2}}$	539±3	(331±3)×10	(168±1)×10	(G/cm)
$L_{\boldsymbol{G}}$	17.1±0.8	2.2±0.2	3.2±0.2	(μm)
$\left(\frac{S_0}{V_0}\right)_{\boldsymbol{G}}$	(6±2)×10^4	(5±2)×10^5	(3±1)×10^5	(m^{-1})

Table 4.5: Values extracted from the short-time behavior of autocorrelation via a fit of Eq.(4.35) on each corresponding data set.

$0.35 \leq \phi \leq 0.41$ [32]. Thus, $1.9\times10^4 \leq S_0/V_0 \leq 2.4\times10^4$ and $1.7\times10^5 \leq S_0/V_0 \leq 2.2\times10^5$ in m^{-1} for the less and more confined samples respectively, provided polydispersity effects can be neglect and the mean diameter of beads is used.

4.4 Conclusion and prospects for future work

Internal field encoding protocols, like the DDIF method, can be a reasonable alternative to relaxation techniques for probing confinement lengths scales. They combine elements of diffusion methods and are considerably simpler from a experimental perspective since they do not require pulsing gradient apparatuses for implementation. However, it is still necessary a lot more of experimentation with these methods, particularly, over model porous media, to assess what sort of information they are actually able to provide. A clearer understanding of internal field conformation and how it scales with the pore geometry is evidently beneficial and it is firmly believed that some general guidelines for interpretation can come out of such studies. In this aspect, the results of computer simulations done over model geometries or over pore structures derived from micro-X-ray computerized tomography are essential. Recent literature shows there is a considerable effort in the community towards this realization.

By combining microscopic knowledge of internal fields with the techniques presented on Chapter 2, it might be possible to develop a deeper understanding of internal field autocorrelations and learn to recognize diffusion regimes directly from data. These ideas also sit well with the particularly modern trend of using artificial intelligence for pattern identification and to assist on data interpretation, as the ability to recognize features can be learned from model materials and from tests in improved conditions and applied to more complex structures or to results obtained

in sub-optimum set-ups.

As discussed, the loss of autocorrelation can, in principle, be used to identify multiply confinement length scales in time domain, provided there is sufficient separation between the characteristic sizes of each region. It would be nice to be able to reproduce this effect experimentally by interlayering stacks of glass beads of different sizes in such a way that smaller spheres do not fall in between the pores of the larger system. Experiments of this sort will be performed in due time.

Finally, it is necessary to determine whether these techniques can perform adequately in lower fields. It is common to find high field NMR spectrometers, like the one evoked throughout this thesis, being used for chemical characterization of fossil fuels in the oil industry, but NMR applications in petrophysical characterization remain in practice confined to lower fields mainly due to the fact NMR logging tools operate under low fields, so it is easier to match laboratory and field results, but there are also restrictions imposed by sample size (high field samples tend to be relatively small) and equipment cost. It is hoped that, once the concept is proved at higher fields, the protocol could enrich the suite of experimental methods already available at lower fields for pore structure characterization.

APPENDIX A

Phase Cycling and Temporal Profiling

Magnetic field (RF) pulses are essential to NMR methods. They are used for sample excitation in relaxation and diffusion techniques, voxel selection in MRI, phase reversal, storage and detection of longitudinal magnetic moment. As discussed, an important practical aspect of RF-pulses is that they are able to performed all these tasks very quickly and so, from a theoretical standpoint, be considered solely by their effects in the nuclear magnetization of the system. Accordingly, a RF-pulse can be denoted simply by its nutation angle and phase, which is the property that distinguishes the direction of nutation. Nuclear spin magnetization can naturally be nutated of arbitrary angles and into any given direction, but common practice distinguishes $\pi/2$- and π-pulses due to their general applicability. Pulse phase, on the other hand, is more seriously limited by the number of channels the spectrometer has in its oscillator gate. The most versatile spectrometers are equipped with four-channel gates, which means they are able to pulse in the four principal directions of the nuclear rotating frame, namely, $+x, +y, -x, -y$ or, said differently, generate pulses with a specific phase $n\pi/2$, wherein $n = 0, 1, 2, 3$. The pulse phase therefore is the polar angle of the RF field rotating component.

It is possible to summarize effect of pulses on both longitudinal and transverse surviving magnetizations. For example, a $\pi/2$-pulse changes the nuclear spin according

to

$$\begin{aligned} M_z(\boldsymbol{X}, t+) &= \mathrm{Im}\left[e^{-i\frac{n\pi}{2}} M(\boldsymbol{X}, t-)\right], \\ \mathrm{Im}\left[e^{-i\frac{n\pi}{2}} M(\boldsymbol{X}, t+)\right] &= -M_z(\boldsymbol{X}, t-), \end{aligned} \tag{A.1}$$

whereas a π-pulse

$$\begin{aligned} M_z(\boldsymbol{X}, t+) &= -M_z(\boldsymbol{X}, t-) \\ M(\boldsymbol{X}, t+) &= (-1)^n M^*(\boldsymbol{X}, t-) \end{aligned} \tag{A.2}$$

wherein n is the phase number of the RF pulse.

Now, any given implementation of a NMR sequence presupposes a template in which the position and type of the RF pulses is listed. The template of a CPMG sequence, for example, consists of a single initial $\pi/2$-pulse, for excitation, followed by a train of equally spaced π-pulses. The template for a stimulated echo PFG sequence is shown at 1. But it also happens that a given template can produce results that depend directly upon the choice of pulse phases. This, in turn, can be used to correct or remove certain features of the NMR signal by simply stacking the outputs of distinct implementations of the same template. Any of such procedures is called a phase cycling of the given sequence.

To illustrate how phase cycling is an important aspect of NMR methods and its relation to effective temporal profiles, consider the stimulated echo PFG template. Here, the matrix formalism is particularly instructive, so Eq.(2.80) is used.

The excitation pulse establishes a transverse magnetization that is defined by

$$|M_0\rangle = e^{i\frac{(n_0-1)\pi}{2}} |0\rangle \tag{A.3}$$

over an encoding period, t_e, the magnetization evolves under a constant field inhomogeneity, irrespective of its origin, therefore, by the end of encoding

$$|M(t_e)\rangle = e^{i\frac{(n_0-1)\pi}{2}} e^{-\left(i\gamma B + D_0\Lambda^2\right)t_e} |0\rangle . \tag{A.4}$$

Then, a second $\pi/2$-pulse is applied to store nuclear magnetization on the longitudinal axis and spin diffusion sets in unaffected by dephasing field, so after a time t_d,

$$|M_z(t_d)\rangle = e^{-D_0\Lambda^2 t_d} \mathrm{Im}\left[e^{-i\frac{n_1\pi}{2}} |M_0(t_e)\rangle\right] . \tag{A.5}$$

Finally, a third $\pi/2$-pulse brings the magnetization back to transverse plane and once again field inhomogeneities must be considered and acquisition is performed after another period of duration t_e. Thus,

$$\begin{aligned} |M(t)\rangle &= e^{i\frac{(n_2-1)\pi}{2}} e^{-\left(i\gamma B + D_0\Lambda^2\right)t_e} |M_z(t_d)\rangle \\ &= e^{i\frac{(n_2-1)\pi}{2}} e^{-\left(i\gamma B + D_0\Lambda^2\right)t_e} e^{-D_0\Lambda^2 t_d} \mathrm{Im}\left[e^{i\frac{(n_0-n_1-1)\pi}{2}} e^{-\left(i\gamma B + D_0\Lambda^2\right)t_e} |0\rangle\right]. \end{aligned} \tag{A.6}$$

Notice how the choice of pulse phase affects the final magnetization. For example, a choice for which $n_0 - n_1 = 1$ is governed by the imaginary part of $e^{-\left(i\gamma B + D_0\Lambda^2\right)t_e} |0\rangle$, while a choice for which $n_0 - n_1 = 2$ is determined by the real part. Recall that any $|M\rangle$ is just a (infinite) vector of components, so complex expansion and conjugation are simply defined. Incidentally, notice that $|M(t)\rangle^*$ is a solution at a time t of the complex conjugated Bloch-Torrey equation,

$$\frac{\mathrm{d}}{\mathrm{d}t} |M\rangle^* = i\gamma B |M\rangle^* - D_0\Lambda^2 |M\rangle^* \tag{A.7}$$

therefore

$$\left(e^{-\left(i\gamma B + D_0\Lambda^2\right)t_e}\right)^* = e^{-\left(-i\gamma B + D_0\Lambda^2\right)t_e}. \tag{A.8}$$

Hence, by stacking results produced by different implementations of the sequence, it is possible to produce a signal that follows from a magnetization field effectively determined by

$$|M(t)\rangle = e^{-\left(i\gamma B + D_0\Lambda^2\right)t_e} e^{-D_0\Lambda^2 t_d} e^{-\left(-i\gamma B + D_0\Lambda^2\right)t_e} |0\rangle. \tag{A.9}$$

Compare the above result with that produced in the context of piecewise constant sequences, Eq.(2.84), to recognize that phase cycling is what operationally allows the reduction of quite involved experimental protocols to simple effective temporal profiles.

APPENDIX B

Normal process characteristics

The epitome of a normal stochastic process is the Wiener process, namely, a Markovian random process whose jump probability density function is distributed as a Gaussian variable of zero mean and standard deviation $\sqrt{2D_0 t}$, where in t is the time-lapse of the considered jump. Accordingly, the N-point probability function of the 3D Wiener process is defined by

$$P(\boldsymbol{X}_N, t_N; \ldots; \boldsymbol{X}_1, t_1 | \boldsymbol{X}_0) = G_{t_N - t_{N-1}}(\boldsymbol{X}_N, \boldsymbol{X}_{N-1}) \ldots G_{t_1}(\boldsymbol{X}_1, \boldsymbol{X}_0). \tag{B.1}$$

as it is the case with any Markovian process, but, specifically,

$$G_{t_k - t_{k-1}}(\boldsymbol{X}_k, \boldsymbol{X}_{k-1}) = \frac{1}{\left[4\pi D_0 \left(t_k - t_{k-1}\right)\right]^{3/2}} \exp\left[-\frac{|\boldsymbol{X}_k - \boldsymbol{X}_{k-1}|^2}{4D_0 \left(t_k - t_{k-1}\right)}\right] \tag{B.2}$$

for arbitrary $k \leq N$.

Multidimensional Wiener processes have one important feature: The jumps in orthogonal directions are uncorrelated but identically distributed if the stochastic motion is statistically isotropic as considered in the above. Thus, it is possible to focus on one-dimensional processes with no loss to generality.

A more fundamental representation of jointly distributed random variables is made through the definition of joint characteristic functions. Whenever probability density functions are defined, the associated characteristic function to a set of jointly dis-

tributed random variables is determined by the Fourier transform of their probability density, that is,

$$\Phi(u_1, ..., u_N) = \int_{I^N} \mathrm{d}\, x_1 ... \mathrm{d}\, x_N e^{iu_1 x_1} ... e^{iu_N x_N} P(x_1, ..., x_N) \tag{B.3}$$

assuming all variables are can be defined over the same interval I. The characteristic function contains all the statistical information pertaining to the set of random variables, offering in fact a more basic definition of their probabilistic character than probability density functions[84]. For example, all statistical moments of the set are determine by partial differentiation of $\Phi(u_1, ..., u_N)$,

$$\langle x_{k_1} ... x_{k_m} \rangle = (-i)^m \frac{\partial^m \Phi(0, ..., 0)}{\partial u_{k_1} ... \partial u_{k_m}} \tag{B.4}$$

for an arbitrary selection of $m \leq N$ variables. Furthermore, all m-point characteristic functions, $m \leq N$, are determined from $\Phi(u_1, ..., u_N)$ by simply setting $u_k = 0$ for the unwanted variables and the characteristic function of independent variables factor out. These properties follow easily from Eq.(B.3).

Applied to the 1D Wiener process, these ideas imply

$$\begin{aligned} \Phi(u_1, ..., u_N|x_0) = & \int \mathrm{d}\, x_1 ... \mathrm{d}\, x_N e^{iu_1 x_1} ... e^{iu_N x_N} \\ & \times g_{t_N - t_{N-1}}(x_N, x_{N-1}) ... g_{t_1}(x_1, x_0) \\ = & \psi_{t_N - t_{N-1}}(u_N) \Phi(u_1, ..., u_{N-2}, u_{N-1} + u_N|x_0) \\ = & ... \\ = & \psi_{t_N - t_{N-1}}(u_N) ... \psi_{t_1}(u_N + ... + u_1) e^{i(u_N + ... + u_1)x_0} \end{aligned} \tag{B.5}$$

wherein x_k represents the kth position of the considered set and ψ_t is the characteristic function associated to the jump process. The induction above follows simply from the fact that $g_t(x, x')$ is a function of the difference $x - x'$ and a substitution of variables. Because the jump process is normally distributed,

$$\psi_t(u) = e^{-D_0 t u^2}. \tag{B.6}$$

The above relations can be used to determined the two first moments of a 1D

Wiener process,

$$\langle x_1 \rangle_0 = -i \frac{\partial \Phi(0|x_0)}{\partial u_1} = x_0, \tag{B.7a}$$

$$\langle x_1 x_2 \rangle_0 = -\frac{\partial^2 \Phi(0,0|x_0)}{\partial u_1 \partial u_2} = 2D_0 t_1 + x_0^2, \tag{B.7b}$$

which in turn can be used together with the statistical independence of orthogonal components in the multidimensional process to prove

$$\langle X_{1,j} \rangle_0 = X_{0,j}, \tag{B.8a}$$

$$\langle X_{1,j} X_{2,k} \rangle_0 = 2D_0 t_1 \delta_{jk} + X_{0,j} X_{0,k}. \tag{B.8b}$$

APPENDIX C

A representation for Robin-Laplace operators

Consider the Robin and Neumann diffusion propagators in the same domain, Ω, assumed bounded and of regular boundary. The differential equations satisfied by each can be respectively written in Laplace transformed domain as

$$\begin{aligned} sG_s^{(\rho)}(\boldsymbol{X}', \boldsymbol{X}_0) - \delta(\boldsymbol{X}' - \boldsymbol{X}_0) &= D_0 \nabla^2 G_s^{(\rho)}(\boldsymbol{X}', \boldsymbol{X}_0) \\ sG_s^{(0)}(\boldsymbol{X}', \boldsymbol{X}_0) - \delta(\boldsymbol{X}' - \boldsymbol{X}_0) &= D_0 \nabla^2 G_s^{(0)}(\boldsymbol{X}', \boldsymbol{X}_0). \end{aligned} \tag{C.1}$$

By multiplying the first by $G_s^{(0)}(\boldsymbol{X}, \boldsymbol{X}')$, the second by $G_s^{(\rho)}(\boldsymbol{X}, \boldsymbol{X}')$, taking the difference of resultant expressions, integrating over $\boldsymbol{X}'$ and using Green's theorem and boundary conditions, the following identity is obtained

$$G_s^{(\rho)}(\boldsymbol{X}, \boldsymbol{X}_0) = G_s^{(0)}(\boldsymbol{X}, \boldsymbol{X}_0) - \int_{\partial\Omega} \mathrm{d}S' \rho(\boldsymbol{X}') G_s^{(0)}(\boldsymbol{X}, \boldsymbol{X}') G_s^{(\rho)}(\boldsymbol{X}', \boldsymbol{X}_0). \tag{C.2}$$

It can be used iteratively to express the Robin propagator in terms of the Neumann one, provided the issuing sequence converges. Namely,

$$G_s^{(\rho)}(\boldsymbol{X}, \boldsymbol{X}_0) = \left(\sum_{n=0}^{\infty} (-1)^n \mathcal{L}_\rho^n \right) G_s^{(0)}(\boldsymbol{X}, \boldsymbol{X}_0) \tag{C.3}$$

in which

$$\mathcal{L}_\rho f(\boldsymbol{X}) = \int_{\partial\Omega} \mathrm{d}S' \rho(\boldsymbol{X}') G_s^{(0)}(\boldsymbol{X}, \boldsymbol{X}') f(\boldsymbol{X}') \tag{C.4}$$

is the linear operator induced by the iteration.

Now, the Neumann propagator can be written in terms of the eigenstructure of Neumann Laplace operator:

$$G_s^{(0)}(\boldsymbol{X},\boldsymbol{X}_0)=\sum_{m=0}^{\infty}\frac{u_m(\boldsymbol{X})u_m^*(\boldsymbol{X}_0)}{s+D_0\lambda_m^2},\quad s>0. \tag{C.5}$$

Then, because the eigenfunctions form a complete basis in Ω, any $f(\boldsymbol{X})=\sum_n f_n u_m(\boldsymbol{X})$ and

$$\mathcal{L}_\rho f(\boldsymbol{X})=\sum_{mn}u_m(\boldsymbol{X})\frac{R_{mn}}{s+D_0\lambda_m^2}f_n\equiv\left(sI+D_0\Lambda^2\right)^{-1}R\,|f\rangle \tag{C.6}$$

wherein R is the self-adjoint operator whose matrix elements on the chosen basis are defined by

$$R_{mn}=\int_{\partial\Omega}\mathrm{d}S'\rho(\boldsymbol{X'})u_m^*(\boldsymbol{X}')u_n(\boldsymbol{X}'). \tag{C.7}$$

Notice that, because of the normalization of eigenfunctions, R has inverse time dimensions and scales with the ratio $\bar{\rho}S/V$. On the other hand, $(sI+D_0\Lambda^2)^{-1}$ has its magnitude essentially controlled by the Laplace rate variable, $s>0$, given the fact that Λ^2 is semi-positive definite. Thus, it is reasonable to assume that $|\mathcal{L}_\rho|<1$ in the region defined by $s>\bar{\rho}S/V$ and then

$$\mathcal{L}_\rho^n G_s^{(0)}(\boldsymbol{X},\boldsymbol{X}_0)\equiv\left[\left(sI+D_0\Lambda^2\right)^{-1}R\right]^n\left(sI+D_0\Lambda^2\right)^{-1} \tag{C.8}$$

implies

$$\begin{aligned}G_s^{(\rho)}(\boldsymbol{X},\boldsymbol{X}_0)&\equiv\left(sI+D_0\Lambda^2\right)^{-1}\sum_{n=0}^{\infty}(-1)^n\left[R\left(sI+D_0\Lambda^2\right)^{-1}\right]^n\\&=\left(sI+D_0\Lambda^2\right)^{-1}\left[I+R\left(sI+D_0\Lambda^2\right)^{-1}\right]^{-1}\\&=\left[sI+D_0\Lambda^2+R\right]^{-1}.\end{aligned} \tag{C.9}$$

This result can be easily put into the usual notation of diffusion propagators,

$$G_s^{(\rho)}(\boldsymbol{X},\boldsymbol{X}_0)=\sum_{mn}u_m(\boldsymbol{X})\left[sI+D_0\Lambda^2+R\right]^{-1}_{mn}u_n^*(\boldsymbol{X}_0). \tag{C.10}$$

Let U_{mn} be the matrix elements of the unitary transformation that diagonalizes $D_0M^2=D_0\Lambda^2+R$. That such an unitary exists is guaranteed by the spectral

decomposition theorem and the fact that the latter operator is self-adjoint. Then,

$$G_s^{(\rho)}(\boldsymbol{X},\boldsymbol{X}_0)=\sum_{mn}u_m(\boldsymbol{X})\left(\sum_k\frac{U_{mk}U_{kn}^{\dagger}}{s+D_0\mu_k^2}\right)u_n^*(\boldsymbol{X}_0)=\sum_k\frac{v_k(\boldsymbol{X})v_k^*(\boldsymbol{X}_0)}{s+D_0\mu_k^2}. \quad \text{(C.11)}$$

Notice that the new system of functions, $v_k(\boldsymbol{X})=\sum_m u_m(\boldsymbol{X})U_{mk}$, is by construction orthonormal; each function is in effect the k-th eigenvector of the operator that represents the Robin diffusion propagator. This identification is powerful because it allows one to extend the domain of validity of the deduced series over $0<s\leq\bar{\rho}S/V$ through analytic continuation. In retrospect, it is not difficult to show that the matrix representations of both propagators satisfy Eq.(C.2) for all $s>0$ provided only D_0M^2 is positive definite, consequently, establishing that the eigenstructure of the Robin Laplace operator can be obtained[1] from the eigenstructure of the Neumann Laplace operator simply through the diagonalization of $D_0\Lambda^2+R$.

By itself, this result might be useful as a numerical recipe for it reduces the computation of the eigenstructure of various problems to that of a basic one plus a particular diagonalization. But, also, it can be used to account for the effect of surface relaxation in situations in which R can be considered a small perturbation on $D_0\Lambda^2$. This can be done readily through the usual time-independent perturbation techniques used in Quantum Mechanics, though the analysis may lose some of its explicitness in the case of pore structures exhibiting degenerate Neumann modes.

Nevertheless, it is known that the fundamental Neumann-Laplace eigenfunction is homogeneous and non-degenerate for any structure, so

$$v_0(\boldsymbol{X})=u_0(\boldsymbol{X})-\sum_{n=1}^{\infty}\frac{R_{0n}}{D_0\lambda_n^2}u_n(\boldsymbol{X}) \quad \text{and} \quad D_0\mu_0^2=R_{00}=\frac{\bar{\rho}S}{V} \quad \text{(C.12)}$$

always follows in the fast diffusion regime. But it can also be argued that realistic pore systems lack the symmetries that otherwise should produce degeneracies. Quasi-degeneracy may still be an issue for very high eigenmodes, but these, in diffusion studies, typically play a negligible role. If these conditions are met, first order non-degenerate perturbation theory can be used for all modes and it implies

$$v_m(\boldsymbol{X})=u_m(\boldsymbol{X})+\sum_{n\neq m}^{\infty}\frac{R_{mn}}{D_0\left(\lambda_m^2-\lambda_n^2\right)}u_n(\boldsymbol{X}) \quad \text{and} \quad D_0\mu_m^2=D_0\lambda_m^2+R_{mm}, \quad \text{(C.13)}$$

[1] Though, only in the mean square sense, for the case of eigenfunctions.

for all m. Parenthetically, recall that any non-degenerate eigenfunction of the Laplace operator must be real, thus, if all modes are non-degenerate, R has only real matrix elements. Finally, a general approximate expression for the Robin propagator can be given in terms of the Neumann eigenstructure

$$G_t^{(\rho)}(\boldsymbol{X}, \boldsymbol{X}_0) = \sum_{m=0}^{\infty} e^{-\left(D_0\lambda_m^2 + R_{mm}\right)t} u_m(\boldsymbol{X}) u_m(\boldsymbol{X}_0) + \sum_{m,n\neq m} e^{-\left(D_0\lambda_m^2 + R_{mm}\right)t} \frac{R_{mn}}{D_0\left(\lambda_m^2 - \lambda_n^2\right)} \left(u_m(\boldsymbol{X}) u_n(\boldsymbol{X}_0) + u_n(\boldsymbol{X}) u_m(\boldsymbol{X}_0)\right). \tag{C.14}$$

APPENDIX D

The hyperfine interaction

The contribution of a single unpaired electron to the local field operator is defined by the sum of contact, dipolar and spin-orbit couplings[56] and so it depends on the **relative** motion of the electron to a considered nucleus. Electron motion however is typically so fast that modulations produced by it could only be of any relevance for NMR relaxation at exceedingly high probing frequencies. As a result, it is reasonable to throw out all orbital correlations in Eq.(3.6) or, to what amounts to the same, to consider instead *electron-averaged* field contributions. The approximation leads to a coupling of the nucleus to an effective paramagnetic core. Under the assumption of orbital angular momentum quenching, the local field generated by such a reduced system is[1]

$$\mathbf{b}(\boldsymbol{X}) = \frac{2\mu_0}{3}\gamma_e\hbar\psi(\boldsymbol{X})\boldsymbol{S} + \nabla\Phi(\boldsymbol{X}), \tag{D.1}$$

in which $\boldsymbol{X}$ denotes the position vector relative to the effective center. The first contribution is the contact coupling with $\psi(\boldsymbol{X})$, the probability density of an unpaired electron at the nucleus position; $\boldsymbol{S}$ is the total spin of the paramagnetic center. The magnetic scalar potential introduced above is defined by the expression

$$\Phi(\boldsymbol{X}) = \frac{\mu_0}{4\pi}\gamma_e\hbar\int \mathrm{d}^3\boldsymbol{X}'\frac{\nabla\cdot(\psi(\boldsymbol{X}')\boldsymbol{S})}{|\boldsymbol{X}-\boldsymbol{X}'|} \tag{D.2}$$

which is simply the classical potential associated with a magnetization field $\gamma_e\hbar\psi(\boldsymbol{X}')\boldsymbol{S}$.

Refraining from having to advance a theory for the electronic orbital states, the most useful development of the above equation is made through a moment expansion. Accordingly, the two leading terms are

$$\Phi(\boldsymbol{X}) = \frac{\mu_0}{4\pi}\gamma_e\hbar\boldsymbol{S}\cdot\nabla\left(\frac{1}{|\boldsymbol{X}|}\right) - \frac{\mu_0}{4\pi}\gamma_e\hbar\boldsymbol{S}\cdot\nabla\left(\langle\boldsymbol{X}'\rangle\cdot\nabla\left(\frac{1}{|\boldsymbol{X}|}\right)\right). \tag{D.3}$$

From the zero order term ensues a dipole-dipole coupling between the total spin of the paramagnetic center and the nuclear spin as if both systems were point dipoles; incidentally, this is the contribution normally referred to as the dipolar interaction in relaxation theories[41,64,65]. The subsequent term represents the first order correction and introduces the average position of an unpaired electron, $\langle\boldsymbol{X}'\rangle$. It is expected that the probability density of electrons on a paramagnetic site attached to the surface of a solid wall is non-isotropic. Hence, $\langle\boldsymbol{X}'\rangle \neq 0$ and, consequently, one must consider to what extent the correction introduced by this term is relevant.

Clearly, the dipolar contribution falls as $|\boldsymbol{X}|^{-3}$ whereas the first order correction exhibits a dependence as $|\boldsymbol{X}|^{-4}$. Over regions $|\boldsymbol{X}| \approx |\langle\boldsymbol{X}'\rangle|$, however, the two contributions should have similar magnitudes. The scalar coupling, on the other hand, mediated by $\psi(\boldsymbol{X})$, is expected to fall even faster, possibly exponentially scaled by some measure in the order of $|\langle\boldsymbol{X}'\rangle|$. Therefore, unless nuclei typically reside too close to the core of paramagnetic centers, that is, unless the typical values of $|\boldsymbol{X}|$ are in the order of $|\langle\boldsymbol{X}'\rangle|$, the dipolar field must be the most relevant contribution to the local field.

Given that for the majority of paramagnetic ions the ionic radius is in the order of tens of picometers, if such scale is taken to be representative of $|\langle\boldsymbol{X}'\rangle|$, then even for a small coordinated molecule, like a water molecule, typical values of $|\boldsymbol{X}|$ should be about ten times larger than the average position of an unpaired electron. The disparity may not seem sufficiently large to justify the neglect of the first order correction, but it is more than enough to ignore the contact interaction completely provided the assumed exponential behavior holds.

It is not possible to advance further arguments in this respect without a proper characterization of unpaired electron density on a paramagnetic center, but it is hoped that the discussion above may serve as sufficient indication that the most relevant mechanism inducing NMR relaxation, stemming from the hyperfine interaction, is indeed the dipolar coupling. Accordingly, the theory presented in Chapter 3 is based

solely on this interaction[1].

[1]It is perhaps instructive to mention that it is the modulation of the deviation of the local field to its static value, rather than its actual value, that which produces NMR relaxation. So it is possible that the reputed weaker contributions play an even smaller role in the local relaxation mechanisms, provided they deviate only slightly from equilibrium values. If, on the other hand, the static field they introduce is somewhat relevant, they can contribute to the overall transverse relaxation through induced first order frequency shifts.

Bibliography

[1] A Abragam. *The principles of nuclear magnetism*. Number 32. Oxford university press, 1961.

[2] A Abragam and B Bleaney. *Electron paramagnetic resonance of transition ions*. OUP Oxford, 2012.

[3] S Axelrod and PN Sen. Nuclear magnetic resonance spin echoes for restricted diffusion in an inhomogeneous field: Methods and asymptotic regimes. *The Journal of Chemical Physics*, 114(15):6878–6895, 2001.

[4] R Balian. *From microphysics to macrophysics: methods and applications of statistical physics*, volume 2. Springer Science & Business Media, 2007.

[5] PS Belton, BP Hills, and ER Raimbaud. The effects of morphology and exchange on proton nmr relaxation in agarose gels. *Molecular Physics*, 63(5):825–842, 1988.

[6] M Bertero, C De Mol, and ER Pike. Linear inverse problems with discrete data. i. general formulation and singular system analysis. *Inverse problems*, 1(4):301, 1985.

[7] M Bertero, C De Mol, and ER Pike. Linear inverse problems with discrete data: Ii. stability and regularisation. *Inverse problems*, 4(3):573, 1988.

[8] F Bloch. Nuclear relaxation in gases by surface catalysis. *Physical Review*, 83(5):1062, 1951.

[9] Felix Bloch. Nuclear induction. *Physical review*, 70(7-8):460, 1946.

[10] N Bloembergen. Proton relaxation times in paramagnetic solutions. *The Journal of Chemical Physics*, 27(2):572–573, 1957.

[11] N Bloembergen, EM Purcell, and RV Pound. Relaxation effects in nuclear magnetic resonance absorption. *Physical review*, 73(7):679, 1948.

[12] RJS Brown. Measurements of nuclear spin relaxation of fluids in bulk and for large surface-to-volume ratios. *Bulletin of the American Physics Society, Series II*, 1:216, 1956.

[13] RJS Brown. Distribution of fields from randomly placed dipoles: free-precession signal decay as result of magnetic grains. *Physical Review*, 121(5):1379, 1961.

[14] RJS Brown. Proton relaxation in crude oils. *Nature*, 189(4762):387–388, 1961.

[15] RJS Brown and I Fatt. Measurements of fractional wettability of oil fields' rocks by the nuclear magnetic relaxation method. In *Fall Meeting of the Petroleum Branch of AIME*. Society of Petroleum Engineers, 1956.

[16] KR Brownstein and CE Tarr. Spin-lattice relaxation in a system governed by diffusion. *Journal of Magnetic Resonance (1969)*, 26(1):17–24, 1977.

[17] KR Brownstein and CE Tarr. Importance of classical diffusion in nmr studies of water in biological cells. *Physical Review A*, 19(6):2446, 1979.

[18] TR Bryar, CJ Daughney, and RJ Knight. Paramagnetic effects of iron (iii) species on nuclear magnetic relaxation of fluid protons in porous media. *Journal of magnetic resonance*, 142(1):74–85, 2000.

[19] JP Butler, JA Reeds, and SV Dawson. Estimating solutions of first kind integral equations with nonnegative constraints and optimal smoothing. *SIAM Journal on Numerical Analysis*, 18(3):381–397, 1981.

[20] Paul T Callaghan. A simple matrix formalism for spin echo analysis of restricted diffusion under generalized gradient waveforms. *Journal of Magnetic Resonance*, 129(1):74–84, 1997.

[21] Paul T Callaghan, Andrew Coy, David MacGowan, Ken J Packer, and Fernando O Zelaya. Diffraction-like effects in nmr diffusion studies of fluids in porous solids. *Nature*, 351(6326):467–469, 1991.

[22] PT Callaghan. *Principles of nuclear magnetic resonance microscopy*. Oxford University Press on Demand, 1993.

[23] HY Carr and EM Purcell. Effects of diffusion on free precession in nuclear magnetic resonance experiments. *Physical review*, 94(3):630, 1954.

[24] B Chencarek, MS Nascimento, AM Souza, RS Sarthour, BCC Santos, MD Correia, and IS Oliveira. Multi-exponential analysis of water nmr spin–spin relaxation in porosity/permeability-controlled sintered glass. *Applied Magnetic Resonance*, 50(1-3):211–225, 2019.

[25] MH Cohen and KS Mendelson. Nuclear magnetic relaxation and the internal geometry of sedimentary rocks. *Journal of Applied Physics*, 53(2):1127–1135, 1982.

[26] MD Correia, AM Souza, JP Sinnecker, RS Sarthour, BCC Santos, W Trevizan, and IS Oliveira. Superstatistics model for t2 distribution in nmr experiments on porous media. *Journal of Magnetic Resonance*, 244:12–17, 2014.

[27] R Courant and D Hilbert. *Methods of mathematical physics*, volume 1. CUP Archive, 1966.

[28] B Cowan. *Nuclear magnetic resonance and relaxation*. Cambridge University Press, 2005.

[29] J Crank. *The mathematics of diffusion*. Oxford university press, 1979.

[30] GD De Villiers, B McNally, and ER Pike. Positive solutions to linear inverse problems. *Inverse Problems*, 15(2):615, 1999.

[31] F D'Orazio, S Bhattacharja, WP Halperin, K Eguchi, and T Mizusaki. Molecular diffusion and nuclear-magnetic-resonance relaxation of water in unsaturated porous silica glass. *Physical Review B*, 42(16):9810, 1990.

[32] Francis AL Dullien. *Porous media: fluid transport and pore structure*. Academic press, 2012.

[33] KJ Dunn, DJ Bergman, and GA LaTorraca. *Nuclear magnetic resonance: Petrophysical and logging applications*, volume 32. Elsevier, 2002.

[34] RR Ernst, G Bodenhausen, and A Wokaun. *Principles of nuclear magnetic resonance in one and two dimensions*, volume 14. Clarendon press Oxford, 1987.

[35] Paola Fantazzini and Robert JS Brown. Units in distributions of relaxation times. *Concepts in Magnetic Resonance Part A: An Educational Journal*, 27(2):122–123, 2005.

[36] DA Faux, SHP Cachia, PJ McDonald, JS Bhatt, NC Howlett, and SV Churakov. Model for the interpretation of nuclear magnetic resonance relaxometry of hydrated porous silicate materials. *Physical Review E*, 91(3):032311, 2015.

[37] I Foley, SA Farooqui, and RL Kleinberg. Effect of paramagnetic ions on nmr relaxation of fluids at solid surfaces. *Journal of Magnetic Resonance, Series A*, 123(1):95–104, 1996.

[38] JJ Fripiat, M Letellier, and P Levitz. Interaction of water with clay surfaces. *Phil. Trans. R. Soc. Lond. A*, 311(1517):287–299, 1984.

[39] Zsolt Gengeliczki, Daniel E Rosenfeld, and MD Fayer. Theory of interfacial orientational relaxation spectroscopic observables. *The Journal of chemical physics*, 132(24):244703, 2010.

[40] B Ghanbarian, AG Hunt, RP Ewing, and M Sahimi. Tortuosity in porous media: a critical review. *Soil science society of America journal*, 77(5):1461–1477, 2013.

[41] S Godefroy, JP Korb, M Fleury, and RG Bryant. Surface nuclear magnetic relaxation and dynamics of water and oil in macroporous media. *Physical Review E*, 64(2):021605, 2001.

[42] Carolyn Gordon, David L Webb, and Scott Wolpert. One cannot hear the shape of a drum. *Bulletin of the American Mathematical Society*, 27(1):134–138, 1992.

[43] Denis S Grebenkov. Nmr survey of reflected brownian motion. *Reviews of Modern Physics*, 79(3):1077, 2007.

[44] Denis S Grebenkov. Laplacian eigenfunctions in nmr. i. a numerical tool. *Concepts in Magnetic Resonance Part A: An Educational Journal*, 32(4):277–301, 2008.

[45] Denis S Grebenkov. Use, misuse, and abuse of apparent diffusion coefficients. *Concepts in Magnetic Resonance Part A: An Educational Journal*, 36(1):24–35, 2010.

[46] Denis S Grebenkov. From the microstructure to diffusion nmr, and back. In *Diffusion NMR of Confined Systems*, pages 52–110. 2016.

[47] DS Grebenkov. Residence times and other functionals of reflected brownian motion. *Physical Review E*, 76(4):041139, 2007.

[48] DS Grebenkov and BT Nguyen. Geometrical structure of laplacian eigenfunctions. *siam REVIEW*, 55(4):601–667, 2013.

[49] HS Gutowsky, DW McCall, and CP Slichter. Nuclear magnetic resonance multiplets in liquids. *The Journal of Chemical Physics*, 21(2):279–292, 1953.

[50] EL Hahn. Spin echoes. *Physical review*, 80(4):580, 1950.

[51] EL Hahn and DE Maxwell. Spin echo measurements of nuclear spin coupling in molecules. *Physical Review*, 88(5):1070, 1952.

[52] PC Hansen. *Discrete inverse problems: insight and algorithms*. SIAM, 2010.

[53] PS Hubbard. Some properties of correlation functions of irreducible tensor operators. *Physical Review*, 180(1):319, 1969.

[54] MD Hurlimann, Karl G Helmer, LL Latour, and Christopher H Sotak. Restricted diffusion in sedimentary rocks. determination of surface-area-to-volume ratio and surface relaxivity. *Journal of Magnetic Resonance, Series A*, 111(2):169–178, 1994.

[55] AA Istratov and OF Vyvenko. Exponential analysis in physical phenomena. *Review of Scientific Instruments*, 70(2):1233–1257, 1999.

[56] JD Jackson. *Classical electrodynamics*. John Wiley & Sons, 2012.

[57] DL Johnson and LM Schwartz. Analytic theory of two-dimensional nmr in systems with coupled macro-and micropores. *Physical Review E*, 90(3):032407, 2014.

[58] DL Johnson and LM Schwartz. Three-state analytic theory of two-dimensional nuclear magnetic resonance in systems with coupled macro-and micropores. *Physical Review E*, 91(6):062406, 2015.

[59] Mark Kac. Can one hear the shape of a drum? *The american mathematical monthly*, 73(4P2):1–23, 1966.

[60] K Keating and R Knight. A laboratory study to determine the effect of iron oxides on proton nmr measurements. *Geophysics*, 72(1):E27–E32, 2007.

[61] VM Kenkre, Eiichi Fukushima, and D Sheltraw. Simple solutions of the torrey–bloch equations in the nmr study of molecular diffusion. *Journal of Magnetic Resonance*, 128(1):62–69, 1997.

[62] WE Kenyon, PI Day, C Straley, and JF Willemsen. A three-part study of nmr longitudinal relaxation properties of water-saturated sandstones. *SPE formation evaluation*, 3(03):622–636, 1988.

[63] RL Kleinberg. 9. nuclear magnetic resonance. In *Experimental methods in the physical sciences*, volume 35, pages 337–385. Elsevier, 1999.

[64] RL Kleinberg, WE Kenyon, and PP Mitra. Mechanism of nmr relaxation of fluids in rock. *Journal of Magnetic Resonance, Series A*, 108(2):206–214, 1994.

[65] JP Korb. Nuclear magnetic relaxation of liquids in porous media. *New Journal of Physics*, 13(3):035016, 2011.

[66] JP Korb, M Whaley-Hodges, and RG Bryant. Translational diffusion of liquids at surfaces of microporous materials: Theoretical analysis of field-cycling magnetic relaxation measurements. *Physical Review E*, 56(2):1934, 1997.

[67] J Korringa, DO Seevers, and HC Torrey. Theory of spin pumping and relaxation in systems with a low concentration of electron spin resonance centers. *Physical Review*, 127(4):1143, 1962.

[68] R Kubo, M Toda, and N Hashitsume. *Statistical physics II: nonequilibrium statistical mechanics*, volume 31. Springer Science & Business Media, 2012.

[69] Lawrence L Latour, LM Li, and Christopher H Sotak. Improved pfg stimulated-echo method for the measurement of diffusion in inhomogeneous fields. *Journal of magnetic resonance, Series B*, 101(1):72–77, 1993.

[70] FB Laun. Restricted diffusion in nmr in arbitrary inhomogeneous magnetic fields and an application to circular layers. *The Journal of Chemical Physics*, 137(4):044704, 2012.

[71] FB Laun, TA Kuder, W Semmler, and B Stieltjes. Determination of the defining boundary in nuclear magnetic resonance diffusion experiments. *Physical review letters*, 107(4):048102, 2011.

[72] JHi Lee, C Labadie, CS Springer, and GS Harbison. Two-dimensional inverse laplace transform nmr: altered relaxation times allow detection of exchange correlation. *JOURNAL-AMERICAN CHEMICAL SOCIETY*, 115:7761–7761, 1993.

[73] NV Lisitza and Y-Q Song. The behavior of diffusion eigenmodes in the presence of internal magnetic field in porous media. *The Journal of Chemical Physics*, 114(20):9120–9124, 2001.

[74] RW Mair, GP Wong, D Hoffmann, Martin D Hürlimann, S Patz, LM Schwartz, and RL Walsworth. Probing porous media with gas diffusion nmr. *Physical review letters*, 83(16):3324, 1999.

[75] KR McCall, DL Johnson, and RA Guyer. Magnetization evolution in connected pore systems. *Physical Review B*, 44(14):7344, 1991.

[76] HM McConnell. Reaction rates by nuclear magnetic resonance. *The Journal of Chemical Physics*, 28(3):430–431, 1958.

[77] KS Mendelson. Percolation model of nuclear magnetic relaxation in porous media. *Physical Review B*, 41(1):562, 1990.

[78] J Mitchell, JD Griffith, JHP Collins, AJ Sederman, LF Gladden, and ML Johns. Validation of nmr relaxation exchange time measurements in porous media. *The Journal of chemical physics*, 127(23):234701, 2007.

[79] Partha P Mitra and Bertrand I Halperin. Effects of finite gradient-pulse widths in pulsed-field-gradient diffusion measurements. *Journal of Magnetic Resonance, Series A*, 113(1):94–101, 1995.

[80] Partha P Mitra, Pabitra N Sen, and Lawrence M Schwartz. Short-time behavior of the diffusion coefficient as a geometrical probe of porous media. *Physical Review B*, 47(14):8565, 1993.

[81] S Muncaci and I Ardelean. Probing the pore size of porous ceramics with controlled amount of magnetic impurities via diffusion effects on the cpmg technique. *Applied Magnetic Resonance*, 44(7):837–848, 2013.

[82] Hideo Nakajima. *Porous metals with directional pores*. Springer, 2013.

[83] M Nascimento, B Chencarek, AM Souza, RS Sarthour, B Coutinho, MD Correia, and IS Oliveira. Enhanced nmr relaxation of fluids confined to porous media: A proposed theory and experimental tests. *Physical Review E*, 99(4):042901, 2019.

[84] E Parzen. *Stochastic processes*. SIAM, 1999.

[85] RF Pawula. Approximation of the linear boltzmann equation by the fokker-planck equation. *Physical review*, 162(1):186, 1967.

[86] Jean Philibert. One and a half century of diffusion: Fick, einstein, before and beyond. *Diffusion Fundamentals*, 2(1):1–10, 2005.

[87] Baldwin Robertson. Spin-echo decay of spins diffusing in a bounded region. *Physical Review*, 151(1):273, 1966.

[88] P Roose, J Van Craen, G Andriessens, and H Eisendrath. Nmr study of spin–lattice relaxation of water protons by mn2+ adsorbed onto colloidal silica. *Journal of Magnetic Resonance, Series A*, 120(2):206–213, 1996.

[89] S Ryu. Effect of inhomogeneous surface relaxivity, pore geometry and internal field gradient on nmr logging: Exact and perturbative theories and numerical investigations. In *SPWLA 50th Annual Logging Symposium*. Society of Petrophysicists and Well-Log Analysts, 2009.

[90] S Ryu and DL Johnson. Aspects of diffusive-relaxation dynamics with a nonuniform, partially absorbing boundary in general porous media. *Physical review letters*, 103(11):118701, 2009.

[91] Pabitra N Sen, Lawrence M Schwartz, Partha P Mitra, and Bertrand I Halperin. Surface relaxation and the long-time diffusion coefficient in porous media: periodic geometries. *Physical Review B*, 49(1):215, 1994.

[92] PN Sen. Time-dependent diffusion coefficient as a probe of geometry. *Concepts in Magnetic Resonance Part A: An Educational Journal*, 23(1):1–21, 2004.

[93] SD Senturia and JD Robinson. Nuclear spin-lattice relaxation of liquids confined in porous solids. *Society of Petroleum Engineers Journal*, 10(03):237–244, 1970.

[94] I Seroussi, DS Grebenkov, O Pasternak, and N Sochen. Microscopic interpretation and generalization of the bloch-torrey equation for diffusion magnetic resonance. *Journal of Magnetic Resonance*, 277:95–103, 2017.

[95] JH Simpson and HY Carr. Diffusion and nuclear spin relaxation in water. *Physical Review*, 111(5):1201, 1958.

[96] CP Slichter. *Principles of magnetic resonance*, volume 1. Springer Science & Business Media, 2013.

[97] I Solomon. Relaxation processes in a system of two spins. *Physical Review*, 99(2):559, 1955.

[98] R Song, YQ Song, M Vembusubramanian, and JL Paulsen. The robust identification of exchange from t2–t2 time-domain features. *Journal of Magnetic Resonance*, 265:164–171, 2016.

[99] Y-Q Song, L Venkataramanan, MD Hürlimann, M Flaum, Pi Frulla, and C Straley. T1–t2 correlation spectra obtained using a fast two-dimensional laplace inversion. *Journal of Magnetic Resonance*, 154(2):261–268, 2002.

[100] Yi-Qiao Song. Determining pore sizes using an internal magnetic field, 2000.

[101] Yi-Qiao Song. Using internal magnetic fields to obtain pore size distributions of porous media. *Concepts in Magnetic Resonance Part A: An Educational Journal*, 18(2):97–110, 2003.

[102] Yi-Qiao Song, Seungoh Ryu, and Pabitra N Sen. Determining multiple length scales in rocks. *Nature*, 406(6792):178–181, 2000.

[103] YQ Song. Magnetic resonance of porous media (mrpm): A perspective. *Journal of Magnetic Resonance*, 229:12–24, 2013.

[104] YQ Song, G Carneiro, LM Schwartz, and DL Johnson. Experimental identification of diffusive coupling using 2d nmr. *Physical review letters*, 113(23):235503, 2014.

[105] I Stakgold. *Boundary Value Problems of Mathematical Physics: Volume 1*. SIAM, 2000.

[106] Frank Stallmach and Petrik Galvosas. Spin echo nmr diffusion studies. *Annual Reports on NMR Spectroscopy*, 61:51–131, 2007.

[107] Edward O Stejskal and John E Tanner. Spin diffusion measurements: spin echoes in the presence of a time-dependent field gradient. *The journal of chemical physics*, 42(1):288–292, 1965.

[108] EO Stejskal. Use of spin echoes in a pulsed magnetic-field gradient to study anisotropic, restricted diffusion and flow. *The Journal of Chemical Physics*, 43(10):3597–3603, 1965.

[109] SD Stoller, William Happer, and Freeman J Dyson. Transverse spin relaxation in inhomogeneous magnetic fields. *Physical Review A*, 44(11):7459, 1991.

[110] HC Torrey. Nuclear spin relaxation by translational diffusion. *Physical Review*, 92(4):962, 1953.

[111] HC Torrey. Bloch equations with diffusion terms. *Physical review*, 104(3):563, 1956.

[112] HC Torrey, J Korringa, DO Seevers, and J Uebersfeld. Magnetic spin pumping in fluids contained in porous media. *Physical Review Letters*, 3(9):418, 1959.

[113] Monique C Tourell, Ionut-Alexandru Pop, Lynda J Brown, Richard CD Brown, and Giuseppe Pileio. Singlet-assisted diffusion-nmr (sad-nmr): redefining the limits when measuring tortuosity in porous media. *Physical Chemistry Chemical Physics*, 20(20):13705–13713, 2018.

[114] CC Wang and R Pecora. Time-correlation functions for restricted rotational diffusion. *The Journal of Chemical Physics*, 72(10):5333–5340, 1980.

[115] KE Washburn and PT Callaghan. Tracking pore to pore exchange using relaxation exchange spectroscopy. *Physical review letters*, 97(17):175502, 2006.

[116] KP Whittall and AL MacKay. Quantitative interpretation of nmr relaxation data. *Journal of Magnetic Resonance (1969)*, 84(1):134–152, 1989.

[117] DE Woessner. Nmr spin-echo self-diffusion measurements on fluids undergoing restricted diffusion. *The Journal of Physical Chemistry*, 67(6):1365–1367, 1963.

[118] LJ Zielinski and PN Sen. Combined effects of diffusion, nonuniform-gradient magnetic fields, and restriction on an arbitrary coherence pathway. *The Journal of chemical physics*, 119(2):1093–1104, 2003.

[119] JR Zimmerman and WE Brittin. Nuclear magnetic resonance studies in multiple phase systems: lifetime of a water molecule in an adsorbing phase on silica gel. *J. phys. Chem*, 61(10):1328–1333, 1957.